The glutamate dehydrogenase of the slow-growing mycobacteria: its function in nitrogen metabolism and importance to *in vitro* and intracellular survival.

by

Albertus Johannes Viljoen

BSc Human Life Sciences, Stellenbosch University, 2008

BScMedScHons Human Genetics, Stellenbosch University, 2009

Dissertation presented for the degree of Doctor of Philosophy in the Faculty of Medicine and Health Sciences at Stellenbosch University

Supervisor: **Prof. Ian J.F. Wiid**

Co-supervisor: **Dr. Catriona J. Kirsten (née Harper)**

Stellenbosch University

December 2013

Declaration

By submitting this dissertation electronically, I declare that the entirety of the work contained therein is my own, original work, that I am the sole author thereof (save to the extent explicitly otherwise stated), that reproduction and publication thereof by Stellenbosch University will not infringe any third party rights and that I have not previously in its entirety or in part submitted it for obtaining any qualification.

Date: December 2013

Summary

Recent studies have implicated the metabolism of glutamate in *Mycobacterium tuberculosis*, the causative agent of tuberculosis disease, as an important factor in survival of the bacterium in the human host macrophage cells. Glutamine oxoglutarate aminotransferase (GOGAT) and glutamate dehydrogenase (GDH), the major enzymes involved in the production and break-down of glutamate respectively, are controlled through their interaction with glycogen accumulation regulator A (GarA) which is phosphorylated by protein kinase G (PknG), a determinant of virulence. However, GOGAT and GDH have not been investigated for their roles in the survival of *M. tuberculosis* in macrophage cells. In this study, the regulation of GOGAT and GDH in response to fluctuations in nitrogen availability is described in *Mycobacterium bovis* BCG, a close relative of *M. tuberculosis*. Evidence is presented that the amino acid residue of GarA which is phosphorylated by PknG is required for *in vitro* growth of *M. bovis* BCG. Although the genes encoding for GOGAT and GDH in *M. tuberculosis* are essential, *M. bovis* BCG mutants of the corresponding genes were generated successfully in this study. It is shown that GOGAT is required for *de novo* synthesis of glutamate, while GDH is required for utilization of the amino acid as a sole nitrogen source and in the metabolism of asparagine. While growth of the GOGAT mutant in macrophage cells was not appreciably different from wild type *M. bovis* BCG, intracellular growth of the GDH mutant was impaired, suggesting that GDH plays an important role during infection of macrophage cells. It is shown that the intracellular requirement for GDH may be linked to functions of this enzyme in acidic conditions or in the utilization of glutamate as a carbon source. The *M. tuberculosis* GDH is a unique enzyme which differs largely from its human homologue or the homologues found in the human gut flora and present a potential route for development of novel chemotherapeutic intervention strategies in tuberculosis disease.

Opsomming

Die metabolisme van glutamiensuur in *Mycobacterium tuberculosis*, die oorsaaklike agent in die siekte tuberkulose, is in onlangse studies as ‘n belangrike faktor in die oorlewing van die bakterium in gasheer-mensmakrofaagselle geïmpliseer. Glutamien oksoglutaraat aminotransferase (GOGAT) en glutamiensuur dehidrogenase (GDH), die belangrikste ensieme wat onderskeidelik by die produksie en af-braak van glutamiensuur betrokke is, word deur hulle interaksie met glikogeen akkumulasie reguleerder (GarA) beheer, wat deur proteïen kinase G (PknG), ‘n virulensie faktor, gefosforileer word. Die rolle wat GOGAT en GDH in die oorlewing van *M. tuberculosis* in makrofaagselle vertolk is egter nog nie bestudeer nie. In hiérdie studie word die regulasie van GOGAT en GDH in respons op fluktuasies in stikstof beskikbaarheid in *Mycobacterium bovis* BCG, ‘n nabye familielid van *M. tuberculosis*, beskryf. Bewyse word voorgelê dat die aminosuur-residu wat deur PknG in GarA gefosforileer word, deur *M. bovis* BCG benodig word om *in vitro* te kan groei. Alhoewel die gene wat vir GOGAT en GDH in *M. tuberculosis* kodeer essensieël is, is *M. bovis* BCG mutante van die korresponderende gene suksesvol in hiérdie studie geskep. Daar word aangetoon dat GOGAT vir die *de novo* sintese van glutamiensuur benodig word, terwyl GDH noodsaaklik is vir die verbruik van die aminosuur as ‘n uitsluitlike stikstof-bron asook in die metabolisme van asparagien. Alhoewel groei van die GOGAT mutant in makrofaagselle nie aansienlik verskil het van wilde tipe *M. bovis* BCG nie, was die intrasellulêre groei van die GDH mutant verswak, wat daarop dui dat GDH ‘n belangrike funksie tydens infeksie van makrofaagselle verrig. Daar word verder aangetoon dat die intrasellulêre vereiste vir GDH aan funksies van dié ensiem onder suur-omstandighede of in die gebruik van glutamiensuur as ‘n enigste koostofbron gekoppel kan word. Die *M. tuberculosis* GDH is ‘n unieke ensiem, wat grootliks verskil van sy menshomoloog of die homoloë wat in die menslike ingewande flora voorkom en bied ‘n potensiële roete vir die ontwikkeling van nuwe chemoterapeutiese intervensie strategieë in die siekte tuberkulose.

Presentations and publications

Poster presentation at the Stellenbosch University Faculty of Health Sciences Annual Academic Day 2010: Viljoen, A.J.; Kirsten, C.; Hayward, D.; Wiid, I.J.F.; Van Helden, P.D.; **Regulation of the nitrogen assimilatory enzymes, glutamine synthetase and glutamate dehydrogenase in *Mycobacterium smegmatis* and *Mycobacterium bovis* BCG.**

Poster presentation at the Stellenbosch University Faculty of Health Sciences Annual Academic Day 2011: Viljoen, A.J.; Kirsten, C.; Wiid, I.J.F.; Van Helden, P.D.; **Investigation of two key enzymes in nitrogen assimilation of *Mycobacterium bovis* BCG: A molecular approach.**

Oral presentation at the Stellenbosch University Faculty of Health Sciences Annual Academic Day 2012: Viljoen, A.J.; Kirsten, C.; Hayward, D.; Wiid, I.J.F.; Van Helden, P.D.; **Genetic study of the nitrogen assimilatory pathways: GDH & GOGAT in *Mycobacterium bovis* BCG.**

Poster presentation at the European Molecular Biology Organization (EMBO) Tuberculosis 2012: Biology, Pathogenesis, Intervention strategies conference, Paris, France, 11-15 September 2012: Viljoen, A.J.; Kirsten, C.; Wiid, I.J.F.; Van Helden, P.D.; **Genetic study of the nitrogen assimilatory pathways of *Mycobacterium bovis* BCG.**

Poster presentation at the Stellenbosch University Faculty of Health Sciences Annual Academic Day 2013: Viljoen, A.J.; Kirsten, C.; Pietersen, R.D.; Baker, B; Wiid, I.J.F.; **Glutamate metabolism: a potential determinant of *Mycobacterium tuberculosis* virulence.**

Manuscript entitled **The role of glutamine oxoglutarate aminotransferase and glutamate dehydrogenase in nitrogen metabolism in *Mycobacterium bovis* BCG** submitted to PLoS One.

Acknowledgements

Aan my oupa, Ben Uys. Hy het my meer as 20 jaar gelede met sy "dinkbokse" die eerste lesse in navorsing gegee.

Firstly I would like to thank my supervisor, Prof. Ian Wiid, and co-supervisor Dr. Carrie Kirsten, for never hesitating to provide me with the resources I needed to be successful in this PhD study. They really are two of the nicest, kindest, warmest people I know. I owe a massive dept of gratitude to Prof. Paul van Helden, for his support as well as for the stimulating and exceptionally well-equiped research environment he has created at the Division of Molecular Biology and Human Genetics.

I would like to thank Mae Newton-Foot for the plasmid pMNFhyg, for her friendliness and everlasting willingness to teach me so many things; Zhuo Fang, Nelita du Plessis, Leanie Kleynhans, Lyntha Paul and Marlo Möller for kind and ample advice given on various aspects of this study; Ruzayda van Aarde for her assistance with mycobacterial genomic DNA extractions and Southern blotting analyses and Ray-Dean Pietersen for his kind help with the cell culture techniques employed in this study. I must acknowledge the invaluable intellectual and technical advice given to me by Monique Williams and thank her for her friendliness and undying patience. I would like to thank my good friends and colleagues, Lance Lucas and Carine Sao Emani, with whom I had countless insightfull conversations on science and a great deal of other things. I have to acknowledge the honours students, Claudia Ntsapi and James Gallant, and MSc student, Siyanda Tshoko, for very pleasant company when they joined me in the investigation of nitrogen-metabolism in mycobacteria. I need to thank all the members of the TBdrug group, present and past, who I have not yet acknowledged for their helpful input in this study: Bienyameen Baker, Andile Ngwane, Gina Leishing, Gustav Styger (who kindly revised several drafts of this thesis), Lubabalo Macingwana, Vuyiseka Mpongoshe and Don Hayward.

The financial assistance of the National Research Foundation (DAAD-NRF) towards this research is hereby acknowledged. Opinions expressed and conclusions arrived at, are those of the author and are not necessarily to be attributed to the DAAD-NRF.

I would also like to thank the Harry Crossley Foundation for personal financial support as well as for project funding.

Ek is geweldig dankbaar vir my ouers Nico en Berna Viljoen. Hulle het baie groot opofferings gemaak en risikos geneem om my te kry tot waar ek vandag is. Ek is net so dankbaar vir my grootouers, Ben en Maggie Uys en Bert en Lida Viljoen, vir die mense wie hulle is (en moes gewees het) en is baie trots om hulle kleinseun te wees. Een persoon aan wie ek veral verskuldig is vir sy bystand en geduld tydens die donkerder tye is my broer Ben. Ek het ek nog altyd meer opgekyk na hom as wat hy ooit sal weet. En dan is daar my pragtige klein sussie, Marelize Viljoen, wie altyd die kop in die wolke het, maar wie altyd absolute vrolikheid uitstraal en die mees stormagtige dag in lente kan verander. Heel laaste moet ek net my twee goeie vriende, Willem “Die Dagger” “Weskus” Brand en Ian “Ziod Squigles” van Vuuren, erken vir die waarskynlik onbewustelike rol wat hulle ook daarin gespeel het om my deur hierdie PhD studie en tesis te kon kry. Ek het so baie om voor dankbaar te wees.

Table of Contents

Declaration ii
Summary iii
Opsomming iv
Presentations and publications v
Acknowledgements vi
Table of Contents viii
List of Abreviations and Terms xii
Study background 1
1.1 Introduction 2
1.1.1 The need for novel anti-tuberculosis chemotherapy 2
1.1.2 Central nitrogen metabolism is a source of novel anti-TB drug targets 2
1.2 Central nitrogen metabolism in *M. tuberculosis* 3
1.2.1 Glutamine synthetase 4
1.2.2 Glutamine oxoglutarate aminotransferase 12
1.2.3 Glutamate dehydrogenase 12
1.2.4 Regulation of central nitrogen metabolism 13
1.2.4.1 Regulation in response to nitrogen status 13
1.2.4.2 Regulators of central nitrogen metabolism 14
1.2.4.3 Glutamine/glutamate homeostasis 15
1.3 *M. tuberculosis* nitrogen metabolism in the context of the infected host 16
1.3.1 Nitrogen source availability in the host 16
1.3.2 Nitrogen source utilization in the host 17
1.4 The important functions of glutamine and glutamate in *M. tuberculosis* 18
1.4.1 In nitrogen metabolism 18
1.4.2 In carbon metabolism 20
1.4.3 Other possible functions of glutamine/glutamate during infection 21
1.5 Gaps in current knowledge on central nitrogen metabolism in *M. tuberculosis* to be addressed by experimental study 21
1.6 Study design and specific aims 22
Regulation of nitrogen metabolism in *M. bovis* BCG 24
2.1 Introduction 25

2.2 Results and Discussion 25
2.2.1 Regulation of GS in response to nitrogen limitation and excess 25
2.2.2 Regulation of GOGAT in response to nitrogen limitation and excess 29
2.2.3 Regulation of GDH in response to nitrogen limitation and excess 31
2.2.4 Regulation of PknG and GarA in response to nitrogen limitation and excess 33
2.2.5 Regulation of GDH when glutamate is a sole nitrogen and carbon source. 33
2.2.6 Generation of an *M. bovis* BCG *garA* T21A amino acid substitution mutant by method of recombineering 35
2.2.7 Assay of *garA* threonine residue 21 essentiality by recombineering 38
2.2.8 Complementation of wt-BCG with copies of *garA* containing T21A and T21V codon substitutions. 40
2.2.9 Generation of *M. bovis* BCG *garA* T21A or T21V amino acid substitution mutants by method of allelic exchange through homologous recombination. 42
2.3 Conclusion 46
The role of glutamine oxoglutarate aminotransferase and glutamate dehydrogenase in nitrogen metabolism and *ex vivo* growth of *M. bovis* BCG 48
3.1 Introduction 49
3.2 Results and Discussion 49
3.2.1 Generation of an *M. bovis* BCG *ΔgltBD* mutant as well as a *ΔgltBD* genetically complemented strain 49
3.2.2 Generation of an *M. bovis* BCG *Δgdh* mutant as well as a *Δgdh* genetically complemented strain 54
3.2.3 Enzymatic activity of GOGAT and GDH in the *ΔgltBD* and *Δgdh* mutants, respectively 61
3.2.4 Growth of wt-BCG in 7H9 containing different nitrogen sources 63
3.2.5 *In vitro* growth phenotypes of the *ΔgltBD* mutant 66
3.2.6 *In vitro* growth phenotypes of the *Δgdh* mutant 73
3.2.7 Gene expression in the *Δgdh* mutant 82
3.2.8 Growth phenotypes of the *Δgdh* and *ΔgltBD* mutants in murine bone marrow-derived macrophages 84
3.2.9 Growth phenotypes of *Δgdh* and *ΔgltBD* in *in vitro* conditions which may resemble the macrophage phagosome. 85
3.3 Conclusion 87
Study conclusions and future considerations 89

4.1. Study conclusions 90
4.2. Future considerations 91
Materials and methods 92
5.1. Ethical statement 93
5.2. Bacterial strains, plasmids, and primers 93
5.3. Cultivation of bacteria 99
5.4. Genetic manipulation of bacteria 100
5.4.1. Preparation of electrocompetent *E. coli* cells and transformation 100
5.4.2. Preparation of electrocompetent *M. bovis* BCG cells and transformation 101
5.4.3. Generation of recombineering proficient *M. bovis* BCG strains 102
5.4.4. Point mutagenesis of *M. bovis* BCG *garA* codon T21 by method of recombineering 103
5.4.5. Complementation of wt-BCG with a copy of *garA* containing a T21A or T21V codon substitution. 103
5.4.6. Generation of *M. bovis* BCG pAVgarA-T21A-SCO and pAVgarA-T21V-SCO strains 104
5.4.7. Genetic complementation of *M. bovis* BCG pAVgarA-T21A-SCO and pAVgarA-T21V-SCO strains with a wild type copy of *garA* 105
5.4.8. Generation of a *ΔgltBD* strain of *M. bovis* BCG 106
5.4.9. Generation of a genetically complemented *M. bovis* BCG *ΔgltBD* strain 107
5.4.10. Generation of a *Δgdh* strain of *M. bovis* BCG 107
5.4.11. Generation of a genetically complemented *M. bovis* BCG *Δgdh* strain 108
5.5. Working with DNA 108
5.5.1. Isolation of plasmid DNA from *E. coli* 108
5.5.2. Isolation of genomic DNA from *M. bovis* BCG 109
5.5.2.1. Isolation of crude DNA for PCR 109
5.5.2.2. Isolation of high quality and purity DNA 109
5.5.3. Analysis of plasmid/genomic DNA concentration, purity, and integrity 110
5.5.4. PCR 110
5.5.4.1. Conventional polymerase chain reaction (PCR) 110
5.5.4.2. High fidelity PCR and PCR of long fragments 111
5.5.4.3. High resolution melt analysis 112
5.5.4.4. Mismatch amplification mutation assay (MAMA) PCR 113

5.5.4.5. Site directed mutagenesis by double-joint PCR 113
5.5.4.6. Extraction of DNA from PCR reactions 114
5.5.5. Southern blotting 114
5.5.6. Gel electrophoresis and extraction of DNA from agarose gels 115
5.5.7. Restriction, dephosphorylation, ligation and sequencing of DNA 115
5.5.7.1. Precipitation of DNA in order to increase concentrations 116
5.6. Working with RNA 116
5.6.1. Isolation of total RNA from *M. bovis* BCG 116
5.6.2. Analysis of purity and integrity of RNA 117
5.6.3. DNase treatment of total RNA and further purification 117
5.6.4. First strand cDNA synthesis 117
5.6.5. Quantitative real-time PCR (qPCR) 117
5.6.6. Analysis of qPCR data and determination of relative gene expression 118
5.7. Working with proteins 118
5.7.1. Analysis of protein concentration in whole cell lysates of *M. bovis* BCG 118
5.7.2. GS activity assay 119
5.7.3. GOGAT activity assay 120
5.7.4. GDH activity assay 120
5.8. *M. bovis* BCG intracellular survival 121
5.8.1. Culturing and infection of BMDM monolayers 121
5.8.2. Harvesting bacteria and enumeration of BCG infection 122
5.9. Bioinformatic approaches 122
5.10. Growth curve analysis 122
5.11. Statistical analysis 125
References 126

List of Abreviations and Terms

A (growth parameter)	maximal growth attained (maximum OD reached on growth curve)
axenic culture	bacterial culture completely free of other organisms
BCG	Bacillus Calmette-Guérin
BMDM	bone marrow-derived macrophages
Bp	basepairs
Cfu	colony forming units
D	downstream of a gene (nearest to the stop-codon of the gene)
DCO	double cross-over
ex vivo growth	bacterial growth in macrophage cell culture model of infection
GABA	γ-aminobutyric acid
GAD	glutamate decarboxylase
GarA	glycogen accumulation regulator A
GDH	glutamate dehydrogenase
GlnE	GS adenylyl transferase
GOGAT	glutamine oxoglutarate aminotransferase
GS	glutamine synthetase
HIV	human immunodeficiency virus
HLA	5-hydroxylevulinate
HOA	2-hydroxy-3-oxoadipate
HRM	high resolution melt
in vitro growth	bacterial growth in axenic culture
in vivo growth	bacterial growth in animal model of infection
Kb	kilobasepairs
KGD	ketoglutarate decarboxylase
L (growth parameter)	lag time
L180 GDH	class of GDH enzymes with 180 kDa subunits
MAMA-PCR	mismatch amplification mutation assay-PCR
MIC	minimum inhibitory concentration
-N7H9	Nitrogen-depleted 7H9 (see Table 15)
-NKB	Nitrogen-depleted Kirchner's Broth (see Table 15)
OD_{600}	optical density measurement at a wavelength of 600 nm
OdhI	oxoglutarate dehydrogenase inhibitor protein I
PknG	protein kinase G
R (growth parameter)	maximal growth rate
SCO	single cross-over
SSA	α-succinic semialdehyde
TB	tuberculosis
TCA	tricarboxylic acid
THP-1 cells	human macrophage-like cell line
TraSH	transposon site hybridisation
U	upstream of a gene (nearest to the start of the start-codon of the gene)

Chapter 1

Study background

1.1 Introduction

1.1.1 The need for novel anti-tuberculosis chemotherapy

Tuberculosis (TB), an infectious pulmonary disease caused by the gram positive bacillus, *Mycobacterium tuberculosis*, remains a profound burden on developing countries. Despite a global decline in TB figures, the African continent remains severely affected by the disease, with the highest TB incidence, prevalence and mortality per 100 000 population (1). Increasing emergence of drug resistant TB is of particular concern to the high TB incidence African countries where there is also a high prevalence of human immunodeficiency virus (HIV) positivity. At 65%, South Africa has the highest percentage of HIV prevalence in incident TB cases in the world. Of concern is that multiple and extensively drug resistant TB is on the rise in parts of this country and it has been observed that spread of extensively drug resistant strains of *M. tuberculosis* may be facilitated by co-infection with HIV (1–3). To make matters worse, it was shown in a recent study that clinical isolates of *M. tuberculosis* obtained from patients in the Eastern Cape province of South Africa may be progressing to a totally drug resistant phenotype (4). Shortcomings of current anti-TB treatments, including a long treatment period which can result in immense financial burden for patients (5, 6) and side effects, largely associated with second line anti-TB drugs (7, 8), may result in non-compliance and thus contribute to the emergence of increasingly drug resistant strains in poor communities. An expansion of the current arsenal of anti-TB drugs is vital to solving the huge problem of drug resistance in current TB treatment. Moreover, the development of TB chemotherapy is required which acts by novel mechanisms in order to improve treatment outcomes and to better control the spread of infection by drug resistant strains of *M. tuberculosis*.

1.1.2 Central nitrogen metabolism is a source of novel anti-TB drug targets

Elucidation of the full *M. tuberculosis* genomic sequence and the identification and annotation of approximately 4000 genes have allowed for the use of whole genome approaches to characterise transcriptional responses of *M. tuberculosis* as well as for the determination of the genes that are required for growth of the bacillus *in vitro*, *ex vivo* and *in vivo* (9–13). It was revealed that a large percentage of genes involved in the transport and metabolism of nitrogenous molecules such as amino acids and

nucleotides are required for *in vitro* growth of *M. tuberculosis* (10, 14). Although any one of the protein effectors encoded by these genes may present a viable target for chemotherapeutic intervention, it is reasonable to speculate that disruption of the pathways of central nitrogen metabolism, which regulate the levels of the precursor metabolites involved in the production of all nitrogenous molecules, may present a profound vulnerability in the physiology of *M. tuberculosis* (15–17). It is not surprising that a substantial number of observations in mycobacteria and related species, which will be discussed in the following sections of this chapter, point to a crucial importance of the enzymes of central nitrogen metabolism in the viability and growth of *M. tuberculosis*.

1.2 Central nitrogen metabolism in *M. tuberculosis*

The major pathways of central nitrogen metabolism involve the assimilation of ammonia/ammonium and the biosynthesis of glutamine and glutamate (see Figure 1). In most prokaryotes, including the saprophytic *M. smegmatis*, inorganic ammonia/ammonium is assimilated through the activity of glutamine synthetase (GS), glutamine oxoglutarate aminotransferase (GOGAT) and an anabolic glutamate dehydrogenase (NADPH-GDH) leading to the production of glutamine and glutamate (18). In slow growing mycobacteria, such as *M. tuberculosis* and *Mycobacterium bovis* BCG, the anabolic GDH is not present and net glutamine and glutamate biosynthesis from inorganic ammonium occurs solely through the activity of GS and GOGAT (19). However, a second catabolic GDH (NAD^+-GDH) is present in all mycobacteria which may be important in the deamination of glutamate (20). The *M. tuberculosis* genome contains a reduced set of genes in comparison to *M. smegmatis*, possibly as a result of the reductive evolutionary loss of genes involved in the biosynthesis of metabolites available in the host (21, 22). Consequently, far fewer of the genes involved in central nitrogen metabolism in *M. tuberculosis* are redundant in comparison to the genome of *M. smegmatis* (19). It is therefore not surprising that the genes encoding for GS (*glnA1*), GOGAT (*gltB* and *gltD*) and GDH (*gdh*) were found to be required for optimal growth of *M. tuberculosis* in several transposon site hybridisation (TraSH) studies utilising media containing ammonium and glutamate (7H10) or ammonium and asparagine as nitrogen sources (Table 1). Although GS has been studied to a great

extent in *M. tuberculosis*, the roles of GOGAT and GDH in the physiology and pathogenicity of the tubercle bacillus remain largely unknown.

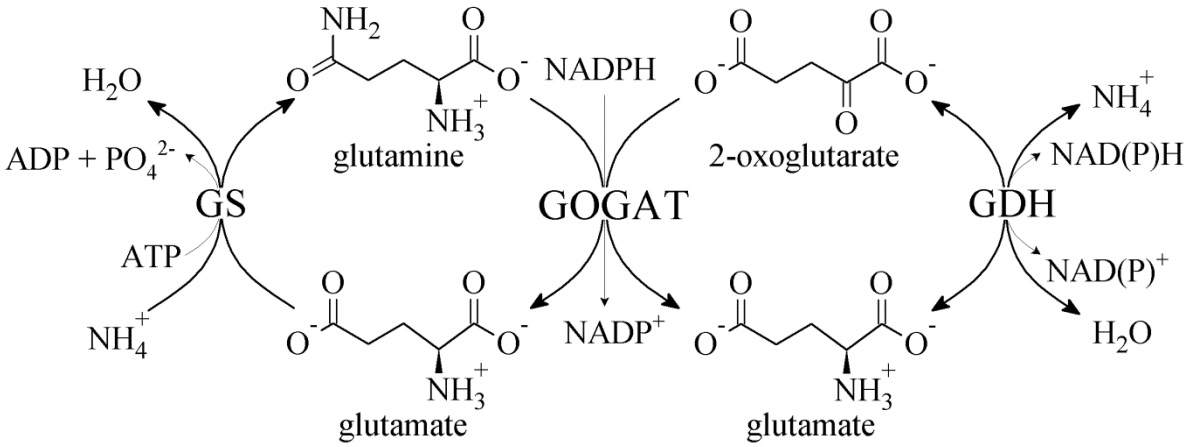

Figure 1: The major biochemical pathways responsible for ammonium assimilation and glutamine and glutamate production in mycobacteria.

1.2.1 Glutamine synthetase

Four major types of prokaryotic GS enzymes (GS type I – III and T) have been identified based on differences in their posttranslational modifications (23). In *M. tuberculosis* all four annotated GS encoding genes (*glnA1-4*) are predicted to encode GS type I enzymes (24). GS type I is composed of 12 identical subunits that are arranged as two hexagonal rings on overlaying planes (25) and is subject to various regulatory mechanisms, including positive and negative substrate feedback (26), oxidative modification (27) and adenylylation (28). The major isoform of GS in *M. tuberculosis* is encoded by *glnA1* and was found to be abundantly expressed and released into the extracellular environment by pathogenic mycobacteria, but not by non-pathogens like *M. smegmatis* and *M. phlei* or other non-mycobacterial genera investigated (24, 29–31). The extracellular release of GS in pathogenic mycobacteria was implicated in the biosynthesis of the poly-L-glutamate-glutamine structure present in the cell walls of pathogenic slow growing mycobacteria (32, 33). Moreover, treatment of *M. tuberculosis* with the potent irreversible GS inhibitor, L-methionine-*S*-sulfoximine (MSO), inhibited growth *in vitro*, in human-like-macrophage cells (THP-1 cells) and in the guinea pig model of tuberculosis (32, 34). In addition, treatment of *M. tuberculosis* with antisense oligonucleotides to *glnA1* led to a marked reduction of

growth *in vitro* and a deletion mutant strain of the gene was glutamine-auxotrophic, attenuated for growth in THP-1 cells and avirulent in guinea pigs and mice (33, 35, 36).

While *glnA2-4* was found to be non-essential to *M. tuberculosis* homeostasis (30), both *glnA1* and *glnA2* have been implicated in the pathogenicity of *M. bovis* (37, 38). As a result of overwhelming data supporting the importance of GS in *M. tuberculosis* pathogenicity and virulence, this enzyme has been proposed as a target for development of novel anti-TB chemotherapy (39). Although MSO is a convulsive agent and *M. tuberculosis* gains resistance to it at a remarkably high rate (40–42), new inhibitors for GS which act by alternative mechanisms are being investigated which may circumvent these issues (43–46).

Table 1. Genes involved in uptake of nitrogen in *M. tuberculosis*: regulation and requirement for growth.

		Regulation[1]							Essentiality							
		Nutrient starvation dormancy	Nutrient starvation dormancy	Wayne model dormancy	Wayne model dormancy	*Ex vivo*	*In vivo*: mice - 7d in hollow fiber, subQ	*In vivo*: mice - 3 & 4 wk	*In vitro*[2]: 7H10	*In vitro*[3]: 7H10	*In vitro*[4]: L-Asn and NH_4^+	*In vitro*[4]: cholesterol	*In vitro*[5]: 7H10	*In vitro*[6]: L-Asn and NH_4^+	*Ex vivo*[7]	*In vivo*[8]
Transport of nitrogen sources:																
Rv0072	probable Gln transporter (ABC)		D		D	D			NR	nd	NR	NR	NR	NR	NR	NR
Rv0073	probable Gln transporter (ABC)		U		D	D			NR	nd	NR	NR	NR	NR	NR	NR
Rv0261c (*narK3*)	membrane nitrite extrusion protein		D		U	U		D	NR	nd	NR	NR	NR	NR	NR	NR
Rv0267 (*narU*)	membrane nitrite extrusion protein		D		U	U			NR	nd	NR	NR	NR	NR	nd	NR
Rv0346c (*ansP2*)	L-Asn permease	D			D	D			NR	nd	NR	NR	NR	NR	nd	NR
Rv0411c (*glnH*)	Gln transporter	D	U		U	U			R	nd	R	na	R	R	nd	na
Rv0522 (*gabP*)	gabA permease/L-Arg import		D		U	U			nd	nd	NR	NR	NR	NR	nd	nd
Rv1496	arginine/ornithine transport system		D			U			NR	nd	NR	NR	NR	NR	NR	NR
Rv1737c^{dosR} (*narK2*)	nitrate/nitrite transporter	D		U	U	U			NR	nd	NR	NR	NR	NR	NR	NR
Rv1999c	probable amino acid permease		D		U	U	U		NR	nd	NR	NR	NR	NR	NR	NR

		Nutrient starvation dormancy	Nutrient starvation dormancy	Wayne model dormancy	Wayne model dormancy	*Ex vivo*	*In vivo*: mice - 7d in hollow fiber, subQ	*In vivo*: mice - 3 & 4 wk	*In vitro*[2]: 7H10	*In vitro*[3]: 7H10	*In vitro*[4]: L-Asn and NH_4^+	*In vitro*[4]: cholesterol	*In vitro*[5]: 7H10	*In vitro*[6]: L-Asn and NH_4^+	*Ex vivo*[7]	*In vivo*[8]
Rv2127 (*ansP1*)	L-asparagine permease		D		D	D		D	NR	nd	NR	NR	NR	NR	nd	NR
Rv2320c (*rocE*)	cationic amino acid transporter		D		U	U			NR	nd	NR	NR	NR	NR	nd	NR
Rv2329c (*narK1*)	nitrate/nitrite transporter	U		U	D	U			nd	nd	NR	NR	NR	NR	NR	nd
Rv2563	Gln transporter (ABC)		D		D	D	U		NR	nd	NR	NR	NR	NR	nd	NR
Rv2564 (*glnQ*)	Gln transporter (ABC)		D		D	U			GD	nd	NR	NR	NR	NR	nd	GD
Rv2690c	probable amino acid permease					D			nd	nd	R	NR	A	R	NR	nd
Rv2920c (*amt*)	ammonium-transporter		D		U	U			NR	nd	NR	NR	NR	NR	NR	NR
Rv3253c	cationic amino acid transporter		U		U	U		D	NR	nd	NR	NR	NR	NR	NR	NR
Rv3756c (*proZ*)	osmoprotectant/glycine betaine uptake	D	D			U		D	NR	nd	NR	NR	NR	NR	NR	NR
Rv3757c (*proW*)	osmoprotectant/glycine betaine uptake		U			U			NR	nd	NR	NR	NR	NR	NR	NR
Rv3758c (*proV*)	osmoprotectant/glycine betaine uptake		U		D	D			NR	nd	NR	NR	NR	NR	NR	R

		Nutrient starvation dormancy	Nutrient starvation dormancy	Wayne model dormancy	Wayne model dormancy	*Ex vivo*	*In vivo*: mice - 7d in hollow fiber, subQ	*In vivo*: mice - 3 & 4 wk	*In vitro*[2]: 7H10	*In vitro*[3]: 7H10	*In vitro*[4]: L-Asn and NH_4^+	*In vitro*[4]: cholesterol	*In vitro*[5]: 7H10	*In vitro*[6]: L-Asn and NH_4^+	*Ex vivo*[7]	*In vivo*[8]
Rv3759c (*proX*)	osmoprotectant/glycine betaine uptake					D			nd	nd	NR	NR	NR	NR	NR	nd
Amino acid degradation:																
Rv0337c (*aspC*)	aspartate aminotransferase				D	U		D	R	nd	R	na	R	R	nd	na
Rv1538c (*ansA*)	L-asparaginase				U	U	U		NR	nd	R	na	NR	R	Rc◇	NR
Rv1832 (*gcvB*)	glycine dehydrogenase		U	U	U	U		U	R	nd	R	na	R	R	nd	na
Rv2589 (*gabT*)	4-aminobutyrate aminotransferase		D						NR	nd	NR	NR	NR	NR	NR	NR
Rv2780 (*ald*)	alanine dehydrogenase	U	U		U	U	U		NR	nd	NR	NR	NR	NR	NR	NR
Rv3432c (*gadB*)	glutamate decarboxylase					U			NR	nd	NR	NR	NR	NR	NR	NR
Rv3565 (*aspB*)	aspartate aminotransferase		D		U	U			nd	nd	R	NR	A	U	NR	nd
Rv3722c	aspartate aminotransferase	D			D	D		D	R	nd	R	na	A	R	nd	na
Nitrate metabolism:																
Rv0252 (*nirB*)	nitrite reductase large subunit		D		U	U		D	NR	nd	NR	NR	NR	NR	NR	NR

		Nutrient starvation dormancy	Nutrient starvation dormancy	Wayne model dormancy	Wayne model dormancy	*Ex vivo*	*In vivo*: mice - 7d in hollow fiber, subQ	*In vivo*: mice - 3 & 4 wk	*In vitro*[2]: 7H10	*In vitro*[3]: 7H10	*In vitro*[4]: L-Asn and NH_4^+	*In vitro*[4]: cholesterol	*In vitro*[5]: 7H10	*In vitro*[6]: L-Asn and NH_4^+	*Ex vivo*[7]	*In vivo*[8]
Rv0253 (*nirD*)	nitrite reductase small subunit		D		U	U			NR	nd	NR	NR	NR	NR	nd	NR
Rv1161 (*narG*)	respiratory nitrate reductase α chain		U		U				NR	R	NR	NR	NR	NR	NR	NR
Rv1162[*relA*] (*narH*)	respiratory nitrate reductase β chain		U	U	D	D			NR	nd	NR	NR	NR	NR	NR	NR
Rv1163[*relA*] (*narJ*)	respiratory nitrate reductase δ chain		D			D			NR	nd	NR	NR	NR	NR	NR	NR
Rv1164 (*narI*)	respiratory nitrate reductase γ chain		D		D	D			NR	nd	NR	NR	NR	NR	NR	NR
Rv1736c (*narX*)	probable nitrate reductase	D	U		U				nd	nd	NR	NR	NR	NR	NR	NR
Urea metabolism:																
Rv1848 (*ureA*)	urease gamma subunit		D		D	U			NR	nd	NR	NR	NR	S	NR	NR
Rv1849 (*ureB*)	urease beta subunit					U		U	NR	nd	NR	NR	NR	U	Ra▽	NR
Rv1850 (*ureC*)	urease alpha subunit		D			U			R	nd	NR	NR	NR	NR	NR	na
Rv1851 (*ureF*)	urease accessory protein		D		U	U			nd	nd	NR	NR	NR	S	nd	nd

		Nutrient starvation dormancy	Nutrient starvation dormancy	Wayne model dormancy	Wayne model dormancy	*Ex vivo*	*In vivo*: mice - 7d in hollow fiber, subQ	*In vivo*: mice - 3 & 4 wk	*In vitro*[2]: 7H10	*In vitro*[3]: 7H10	*In vitro*[4]: L-Asn and NH_4^+	*In vitro*[4]: cholesterol	*In vitro*[5]: 7H10	*In vitro*[6]: L-Asn and NH_4^+	*Ex vivo*[7]	*In vivo*[8]
Rv1852 (*ureG*)	urease accessory protein				U			D	NR	nd	NR	NR	NR	NR	NR	NR
Rv1853 (*ureD*)	urease accessory protein		U	U	U	U		D	NR	nd	NR	NR	NR	NR	NR	NR
Central nitrogen metabolism:																
Rv0410c (*pknG*)	serine/threonine-protein kinase				D	U			R	nd	R	n/a	R	R	NR	na
Rv0818 (*glnR*)	transcriptional regulatory protein		U		D	D		U	NR	nd	NR	NR	NR	NR	NR	NR
Rv1827 (*garA/cfp17*)	regulatory protein (PknG substrate)		U		D	D		U	nd	nd	R	n/a	NR	R	nd	nd
Rv1878 (*glnA3*)	glutamine synthetase		D		U	U			NR	nd	NR	NR	NR	NR	NR	NR
Rv2201 (*asnB*)	asparagine synthetase				D	D			nd	nd	R	n/a	R	R	nd	nd
Rv2220 (*glnA1*)	glutamine synthetase		D		D	D			R	nd	R	n/a	R	R	nd	na
Rv2221c (*glnE*)	GS adenylyl-transferase				U	D		U	R	nd	R	n/a	R	R	nd	na
Rv2222c (*glnA2*)	glutamine synthetase		U		D	D			nd	nd	NR	NR	NR	U	Rc[△]	nd
Rv2476c (*gdh*)	glutamate dehydrogenase				D	D		D	nd	R	R	R*	A	R	NR	nd

		Nutrient starvation dormancy	Nutrient starvation dormancy	Wayne model dormancy	Wayne model dormancy	*Ex vivo*	*In vivo*: mice - 7d in hollow fiber, subQ	*In vivo*: mice - 3 & 4 wk	*In vitro*[2]: 7H10	*In vitro*[3]: 7H10	*In vitro*[4]: L-Asn and NH_4^+	*In vitro*[4]: cholesterol	*In vitro*[5]: 7H10	*In vitro*[6]: L-Asn and NH_4^+	*Ex vivo*[7]	*In vivo*[8]
Rv2860c (*glnA4*)	glutamine synthetase				D			U	NR	nd	NR	NR	A	NR	NR	NR
Rv2918c (*glnD*)	protein-pii uridylyltransferase		U		U	U			nd	nd	NR	NR	NR	NR	Rb○	nd
Rv2919c (*glnB*)	nitrogen regulatory protein P-II		U		U	U		D	nd	nd	NR	NR	NR	NR	Rb	nd
Rv3858c (*gltD*)	GOGAT β subunit				D	D			R	nd	R	n/a	NR	R	nd	na
Rv3859c (*gltB*)	GOGAT α subunit		U		D				R	R	R	n/a	A	R	nd	na

✶ - *gdh* failed to be identified as required for growth in minimal medium with cholesterol as carbon source (p = 0.07, significance was set at p = 0.05). ◇ - just fell short of cut-off ratio of <0.4; 0.446 (0.202 to 0.791), ▽ - just fell short of cut-off ratio of <0.4; 0.496 (0.339 to 0.773), △ - just fell short of cut-off ratio of <0.4; 0.560 (0.380 to 0.775), ○ - just fell short of cut-off ratio of <0.4; 0.347 (0.135 to 0.845)

1.) Data adapted from Table S1 from Murphy *et al*., 2007 .....(11)
2.) Sassetti *et al*., 2003 .....(14)
3.) Lamichhane *et al*., 2003.....(47)
4.) Griffin *et al*., 2011.....(10)
5.) Zhang *et al*., 2012 .....(13)
6.) DeJesus *et al*., 2013 .....(9)
7.) Rengarajan *et al*., 2005.....(48)
8.) Sassetti & Rubin 2003 .....(49)

U - up-regulated, D - down-regulated, R - required for optimal growth, NR - not reguired for optimal growth, GD – growth defect (produce slow growth when mutated) nd – no data, na – not applicable, U – uncertain, A - contains both regions that are and that are not required for optimal growth, S - gene is too short to investigate, Ra - required for optimal growth in unactivated macrophages, Rb - required for optimal growth in macrophages that were activated with INF-γ pre-infection, Rc - required for optimal growth in macrophages that were activated with INF-γ post-infection

1.2.2 Glutamine oxoglutarate aminotransferase

Three distinct types of GOGAT enzymes have been classified according to co-enzyme dependency, namely ferredoxin-GOGAT (Fd-GOGAT) which is found mostly in photosynthesizing organisms (cyanobacteria, algae, and chloroplasts of higher plants), NADPH-GOGAT which is mainly found in bacteria and NADH-GOGAT which is found in the non-green tissues of plants (like seeds and roots), fungi and lower animals (50, 51). Fd-GOGAT and NADH-GOGAT are both monomeric enzymes of 150 kDa and 200 kDa polypeptide chains, respectively, while NADPH-GOGAT consists of a larger α polypeptide chain (≈ 150 kDa) and a smaller β polypeptide chain (≈ 50 kDa) arranged in an $(\alpha/\beta)_8$ hetero-octamer quaternary structure (50, 51). In addition to two putative operons, each containing a gene encoding for the α subunit and a gene encoding for the β subunit, multiple additional putative genes encoding for the α subunit are found in the *M. smegmatis* genome (19). In the slow growing *M. tuberculosis* and *M. bovis* BCG, however, only one putative operon contains the genes encoding for both the α (*gltB*) and β subunits (*gltD*). Notably, it was observed that azaserine, a known GOGAT inhibitor, inhibited *M. tuberculosis* growth with a minimum inhibitory concentration (MIC) < 1.0 µg/ml (47, 52). No GOGAT enzyme has been detected in higher eukaryotes, including humans, and GOGAT has thus been identified as a possible novel anti-TB drug target (53).

1.2.3 Glutamate dehydrogenase

GDH enzymes have very diverse evolutionary, structural and functional properties and four distinct types of GDHs have been identified ($S50_I$, $S50_{II}$, L115 and L180). The $S50_I$ and $S50_{II}$ GDHs are mainly homohexameric enzymes with ≈ 50 kDa polypeptide chains, are specific for NADPH, NADH or have a dual co-factor specificity, function mainly in the assimilation of ammonia and are found in eukaryotes and eubacteria ($S50_I$) or distributed among all domains of life ($S50_{II}$) (54). In contrast, the L115 GDHs are homotetramers with ≈ 115 kDa polypeptide chains, specific for NAD^+, function in the catabolism (deamination) of glutamate and have mostly been found in lower eukaryotes (55). Similar to the L115 class, the L180 GDHs are NAD^+ specific and function in the catabolism of glutamate, however these GDHs have ≈ 180 kDa polypeptide chains arranged as homohexamers (56–58) or homotetramers (59) and

are only found in bacterial genomes. *M. smegmatis* has genes encoding for $S50_I$, L180 and possibly L135 GDH (60), while only a gene for L180 GDH is present in the *M. tuberculosis* and *M. bovis* BCG genomes (http://blast.ncbi.nlm.nih.gov/Blast.cgi). The unique properties of L180 GDH compared to other characterised GDHs, including a very large subunit size, exclusive NAD^+ co-enzyme specificity, apparent function in the deamination of glutamate, exclusive distribution among bacteria and allosteric activation by asparagine and aspartate may have positive implications for the potential of L180 GDH as a specific anti-TB drug target (56–59). Moreover, a protein blast of *M. tuberculosis gdh* against the genomes for common intestinal bacterial genera, including *Bacteroides*, *Enterococcus*, *Escherichia*, *Klebsiella*, *Staphylococcus*, *Lactobacillus* and *Clostridium* delivered no homologues, which may further qualify L180 GDH as a specific anti-TB drug target (query coverage < 40 for only two Lactobacilli and one Bacteroides, http://blast.ncbi.nlm.nih.gov/Blast.cgi).

1.2.4 Regulation of central nitrogen metabolism

1.2.4.1 Regulation in response to nitrogen status

The regulation of the major effector enzymes of central nitrogen metabolism (GS, GOGAT and GDH) is well studied in *Escherichia coli*, *Bacillus subtillis*, *Streptomyces coelicolor* and *Corynebacterium glutamicum* because of their industrial importance in the production of amino acids as well as in the saprophytic *M. smegmatis* (60–63). In *E. coli* high-ammonium affinity GS activity is increased and low ammonium affinity anabolic NADPH-GDH activity is decreased when nitrogen availability is limiting (64, 65). Under nitrogen-rich growth when NADPH-GDH can efficiently assimilate ammonia and the molecule of ATP consumed in the production of glutamine by GS is an unnecessary expenditure, anabolic NADPH-GDH activity is increased and GS activity decreased. Similar regulation of GS in response to nitrogen-rich and nitrogen-limited conditions has been observed for other prokaryotes, including *C. glutamicum* (66), *S. coelicolor* (67), *B. subtillis* (68) and *M. smegmatis* (60). While fewer studies exist on the regulation of GOGAT, there is evidence that the enzyme is strongly up-regulated, like GS, in response to nitrogen limitation (66, 69, 70). A similar trend in the regulation of anabolic NADPH-GDH to that observed in *E. coli* was found in *S. coelicolor* (71), but not in *C. callunae* (72), *C. glutamicum* (69) or *M. smegmatis* (60) cultured under high or low nitrogen conditions.

A unique feature of the mycobacteria is the exceptionally high level at which they express GS. In one study it was observed that mycobacterial species exhibited approximately 20-fold more total GS activity on average than members of the Gram-negative and Gram-positive bacteria (24). In addition, slow growing mycobacteria, including *M. tuberculosis*, had approximately 10-fold more total GS activity on average than did fast growing mycobacteria. Unlike *E. coli* and *M. smegmatis* in which GS is only highly expressed when nitrogen is limiting ([NH_3] < 0.1 mM), in *M. tuberculosis* and other slow growing mycobacteria GS enzymatic activity is high even in the standard mycobacterial growth medium 7H9 which contains at least 7.6 mM NH_4^+. However, *M. tuberculosis* GS activity was observed to be decreased as much as 10-fold in response to a 10-fold increase in the nitrogen source $(NH_4)_2SO_4$, from 3.8 mM (normally present in 7H9) to 38 mM (24). Questions remain on the stimuli which induce changes in GS activity during infection of the host. Moreover, very little is known about the regulation of GOGAT and catabolic NAD^+-GDH in *M. tuberculosis* and the conditions which result in a change in activity of these enzymes are completely unknown in the slow growing pathogenic mycobacteria.

1.2.4.2 Regulators of central nitrogen metabolism

As is the case with the effectors of central nitrogen metabolism, its regulatory mechanism in *M. tuberculosis* contains a reduced set of components in comparison to *M. smegmatis*. However, similarities between the *M. smegmatis* and *M. tuberculosis* genomes include elements of a signal transduction cascade involved in GS regulation in other actinomycetes, namely *glnB, glnD* and the GS-adenylyl transferase, *glnE* (19). In addition, the *M. tuberculosis* genome appears to contain *glnR*, the global transcriptional regulator of nitrogen metabolism present in many Actinomycetes including *M. smegmatis.* The GlnR nitrogen-response regulon was recently determined in a genome wide analysis for *M. smegmatis* and it was found that GlnR controls the expression of more than 100 genes in response to nitrogen limitation (73). The role of *glnR* is unclear in *M. tuberculosis* as it has been found to be non-essential for optimal growth of *M. tuberculosis* in all of the TraSH studies to date (see Table 1). It was observed that *glnA1* is defined by two transcriptional initiation sites in *M. tuberculosis*, one producing a short transcript which is more abundant under standard

growth conditions and the other a long transcript which is more abundant under nitrogen-rich growth conditions (29). However, the transcriptional regulator responsible for expression from either proximal or distal GS transcription initiation sites remains unknown. GS activity is further regulated at a post-translational level in *M. tuberculosis* through adenylylation by GlnE (74).

1.2.4.3 Glutamine/glutamate homeostasis

Interestingly, despite no requirement for *glnB* or *glnD* for *in vitro* growth of *M. tuberculosis*, *glnE*, which may be under control of the products of the aforementioned genes, was shown in an early genetic study of *M. tuberculosis* to be an essential gene and was also identified as required for *in vitro* growth in all of the TraSH studies (see Table 1, (75)). More recently it was shown that the *glnA1-glnE-glnA2* operon in *M. tuberculosis* could be replaced with an antibiotic marker to generate a glutamine auxotroph and that a *glnE* deletion mutant could only be generated when the growth medium was supplemented with both glutamine and MSO, indicating that GS is regulated by GlnE to maintain homeostatic levels of glutamine in the cytosol (35, 76).

A mechanism for homeostatic control of glutamine and glutamate metabolism in *M. tuberculosis* has been elucidated through the activity of the serine threonine protein kinase G (PknG). It was observed that PknG phosphorylates glycogen accumulation regulator A (GarA), a small protein containing a forkhead associated domain near the C-terminal and bearing homology to the *C. glutamicum* protein oxoglutarate dehydrogenase inhibitor protein I (OdhI), thereby modulating its interaction with the glutamate producing enzyme, GOGAT and the glutamate catabolizing enzyme GDH (20, 77–79). Phosphorylation of GarA at the threonine residue 21 by PknG was shown to both abrogate inhibition of GDH activity and stimulation of GOGAT activity, and it was speculated that this type of control would result in a decrease in intracellular glutamate levels (78). PknG has been shown to be important to *ex vivo* and *in vivo* growth of *M. tuberculosis* and is being investigated as a promising drug target (80–83). Although it is thought that PknG phosphorylates host proteins and thereby plays its part in the arrest of phagosomal maturation (84), no such host-protein substrates of PknG have been identified and it is possible to speculate that part of PknGs role in pathogenicity has to do with maintenance of glutamine/glutamate homeostasis.

Studies in enteric bacteria have found that the glutamine to glutamate ratio is of central importance to cellular homeostasis and this may well be the case for *M. tuberculosis* (85–87).

1.3 *M. tuberculosis* nitrogen metabolism in the context of the infected host

1.3.1 Nitrogen source availability in the host

Pathogenic mycobacteria may reside in various environments in the host organism, ranging from the phagosomal or even cytosolic compartments of a macrophage cell to the hypoxic necrotic cavity of a caseous granuloma. The nutritional context is likely to be different in each of the microenvironments encountered by *M. tuberculosis* (88, 89). There remains little certainty about the exact nutritional context within the macrophage and especially within the macrophage phagosome. The concentrations of the 20 common amino acids were measured in THP-1 cells (a human macrophage cell line) cultured under standard conditions and it was found that while all amino acids were present at concentrations higher than 0.1 mM, the most abundant amino acids were glutamate (18.56 mM), glutamine (4.45 mM), aspartate (7.16 mM), glycine (3.82 mM), and asparagine (1.28 mM) (36). However, the authors observed that growth of a glutamine-auxotrophic *glnA1 M. tuberculosis* mutant in the THP-1 cells was markedly impaired, while its growth was chemically complemented by at least 2 mM glutamine in axenic culture, suggesting that the phagosome membrane has a very low permeability for small molecules such as amino acids. A source of nitrogen in the phagosome may become available through the activity of host defence mechanisms which produce reactive nitrogen species like NO which in turn leads to availability of nitrite, nitrate and ammonium (90, 91). Moreover, the genome wide expression profile of *M. tuberculosis* in conditions resembling the environments encountered by the pathogen in the human host and the genes that are required for optimal growth of the organism *in vitro*, *ex vivo* and *in vivo* suggests that the chief nitrogen sources that are utilized by the intracellular mycobacterium include ammonium (possibly obtained from nitrate by the activity of nitrite reductase and nitrate reductase or through deamination of amino acids), glutamine, glutamate, asparagine, aspartate and glycine (Table 1).

1.3.2 Nitrogen source utilization in the host

At least 22 genes encoding for proteins involved in the transport of a nitrogen source could be identified in the *M. tuberculosis* genome (see Table 1). These include transporters for ammonium, glutamine, asparagine, arginine, glycine and nitrate/nitrite. Interestingly, no homologue of the glutamate permeases found in *C. glutamicum* (*GluABCD*, *gltP* and *gltS*) or *M. smegmatis* (*gluD*) are found in *M. tuberculosis* or *M. bovis* BCG despite observations that these strains will grow in medium containing glutamate as a sole nitrogen source (74, 92). However, the requirement of the genes that encode both subunits of GOGAT for growth of *M. tuberculosis* in 7H10 medium which contains 3.4 mM L-Glu, suggests that the glutamate uptake (whether by passive diffusion or a yet unknown system) is inadequate to meet the cellular demand for the amino acid in the absence of the GOGAT biosynthetic pathway. *M. tuberculosis* and *M. bovis* BCG also do not have homologues to any of the genes assigned to encode urea transporters in *M. smegmatis* (19), however the urease of both *M. tuberculosis* and *M. bovis* BCG have been implicated in the alkalization of the phagosome suggesting both the presence of urea as a nitrogen source and urea uptake during infection (93–95).

Surprisingly, only four genes encoding for putative nitrogen uptake systems in *M. tuberculosis*, were found to be essential for optimal growth *in vitro* or *in vivo* (Table 1). These included *glnQ* and *glnH* (both encode proteins involved in glutamine transport), a gene encoding for a putative amino acid permease and *proV* (a putative gene encoding for an osmoprotectant/glycine importer) which was non-essential to *in vitro* growth, but found to be essential *in vivo* (Table 1). Essentiality of the transporters of glutamine illustrates the importance of glutamine production by extracellular GS to homeostasis (see section 1.2.1). Glutamine and glutamate can act as precursors or nitrogen donors in the biosynthesis of all other nitrogenous molecules in the bacterial cell (15–17, 96, 97). Observations that auxotrophic mutants deficient in pathways involved in the biosynthesis of branched-chain amino acids, leucine, arginine, methionine, proline and tryptophan perform poorly *in vivo* further illustrates the importance of glutamine and glutamate and regulation of their levels by central nitrogen metabolism to the pathogenicity of *M. tuberculosis* (98–103).

Unpublished results presented at the EMBO Tuberculosis 2012: Biology, Pathogenesis, Intervention strategies conference held in Paris implicated the asparagine permease encoded by *Rv0346c* (*ansP2*) and aspartate permease encoded by *Rv2127* (*ansP1*) in host colonisation and early infection, respectively, in a mouse model of *M. tuberculosis* infection (104). The authors also reported the important function of asparagine catabolism in pH buffering through ammonia release. Notably, the genes involved in the catabolism of asparagine (*ansA*) and the conversion of aspartate into glutamate (*aspB*, *aspC* and *Rv3722c*) were found to be essential in all the *in vitro* TraSH studies performed to date (Table 1). In addition, the L-asparaginase encoded by *ansA* was one of the few genes of nitrogen metabolism that was also identified as potentially essential in an *ex vivo* TraSH study (Table 1).

The nitrogen sources that are utilized by the infecting mycobacterium may not only be determined by the available nitrogen sources, but may to a considerable extent be a consequence of the metabolic response initiated by the bacilli to subvert host defence mechanisms. For example, alanine and glycine degradation is implicated in entry into the dormancy phase (105–109), the metabolism of ammonium, urea, glutamate, aspartate and asparagine may be important for resistance of the mycobacteria to the acidification of the maturing phagosome (85, 94, 110) and nitrite production from nitrate (which is a natural product of NO) is likely to be important in low oxygen environments, such as the granuloma, where this compound may act as an alternative electron acceptor to oxygen (91, 111). The central importance of glutamine and glutamate to *M. tuberculosis* homeostasis is illustrated in Figure 2.

1.4 The important functions of glutamine and glutamate in *M. tuberculosis*

1.4.1 In nitrogen metabolism

The important roles of glutamine and glutamate as precursors or intermediate molecules in the synthesis of other nitrogenous molecules were discussed in previous sections (see section 1.2 and 1.3). However, an interesting observation was the remarkably high level to which glutamate is accumulated in *M. tuberculosis* and it could be speculated that the high intracellular pool of glutamate may act as a reservoir of nitrogen in environments where nutrients are limiting (112).

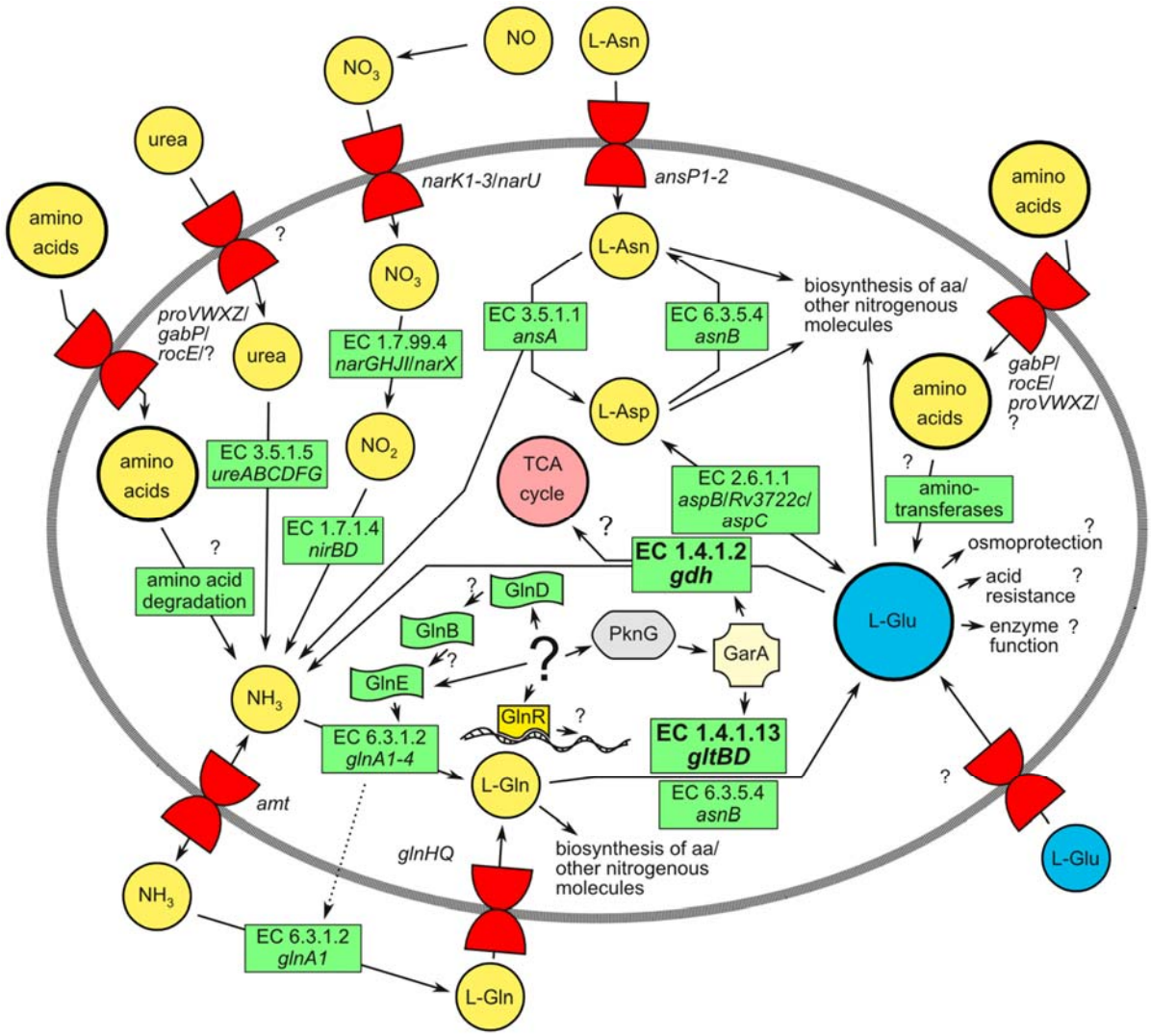

Figure 2: *M. tuberculosis* depends upon central nitrogen metabolism and the production of L-glutamine, and L-glutamate for efficient utilization of the nitrogen sources acquired by the pathogen from the host cell. Metabolism of glutamine and glutamate is regulated possibly to maintain a homeostatic ratio of the cytosolic glutamine to glutamate pools and/or a high glutamate concentration, although the specific stimulus for a regulatory response is unknown. Question marks indicate where experimental inquiry is necessary to better understand nitrogen utilization and metabolism in *M. tuberculosis*. The roles that the highly versatile glutamate may play during infection are of special interest and should become the topic of more investigations.

1.4.2 In carbon metabolism

Both glutamine and glutamate are gluconeogenic amino acids and may be utilised as sources of carbon and energy, although this may vary between different organisms (113). It was observed in early studies of *M. tuberculosis* respiratory metabolism that glutamate is one of only three amino acids (the others being glycine and sarcosine) that may be utilized as an energy and carbon source by *M. tuberculosis* (114, 115). In addition to a role in the regulation of GOGAT and GDH (see section 1.2.4.3), GarA was also found to interact with α-ketoglutarate decarboxylase (KGD) which plays an important role in central carbon metabolism in *M. tuberculosis* (20). Although KGD was originally proposed to be responsible for the production of succinic semialdehyde (SSA), a precursor to the tricarboxylic acid (TCA) cycle intermediate succinate (112), it was more recently shown that this enzyme has a more complex function. KGD couples the decarboxylation of α-ketoglutarate with the condensation of glyoxalate leading to the eventual production of 2-hydroxy-3-oxoadipate (HOA) which then spontaneously decarboxylates to 5-hydroxylevulinate (HLA) (116). The authors speculated that HOA and HLA may be precursors to an essential mycobacterial compound. In addition, the same authors proposed in a more recent communication that instead of KGD, the γ-aminobutyric acid (GABA) shunt pathway is the most likely route of SSA production in this organism (117). Glutamate is a substrate of the first step in the GABA shunt pathway, which is catalysed by glutamate decarboxylase (GAD, *gadB*) and could be speculated to present an important link in a unique alternative TCA cycle in *M. tuberculosis* lacking both conventional KDH and KGD pathways. Interestingly, in a recent TraSH study *gdh* failed to be identified as required for growth in minimal medium with cholesterol as carbon source by just missing statistical significance ($p = 0.07$, significance set at $p = 0.05$ in the experiment) (10). This may suggest that the adaptation of metabolism to utilize cholesterol as a carbon source has an effect on the metabolism of glutamate and thus also on the homeostasis of central nitrogen metabolism. Notably, cholesterol is a preferred carbon source by *M. tuberculosis* during the chronic phase of infection (118).

1.4.3 Other possible functions of glutamine/glutamate during infection

Glutamine and glutamate are osmoprotectants and compatible solutes in bacteria (86, 87, 119, 120). Compatible solutes are organic solutes found in the cell, which when present at a high concentration, facilitate the efficient functioning of enzymes (121). The high intracellular pool of glutamate may thus also be related to the compatible solute qualities of the amino acid. In *E. coli*, decarboxylation of glutamate to γ-aminobutyrate (GABA) by GAD consumes a proton, which is then removed from the cytosol through a glutamate/GABA antiporter and thus plays an important role in acid resistance (85). Although *M. tuberculosis* does not possess the genes for the glutamate/GABA antiporters normally involved in the function of the intracellular GAD system, the presence of a GAD-encoding gene, *gadB*, suggests a possible function of glutamate metabolism in acid resistance (see Table 1), which may be particularly beneficial to *M. tuberculosis* in the phagosome, where the pH has been estimated to range between 4.5 and 5.5 (122, 123).

1.5 Gaps in current knowledge on central nitrogen metabolism in *M. tuberculosis* to be addressed by experimental study

Many questions on nitrogen metabolism in the unique physiology of the tubercle bacilli remain unanswered (illustrated by question marks in Figure 2). While some features regarding the regulators of the enzymes in central nitrogen metabolism have been elucidated, including the importance of GlnE and PknG to pathogenicity and the interactions between these proteins and their respective substrates (see section 1.2.4), the stimuli which result in changes in the expression and activities of GDH and GOGAT specifically have not been elucidated. It is not known if these enzymes are regulated by the same fluctuations in nitrogen supply which regulate GS. Of significant importance may be the high intracellular levels of glutamate, which may be involved in homeostasis of central nitrogen metabolism, homeostasis of central carbon metabolism, efficient enzyme functioning, osmoprotection, acid resistance and which could act as reservoir of nitrogen when nutrients become limiting (see section 1.4.3). Although a disturbance in glutamine and glutamate levels was observed in a PknG deficient mutant of *M. tuberculosis*, which was avirulent in mice (81), it has not been established whether the role of PknG in pathogenicity of *M. tuberculosis* has to do with

its interaction with host proteins or its control of glutamine/glutamate homeostasis. Experimental enquiry is required to further elucidate the function of glutamate metabolism in pathogenicity. Moreover, the contribution to survival and growth in macrophages of the enzyme central to glutamate production, GOGAT, and the enzyme which may play a decisive role in the catabolism of glutamate, GDH, should be determined experimentally. These enzymes may offer unique and specific avenues for development of novel chemotherapeutic intervention strategies.

1.6 Study design and specific aims

In this study questions outlined in section 1.5 (formulated in the aims and objectives listed below), were addressed by experimental enquiry. Throughout the study, slow growing *M. bovis* BCG, which shares a 99.9% similarity with *M. tuberculosis* at nucleotide level (124), was used as a model for *M. tuberculosis*. *M. bovis* BCG survives better in macrophages than other non-pathogenic mycobacteria frequently used as models for *M. tuberculosis*, such as *M. smegmatis* (125, 126).

Aim 1:

To characterise the regulation of central nitrogen metabolism in *M. bovis* BCG in response to stimuli that may be encountered by the tubercle bacilli in the dynamic environments during infection.

Objectives:

i. To investigate the regulation of GS, GOGAT and GDH at the level of mRNA expression as well as enzyme activity in response to transition from growth under nitrogen-excess to growth under nitrogen-limitation.
ii. To investigate the regulation of GS, GOGAT and GDH at the level of mRNA expression as well as enzyme activity in response to transition from growth under nitrogen-limitation to growth under nitrogen-excess.
iii. To generate an amino acid substitution mutant GarA (Thr21Ala) strain of *M. bovis* BCG that is unphosphorylatable by PknG in order to delineate the function of GarA in nitrogen metabolism in *M. bovis* BCG.

Aim 2:

To determine the importance of GOGAT and GDH in the physiology of *M. bovis* BCG under various *in vitro* culturing conditions as well as in a murine bone marrow-derived macrophage (BMDM) model of infection.

Objectives:

i. To generate GOGAT- and GDH-deficient *M. bovis* BCG strains as well as genetically complemented strains of these mutants.
ii. To investigate the *in vitro* growth phenotypes of the strains generated in objective 1 as well as of their wild type *M. bovis* BCG progenitor strain.
iii. To investigate the *ex vivo* growth phenotypes of the strains generated in objective 1 as well as of their wild type *M. bovis* BCG progenitor strain.

Chapter 2

Regulation of nitrogen metabolism in *M. bovis* BCG

2.1 Introduction

In *M. tuberculosis* a substantial amount of research has been focused on the regulation of GS (see chapter 1, section 1.2.4.1), but little is known about the regulation of GOGAT and GDH in response to a transition from nitrogen-rich to nitrogen-limited growth environments and *vice versa*. It was found that GOGAT activity is enhanced and GDH activity is inhibited through their association with a small regulatory protein, GarA (see chapter 1, section 1.2.4.2). It was also found that phosphorylation of GarA at a single threonine residue by the serine-threonine protein kinase, PknG, prevents association between GarA and its substrates GOGAT and GDH. It remains to be determined which growth conditions stimulate or repress phosphorylation of GarA by PknG.

2.2 Results and Discussion

2.2.1 Regulation of GS in response to nitrogen limitation and excess

GS activity was increased by more than 40% within 30 minutes of transferring *M. bovis* BCG cells from a nitrogen-rich (60 mM $(NH_4)_2SO_4$) to a nitrogen-limited (0.1 mM $(NH_4)_2SO_4$) growth condition (Figure 4A1 and B, ○) and decreased by approximately 20% within the same time frame after being transferred from a nitrogen-limited to a nitrogen-rich condition (Figure 4A2 and B, □). These results are in agreement with a previous report from our laboratory for the regulation of GS in *M. smegmatis* (60). However, the expression of *glnA1*, the *M. bovis* BCG homologue to the gene encoding for the major isoform of GS in *M. tuberculosis*, did not change appreciably when bacteria were transferred from an excess nitrogen growth condition to a nitrogen-limiting growth condition or vice versa (Table 2). Out of the four GS-encoding genes (*glnA1-4*) present in the *M. tuberculosis* genome only *glnA1* is abundantly expressed and required for growth in the absence of L-glutamine (30). However, a *glnA1* mutant of *M. bovis* expressing reduced levels of GS was not auxotrophic for L-glutamine (37). In addition, while only *glnA1* was found to be required for the growth of *M. tuberculosis in vivo* (35), the *glnA1 M. bovis* mutant was attenuated for growth in macrophages and a *glnA2* mutant *M. bovis* strain generated by illegitimate recombination was avirulent in guinea pigs (37, 38). These results indicate that both *glnA1* and *glnA2* are potentially important for the expression of GS activity in *M. bovis* BCG which may explain the

discrepancy between changes in GS activity and *glnA1* expression observed in this study. Moreover, the changes in GS activity in this study (less than 2-fold) were meagre in comparison to a previous study in *M. tuberculosis* that reported a 10-fold decrease in activity in response to nitrogen limitation (24). This difference in the extent of up-regulation of GS in response to nitrogen limitation between less-pathogenic *M. bovis* BCG and pathogenic *M. tuberculosis* may correlate with the relatively poor growth and survival of *M. bovis* BCG in macrophages where nitrogen may be a limiting nutrient (36, 125).

Table 2. Relative expression of *M. bovis* BCG genes involved in central nitrogen metabolism in response to nitrogen excess or limitation.

	NH_4^+ Excess to Limitation			NH_4^+ Limitation to Excess		
	30 min	60 min	120 min	30 min	60 min	120 min
glnA1	1.16 ± 0.18	0.82 ± 0.10	1.02 ± 0.29	1.16 ± 0.03	0.88 ± 0.14	1.12 ± 0.45
gltD	0.76 ± 0.13	0.57 ± 0.14	0.73 ± 0.26	0.98 ± 0.01	0.99 ± 0.08	0.90 ± 0.29
gdh	0.56 ± 0.21	0.44 ± 0.17	0.36 ± 0.11	0.92 ± 0.15	0.91 ± 0.09	2.72 ± 1.35
pknG	1.60 ± 0.34	0.93 ± 0.24	1.00 ± 0.43	0.76 ± 0.09	0.77 ± 0.08	0.78 ± 0.24
garA	0.75 ± 0.13	0.56 ± 0.09	0.64 ± 0.23	1.10 ± 0.05	1.10 ± 0.06	1.71 ± 0.65

Data presented are means ± standard errors of 16S-normalized gene expression at 30 minutes, 60 minutes or 120 minutes NH_4^+ excess or limitation relative to 16S-normalized gene expression at 0 minutes calculated for triplicate cultures. 16S-normalised expression of genes of interest at 30 minutes, 60 minutes or 120 minutes NH_4^+ excess or limitation compared to 16S-normalized expression of genes of interest at 0 minutes were analysed with two-way ANOVA with Bonferroni post-testing. None of the data tested significantly different. Significance was set at $p < 0.05$.

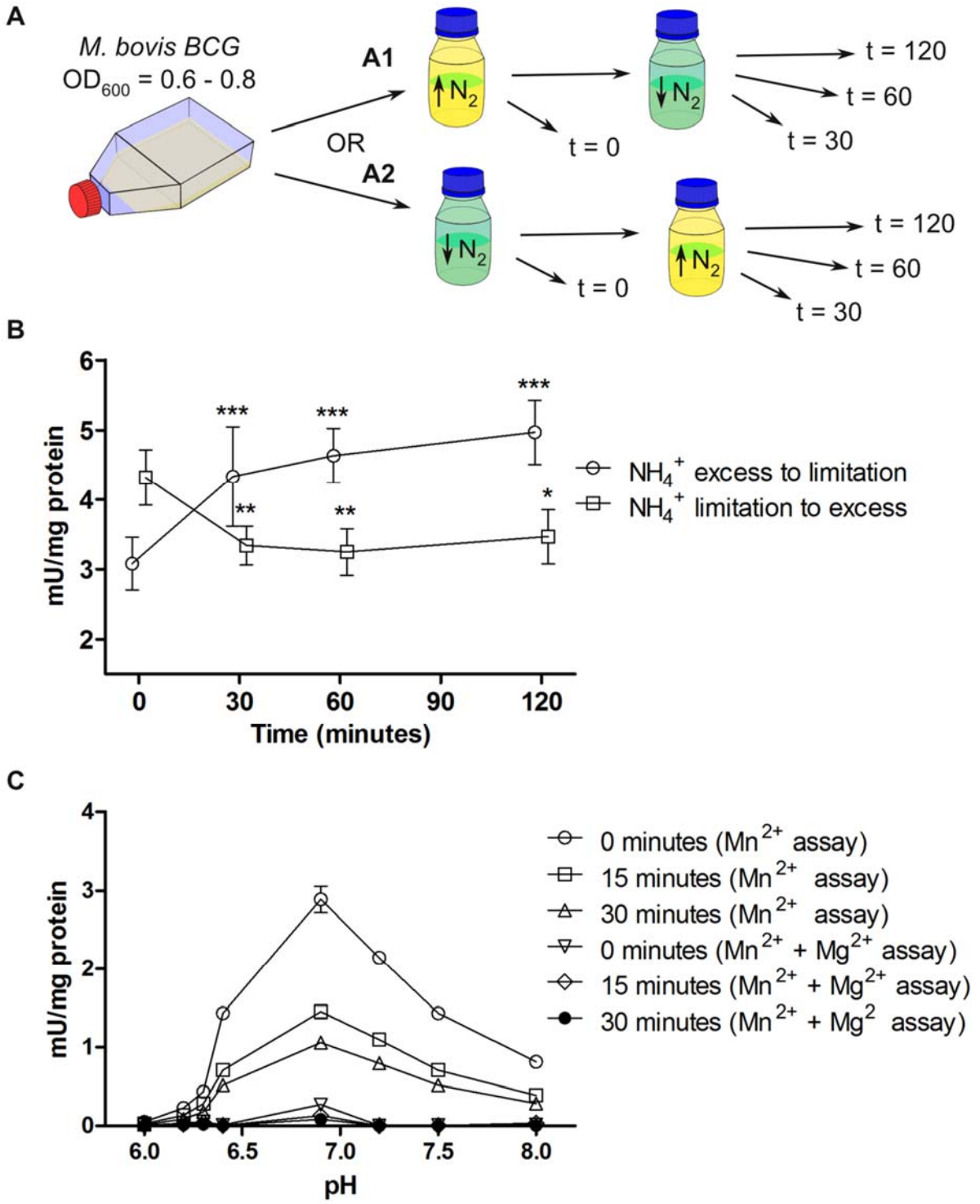

Figure 3: Investigating the regulation of GS activity in *M. bovis* BCG. A) Experiment used to investigate the regulatory response involved in the transition from nitrogen-rich (↑N_2) to nitrogen-limited (↓N_2) growth of *M. bovis* BCG (A1) and vice versa (A2). *M. bovis* BCG cultured in 7H9 to mid-log phase (OD_{600} = 0.6 – 0.8) was washed and re-suspended in -NKB (see chapter 5, section 5.3, Table 15), containing either limiting (0.1 mM) or excess (60 mM) concentrations of the sole nitrogen source $(NH_4)_2SO_4$. After a 1 hour incubation step an aliquot of bacteria was collected for analysis (GS/GOGAT/GDH assay or RNA extraction, t = 0 minutes). The remaining bacteria were collected by centrifugation and re-suspended in the opposite medium composition. Aliquots of bacteria were again

collected for analysis at specific time intervals (t = 30, 60 and 120 minutes). B) Regulation of *M. bovis* BCG GS activity when bacteria that were briefly (1 hour) exposed to conditions of either excess or limiting nitrogen content were transferred to media with a limiting (Figure 3A1) or excess nitrogen content (Figure 3A2), respectively. Data presented are means and standard errors calculated from four independent experiments. Specific GS activities at 30, 60 or 120 minutes NH_4^+ excess or limitation compared to specific GS activity at 0 minutes were analysed using a repeated measures two-way ANOVA and post testing with Bonferroni's multiple comparison test. Asterisks (✶) above error bars indicate significant difference to time = 0 minutes, ✶ $p < 0.05$, ✶✶ $p < 0.01$. C) The pH profiles of whole cell lysate preparates of *M. bovis* BCG containing GS at different states of adenylylation: 0 minutes representing the least adenylylated, 30 minutes most adenylylated and 15 minutes representing an intermediate state of adenylylation between 0 and 30 minutes. *M. bovis* BCG was cultured to exponential growth phase (OD_{600} = 0.6 – 0.8) in 7H9 and exposed to a nitrogen-limiting growth condition (Kirchner's medium containing 0.1 mM $(NH_4)_2SO_4$ as sole nitrogen source) for two hours to induce a low average state of GS adenylylation at which point an aliquot of culture was used to prepare whole cell lysate (0 minutes, see chapter 5, section 5.7.1). The remaining bacteria were transferred to a nitrogen-rich condition (Kirchner's medium containing 60 mM $(NH_4)_2SO_4$ as sole nitrogen source) for 15 or 30 minutes to induce adenylylation before aliquots of culture were used to prepare whole cell lysates. It was reasoned that the modest down-regulation of GS expression in response to nitrogen excess which was observed (< 30% reduction, Figure 4B, □) would be negligible if nitrogen limitation resulted in a low average state of adenylylation and nitrogen excess in a high average state of GS adenylylation in *M. bovis* BCG. GS assays were performed using the mixed imidazole buffer system (see chapter 5, section 5.7.2). The Mn^{2+}-containing assay measured total GS activity, while the Mn^{2+} + Mg^{2+}-containing assay measured the activity of unadenylylated GS exclusively.

Due to the modest changes observed in the expression of GS in response to nitrogen limitation and excess, the contribution of post-translational modification was investigated. Each of the twelve subunits of GS is adenylylated by GlnE at a conserved tyrosine residue resulting in increasing inactivation of the biosynthetic activity of the enzyme (23, 127, 128). The γ-glutamyl transferase GS assay has been employed to measure the state of *E. coli* GS adenylylation as addition of Mg^{2+} to the assay system allows for the exclusive measurement of unadenylylated GS activity (129). The average state of adenylylation (the number adenylylated GS subunits per molecule of GS enzyme divided by twelve) in any *E. coli* GS containing sample is accurately represented by the ratio of unadenylylated GS activity to total GS activity (129). However, equal amounts of totally adenylylated and totally unadenylylated GS will only have the same amount of activity at a specific pH, termed the isoactivity point, which has not yet been determined for *M. bovis* BCG or *M. tuberculosis* GS. In this study, no

isoactivity point was observed for the pH profiles of GS preparates with a low (Figure 3C, ○ and ▽), intermediate (Figure 3C, □ and ◇) or high (Figure 3C, △ and ●) average state of GS adenylylation assayed with or without Mg^{2+}. Limitations of the approach used in this study to determine the isoactivity point of *M. bovis* BCG (see Figure 3C legend) were a failure to measure the absolute quantity of GS protein in each whole cell lysate and the absence of *in vitro* adenylylated and unadenylylated *M. bovis* BCG GS controls. Unequal representation of total GS protein as a result of transcription could thus not be ruled out. However, it may be speculated from the very low activity measured over the pH range 6.0 to 8.0 for all three whole cell lysate preparates using the Mg^{2+}-containing assay, which only detects unadenylylated enzyme (Figure 3C, ▽, ◇ and ●), that *M. bovis* BCG GS is at a high average state of adenylylation even when the bacterium is exposed to limiting nitrogen for two hours. This is in agreement with the well documented absolute requirement for adenylylation of GS in *M. tuberculosis* (35, 75, 76). It was also previously observed that although *Salmonella typhimurium glnE* mutants grew better under nitrogen limitation (130), *M. tuberculosis glnE* mutants could not be generated on nitrogen-limited media (76).

2.2.2 Regulation of GOGAT in response to nitrogen limitation and excess

Despite detection of a *gltD* transcript in *M. bovis* BCG at approximately 20% of *glnA1* transcript levels (see chapter 5, section 5.6.6), effectively no GOGAT activity was detected above non-specific background levels in whole cell lysates of *M. bovis* BCG grown in 7H9, -N7H9 + 4 mM $(NH_4)_2SO_4$ or –N7H9 + 3 mM L-Gln (see chapter 5, section 4.3) and using four different GOGAT assay systems (Table 3). GOGAT activity was also not detected in whole cell lysates of *M. smegmatis* in an early study of the regulation of nitrogen metabolism in this organism (18). However, in a more recent study GOGAT activity was detected in extracts of *M. smegmatis* at approximately 0.7 mU/mg protein, which is 1% – 20% of the levels which have been reported for whole cell lysates of *C. glutamicum* (66, 70, 78). GOGAT activity was also detected in whole cell lysates of *M. bovis* BCG, but the level of activity in this organism was lower than in *M. smegmatis* extracts (78). It is thus possible that reagents and equipment used in this study (see chapter 5, section 5.7.3) was not sufficiently sensitive to detect low levels of GOGAT activity in *M. bovis* BCG extracts. NADPH-GOGAT contains three iron sulfur clusters which are crucial to the activity of the enzyme and it is possible that

these became oxidised during preparation of the whole cell lysates (see chapter 5, section 5.7.1) resulting in inactivation of the enzyme in this study (131, 132).

No significant difference in *gltD* expression was observed when *M. bovis* BCG was exposed to either nitrogen excess or limitation (Table 2). In previous studies, up-regulation of GOGAT mRNA expression and enzymatic activity by nitrogen limitation were reported for *C. glutamicum* (66, 69, 70). However, disruption of a gene encoding for a histidine kinase (*hkm*) upstream of the GOGAT operon in *C. glutamicum* resulted in a nearly 2-fold decrease in GOGAT activity in low-nitrogen medium compared to wild type, while in high-nitrogen medium GOGAT activity was increased approximately 2-fold (66). The authors speculated that *hkm* may play a role in signal transduction of nutritional status affecting the expression of GOGAT in *C. glutamicum*. Neither a pBLAST nor a tBLASTn of the *hkm* (*cg0228*) amino acid and nucleotide sequences, respectively, against the *M. tuberculosis* H37Rv and *M. bovis* BCG str Pasteur 1173P2 genomes delivered any homologues (no query coverages were greater than 40) for *hkm* in either of these organisms. However, it should be noted that a number of differences in the regulatory and effector proteins of nitrogen metabolism exist between *C. glutamicum* and *M. tuberculosis*, such as the absence of homologues of the global regulator of *C. glutamicum* nitrogen metabolism, *amtR* and an anabolic NADPH-GDH in *M. tuberculosis* which may explain differences in the regulation of the effectors of nitrogen metabolism between these organisms (61, 62).

Table 3: Specific GOGAT activity in whole cell lysates of wt-BCG

	mU/mg protein			
Condition	Assay 1*	Assay 2*	Assay 3**	Assay 4**
7H9	0.48 ± 0.31	4.20 ± 8.58	-0.16 ± 1.48	0.18 ± 2.21
-N7H9 + 4 mM $(NH_4)_2SO_4$	-	-	0.12 ± 3.47	-0.50 ± 0.54
–N7H9 + 3 mM L-Gln	-	-	1.74 ± 1.04	-0.35 ± 1.42

✶ - Mean specific activity (mU/mg protein) ± standard deviation for triplicate cultures.
✶✶ - Mean specific activity (mU/mg protein) ± standard deviation for duplicate cultures.
Assay 1, 2 and 3 and 4 represent three independent experiments.
Assay 1: Meers *et al*. (1970) protocol (50 mM tris buffer, pH 7.6) ..... (133)
Assay 2: Miller & Stadtman (1972) protocol (100 mM NaH_2PO_4/K_2HPO_4 buffer, pH 7.0) ..... (134)
Assay 3: Meers *et al*. (1970) protocol (50 mM potassium phosphate buffer, pH 7.5)
Assay 4: Miller & Stadtman (1972) protocol (50 mM potassium phosphate buffer, pH 7.5)

2.2.3 Regulation of GDH in response to nitrogen limitation and excess

NAD^+-GDH activity (assayed for aminating activity, see chapter 5, section 5.7.4) was not affected by the transition from a nitrogen-limiting growth condition to a nitrogen-rich growth condition of *M. bovis* BCG (Figure 4A1-3, □). However, NAD^+-GDH activity was decreased by nitrogen limitation in *M. bovis* BCG by approximately 30% (figure 4A1-3, ○), which is reminiscent of the regulation usually observed for the anabolic NADPH-GDHs. However, this was not reflected by equivalent significant changes in *gdh* transcript levels (Table 2). In addition, NAD^+-GDH deaminating measurements were approximately 10% or less of aminating activity levels under all the conditions tested (Figure 4B). Deaminating GDH activity was thus plotted against L-glutamate concentration in order to optimise the NAD^+-GDH deaminating activity assay (Figure 5). The deaminating NAD^+-GDH activity only reached the minimal level of the specific activity usually observed in the aminating direction (approximately 10 mU/mg protein) when L-glutamate concentration was equal to approximately 0.5 M. Similarly, a very low affinity for L-glutamate (half-maximal activity at 83 mM) in comparison to that for ammonia (K_m = 45 mM) and 2-oxoglutarate (half-maximal activity at 5 mM) was observed for the L180 NAD^+-GDH present in *M. smegmatis* (20). The poor affinity of *M. bovis* BCG NAD^+-GDH for L-glutamate as well as the down-regulation of the enzyme's activity in response to nitrogen limitation may suggest an anabolic function for this enzyme. These observations were surprising, since a catabolic activity is normally characteristic of GDH enzymes with a coenzyme specificity for NAD^+ (135, 136). However, exceptions to this rule have been reported (137, 138) and it remains possible that NAD^+-GDH could play a role in the production of glutamate in *M. bovis* BCG and related mycobacteria rather than in the deamination of the amino acid. On the other hand, exceptionally high intracellular levels of L-glutamate in *M. tuberculosis* and possibly *M. bovis* BCG, which corresponds with the affinity of L180 GDH for L-glutamate (112) and the accumulation of glutamate in a *pknG* mutant of *M. tuberculosis* (81) suggest that L180 GDH is indeed more important for the catabolic function in *M. tuberculosis*.

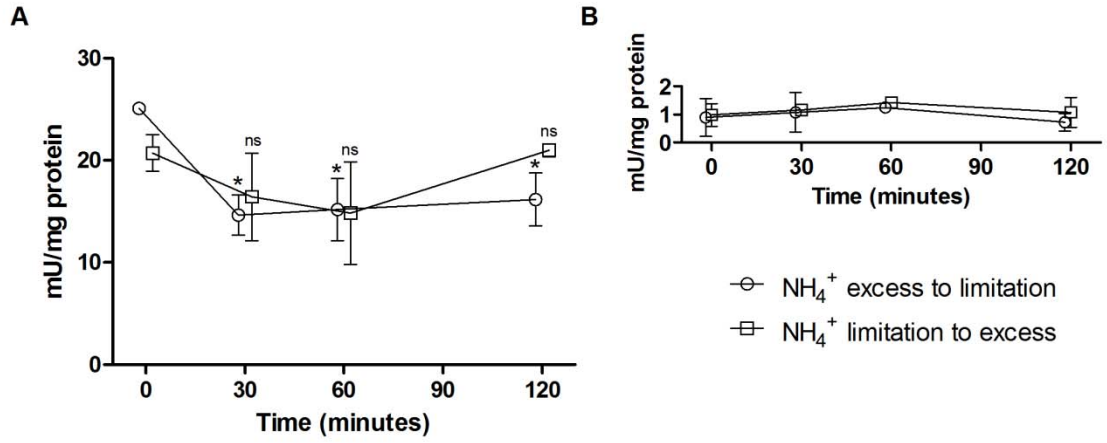

Figure 4: Regulation of *M. bovis* BCG NAD^+-GDH activity when bacteria that were briefly (1 hour) exposed to conditions of either excess or limiting nitrogen content were transferred to media with a limiting or excess nitrogen content, respectively. Means and standard deviations were calculated from two independent experiments. A) Regulation of NAD^+-GDH activity in response to nitrogen limitation or excess. B) Deaminating activity of NAD-GDH (see chapter 5, section 5.7.4). Asterisks (✶) above error bars indicate significant difference between specific GDH activities at 30, 60 or 120 minutes of NH_4^+ limitation or excess and time = 0 minutes as determined by repeated measures two-way ANOVA with Bonferroni post-test, ✶ - $p < 0.05$, ns - no significant difference ($p > 0.05$).

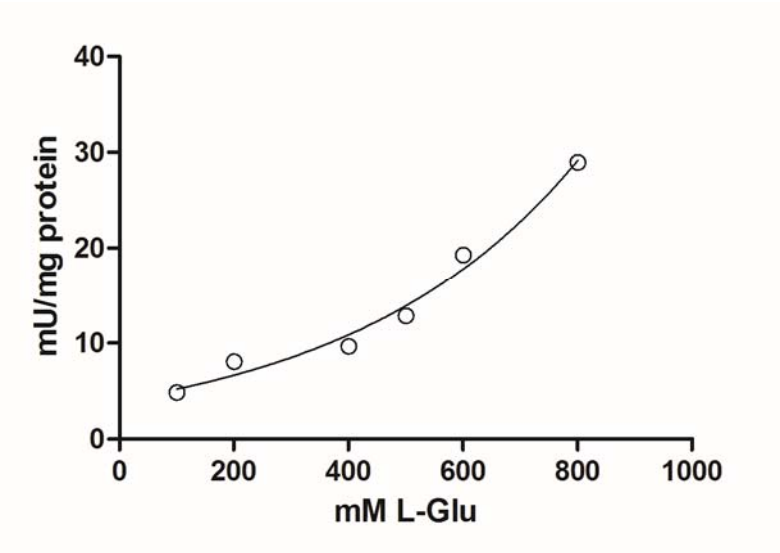

Figure 5: Optimization of the GDH reverse (deaminating) assay using whole cell lysate of exponentially growing *M. bovis* BCG cultured in 7H9. NAD^+ levels were kept at 0.5 mM.

2.2.4 Regulation of PknG and GarA in response to nitrogen limitation and excess

The enzyme activity curve obtained during the optimization of the deaminating NAD^+-GDH assay (Figure 5) was very similar to the glutamate binding curve obtained for the *M. smegmatis* L180 GDH when the purified enzyme was associated with GarA (20). In that study addition of 2 µM GarA to a GDH preparate, increased the half maximal binding of L-glutamate from 83 mM to in excess of 500 mM. This may indicate that NAD^+-GDH is associated with GarA and thus inhibited when *M. bovis* BCG is growing exponentially in 7H9. In addition, the low activities obtained for NAD^+-GDH assayed in the deaminating direction for *M. bovis* BCG subjected to nitrogen limitation or excess (see chapter 2, section 2.2.3) may indicate that the enzyme was also inhibited by GarA under these conditions. As for *gdh* and *gltD*, no significant differences in the expression of *garA* or *pknG* were observed either under nitrogen excess or limitation (Table 2). It was previously found that an *M. bovis* BCG *pknG* deletion mutant showed no differences in intracellular L-glutamine and L-glutamate content compared to a wild type strain, contrary to observations for the equivalent *M. tuberculosis* mutant (139). Although these results suggest that PknG does not affect the regulation of GOGAT or GDH under nitrogen limitation or excess in *M. bovis* BCG, culturing conditions where PknG activity is required for the control of GOGAT or GDH activity may exist. Notably growth conditions under which *M. bovis* BCG requires the degradation of L-glutamate may also promote decreased GOGAT activity and de-repression of GDH activity possibly through the phosphorylation of GarA by PknG and such conditions may not have been modelled by the growth media used in the study by Nguyen *et al*. (2005) (139).

2.2.5 Regulation of GDH when glutamate is a sole nitrogen and carbon source.

Since no induction of GDH activity was observed when excess ammonium was added to the growth medium (Figure 5A-C, □), the effect of the substrates 2-oxoglutarate and glutamate on GDH activity was investigated. When *M. bovis* BCG was cultured to logarithmic growth phase and transferred from 7H9 medium containing approximately 3.4 mM L-glutamate (Figure 6, column A) to minimal medium containing excess (30

mM) glutamate as sole carbon and nitrogen source a more than 2-fold increase in GDH activity was observed (Figure 6, column B). However, when bacteria grown in 7H9 were transferred to minimal medium containing the nitrogen source $(NH_4)_2SO_4$ and carbon source glycerol in addition to excess glutamate, no significant change in GDH activity was observed (Figure 6, column C). This may be evidence of an important role for *M. bovis* BCG NAD-GDH in the deamination of glutamate to produce free ammonium for glutamine production by GS as well as to produce 2-oxoglutarate as an intermediate metabolite of the TCA cycle. It was found in earlier studies that glutamate is one of only three nitrogenous compounds that are oxidised by mycobacteria, suggesting that glutamate may be used as a source of energy by these bacteria (114, 115).

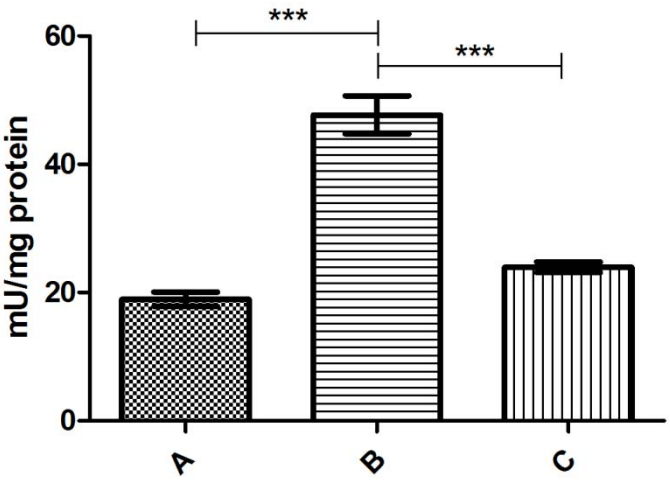

Figure 6: *M. bovis* BCG GDH activity in media where GDH may be required either for its aminating or for its deaminating activity. *M. bovis* BCG cells were cultured to mid-logarithmic growth phase (OD_{600} = 0.6 – 0.8) before being transferred to 7H9 (A), B – -NKB without glycerol (see chapter 5, section 5.3, Table 12) + 30 mM L-Glu (B), -NKB + 10 mM $(NH_4)_2SO_4$ + 30 mM L-Glu (C). Cells were collected after 24 hours of incubation at 37°C, whole cell lysates prepared and GDH activity measured (see chapter 5, section 5.7.4). Means and standard deviations were calculated for triplicate cultures. Asterisks (✶) above error bars indicate significant difference between indicated columns as determined by one-way ANOVA with Bonferroni post-test, ✶✶✶ $p < 0.001$. No significant difference was observed between column A and C ($p > 0.05$).

2.2.6 Generation of an *M. bovis* BCG *garA* T21A amino acid substitution mutant by method of recombineering

A mutant *M. bovis* BCG strain in which a mutated *garA* gene expresses GarA protein with a Thr21Ala amino acid substitution thus rendering the protein unphosphorylatable by PknG may be useful to delineate the function of GarA in nitrogen metabolism in *M. bovis* BCG (see chapter 2, section 2.1). Recombineering was employed to generate an A61G point mutation in *garA* resulting in the amino acid substitution T21A (Figure 7, see chapter 5, section 5.4.4). A total of 149 hygromycin resistant colonies were screened using HRM analysis (see chapter 5, section 5.5.4.3) and another 96 hygromycin resistant colonies using MAMA-PCR with the primers GarA1F, GarA1Fm and GarA1R (see chapter 5, section 5.5.4.4 and Table 14). None of the HRM analysed colonies produced the two first derivative peaks expected for the *garA* T21A mutant genotype (see chapter 5, section 5.5.4.3). However, eighteen colonies were identified with HRM profiles that digressed appreciably from the wild type *garA* genotype (confidence of more than 80%, see chapter 5, section 5.5.4.3) and were further analysed by sequencing to detect mutations. None of the sequenced colonies carried the *garA* A61G mutation. In addition, while all 96 colonies assayed by MAMA-PCR produced the 465 bp internal control fragment, none produced the 323 bp product expected for *garA* A61G mutant colonies (Figure 8). A limitation encountered during analysis of colonies with both the HRM and MAMA techniques was the absence of a positive control. It was thus impossible to optimise the techniques for detection of mutants. Notwithstanding, these results may indicate that the GarA threonine 21 amino acid residue is not amenable to modification by substitution with an alanine residue.

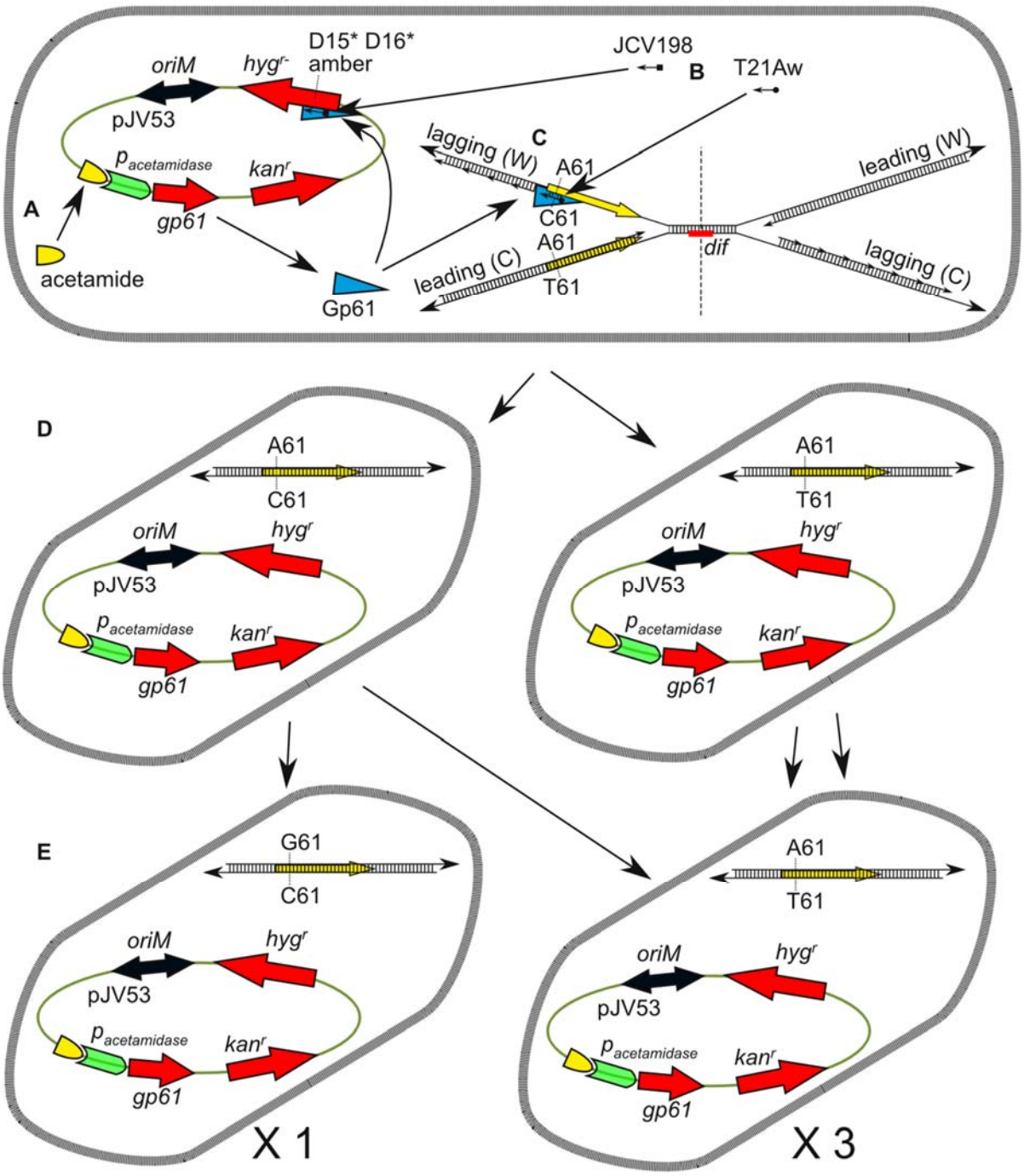

Figure 7: Generation of an *M. bovis* BCG *garA* A61G mutant, expressing GarA protein with a T21A amino acid substitution, by method of recombineering. A) Expression of the Che9c recombineering protein Gp61 was induced in an *M. bovis* BCG strain carrying the self-replicating recombineering plasmid pJV75Amber (wt-BCG::pJV75Amber). B) wt-BCG::pJV75Amber cells expressing Gp61 were co-transformed with the recombineering oligonucleotides, JCV198 and T21Aw (or T21Ac, which was not included in this illustration). C) Gp61 facilitates a process of strand invasion whereby the T21Aw oligonucleotide acts as an Okazaki fragment during DNA replication of the lagging strand and is in this way incorporated into the bacterial genome. It has been shown that a strand bias (with relation to DNA replication) exists towards the lagging strand of DNA replication in recombineering

with single stranded DNA substrates (140). Although it was determined that *garA* is situated on the lagging strand of DNA replication by its relation to the *dif* sequence (141), which suggests that recombineering of *garA* sequences would be more efficiently accomplished with oligonucleotides which are complementary to the Watson sequence, oligonucleotides complementary to both the Watson (T21Aw) and Crick sequence (T21Ac) were used. Incorporation of JCV198 into pJV75Amber was facilitated by Gp61 and repaired two adjacent Amber null-mutations in a non-functional hygromycin (*hyg*$^{r-}$) cassette rendering the *hyg*^{r} cassette functional. D) Subsequent cell division was expected to have resulted in one daughter cell with nucleotide mismatches between the residues introduced by recombineering on the Crick strand and the wild type residues on the Watson strand and another daughter cell without any mutations. E) In a second round of cell division generation of three wild type daughter cells and one *garA* A61G mutant daughter cell were expected. Selection of bacterial colonies on hygromcyin containing media filtered out a large background of bacterial cells that could not be electro-transformed efficiently with the recombineering oligonucleotides. Mutant *garA* A61G *M. bovis* BCG colonies were thus expected at a frequency of one in four screened colonies.

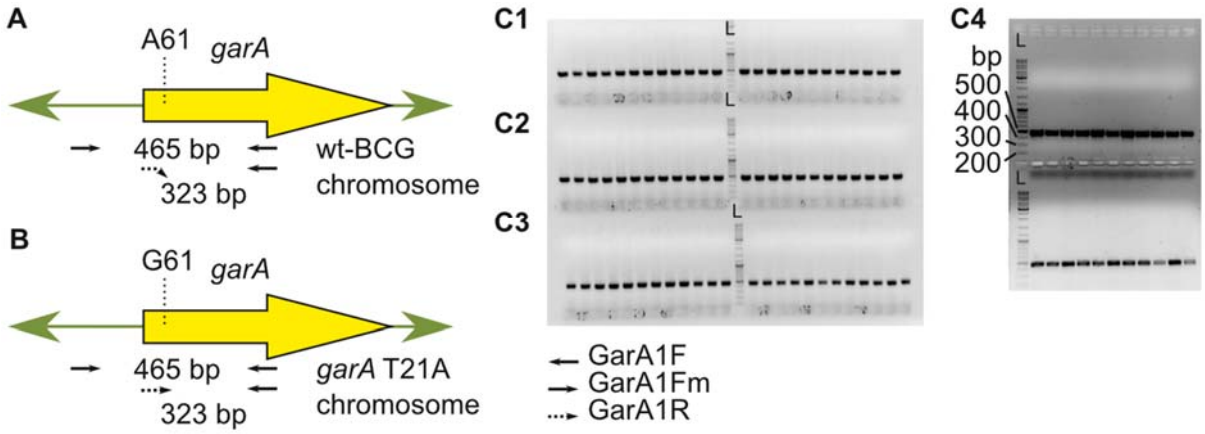

Figure 8: Screening of 96 hygromycin resistant wt-BCG::pJV75Amber colonies transformed with T21Aw and T21Ac. A) Binding of MAMA primers (GarA1F, GarA1Fm and GarA1R) to the wt-BCG *garA* genomic region. The GarA1Fm primer has mismatches with the wt-BCG DNA template at both the penultimate and ultimate nucleotide residues on the 3'-end and does not elongate from wt-BCG DNA template using standard PCR conditions (see chapter 5, section 5.5.4.1). B) Binding of MAMA-PCR primers to *garA* A61G mutant genomic region. The GarA1Fm MAMA-PCR primer only contains a mismatch to the *garA* A61G mutant DNA template at the penultimate nucleotide residue on the 3'-end and is expected to elongate from *garA* A61G mutant DNA template using standard PCR conditions. C1-2) MAMA-PCR analysis of 48 colonies obtained from wt-BCG::pJV75Amber transformed with the T21Aw recombineering oligonucleotide (see chapter 5, Table 14), C3-4) MAMA-PCR analysis of 48 colonies obtained from wt-BCG::pJV75Amber transformed with the T21Ac recombineering oligonucleotide (see chapter 5, Table 14). The same DNA marker (L) was used.

2.2.7 Assay of *garA* threonine residue 21 essentiality by recombineering

Recombineering with oligonucleotides designed to mutate different nucleotide residues within the *garA* threonine 21 codon as well as an adjacent valine 20 codon was used along with the ability of MAMA-PCR to detect a mutant template against a high background of wild type templates (142) to investigate the essentiality of the GarA T21 amino acid residue (Figure 9). When the MAMA-PCR primer set GarA2Fm1 and GarA2R was used a faint 146 bp PCR amplicon could be generated from a control template (pAVGarA-T21A, see chapter 5, section 5.4.6) diluted by at least 1000-fold in a background of 10^5 wt-BCG DNA templates/PCR reaction. However, no 146 bp PCR fragment was observed when 10^5 DNA template prepared from wt-BCG::pJV75Amber co-transformed with JCV198 and T21Ac (Figure 9C1, Lane 7) or T21Aw (Figure 9C2, Lane 19). This result suggests that recombineering may at best be successful at generating *garA* A61G mutations in less than 0.1% of the hygromycin resistant wt-BCG::pJV75Amber population generated by recombineering of pJV75Amber with JCV198, which may indicate that the *garA* A61G mutation impacts negatively on the growth and survival of *M. bovis* BCG. Recombineering efficiency of 3 – 4% of co-selected cells was previously reported (140).

In addition to investigating the permissiveness of a T21A substitution, the permissiveness of a V20I and a T21Q substitution as well as a synonymous nucleotide substitution in the threonine 21 codon was investigated. It was reasoned that substitution of valine residue 20 with a residue from the same amino acid group, such as isoleucine as well as a substitution of the ACG threonine 21 codon with a ACC threonine codon, may occur at optimal recombineering efficiencies and could thus act as controls of recombineering efficiency near the *garA* threonine 21 codon. On the other hand, substitution of threonine 21 with a residue from the same amino acid group, such as glutamine, may indicate that the failure to generate a *garA* A61G mutant may be as a result of a deleterious effect of the T21A amino acid substitution on the structure of the GarA protein as opposed to abolishment of the threonine phosphorylation site of PknG. However, 146 bp PCR amplicons generated by MAMA-PCR with the primer sets GarA2R and GarA2Fm2, GarA2Fm3 or GarAFm4 were not observed for DNA extracted from wt-BCG::pJV75Amber which was transformed with the recombineering oligonucleotides JCV198 and V20Iw (Figure 9C3), T21Tw (Figure

Figure 9C4) or T21Qw (Figure 9C5), respectively. Although no positive control was available for the MAMA-PCR analysis of the V20Iw, T21Qw or T21Tw transformations, these results may suggest that the *garA* nucleotide residues surrounding the threonine 21 codon are highly resistant to changes by recombineering.

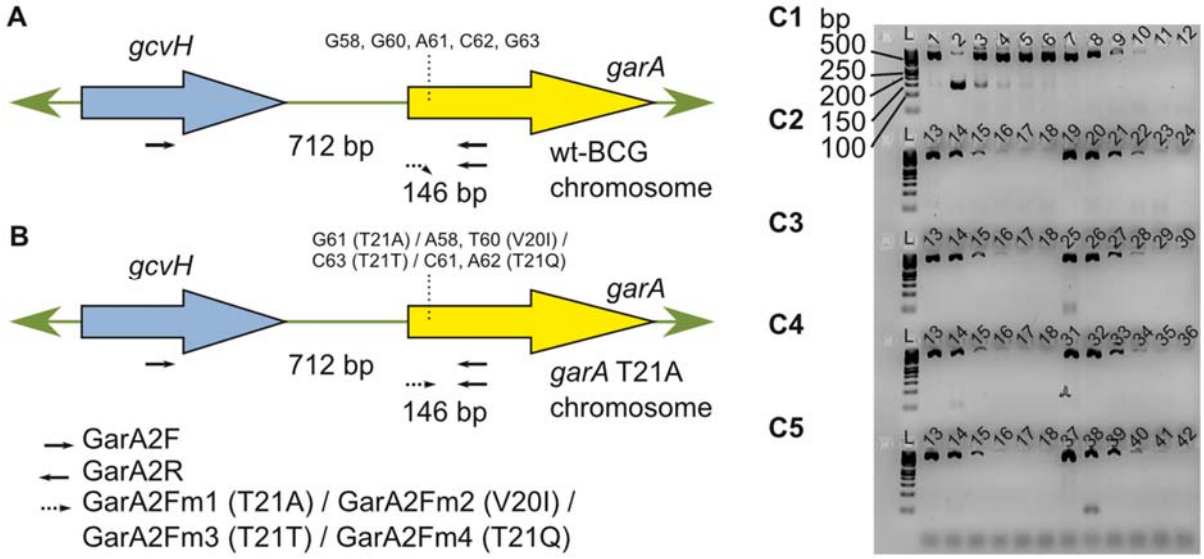

Figure 9: Recombineering coupled with MAMA-PCR analysis to assay the essentiality of the GarA threonine 21 residue. wt-BCG::pJV75Amber was co-transformed with the oligonucleotides JCV198 and T21Aw or T21Ac (A61G non-synonymous missense SNP results in a T21A amino acid substitution) or V20Iw (G58A, G60T non-synonymous missense SNPs result in a V20I amino acid substitution) or T21Tw (G63C synonymous SNP results in a substitution of the ACG Thr21 codon for a ACC Thr21 codon) or T21Qw (A61C, C62A non-synonymous missense SNPs result in a T21Q amino acid substitution) or JCV198 on its own as described in chapter 5, section 5.4.4. However, instead of plating bacteria out onto 7H11 agar, transformed cells were used to inoculate 7H9 medium containing the antibiotic hygromycin (see chapter 5, section 5.2) to an initial OD_{600} = 0.05. The bacteria were grown for approximately 2 weeks until an OD_{600} = 1.0 was reached and genomic DNA was extracted as described in chapter 5, section 5.5.2.2. Ten-fold dilution series of the extracted genomic DNA was prepared as template for analysis with MAMA-PCR. A) Binding of MAMA-PCR primers (GarA2F, GarA2Fm1/ GarA2Fm2/ GarA2Fm3/ GarA2Fm4 and GarA1R) to the wt-BCG *garA* genomic region. The GarA2Fm1, GarA2Fm2, GarA2Fm3 and GarA2Fm4 primers have mismatches with the wt-BCG DNA template at the penultimate and ultimate nucleotide residues on the 3'-end and do not elongate from wt-BCG DNA template using standard PCR conditions (see chapter 5, section 5.5.4.1, Table 14). B) Binding of MAMA-PCR primers to *garA* T21A, V20I, T21T or T21Q codon-mutant genomic regions. The GarA2Fm1, GarA2Fm2 and GarA2Fm3 MAMA-PCR primers only contain mismatches to the *garA* T21A, V20I, and T21T mutant DNA templates at the penultimate nucleotide residues on their 3'-ends and are expected to elongate from *garA* T21A, V20I, and T21T codon-mutant DNA templates, respectively, using standard PCR conditions. The GarA2Fm4 MAMA-PCR primer only contains a

mismatch to the *garA* T21Q codon-mutant DNA template at the third nucleotide residue proximal to the 3'-end and is also expected to elongate from the *garA* T21Q codon-mutant DNA template. C1 & 2) MAMA-PCR analysis of wt-BCG::pJV75Amber transformed with T21Aw using GarA2Fm1. Lane 1: wt-BCG DNA template, Lane 2: Positive control for *garA* A61G nucleotide sequence substitution (pAVGarA-T21A, see chapter 5, section 5.4.6, Table 14), Lane 3 – 6: Ten-fold dilution series of pAVGarA-T21A DNA template starting at 10^5 molecules/PCR reaction and prepared in nuclease free water containing 10^5 molecules wt-BCG DNA template/PCR reaction. Lane 7 – 12: Ten-fold dilution series of JCV198+T21Ac-transformed wt-BCG::pJV75Amber starting at 10^5 molecules/PCR reaction. Lane 13 – 17: Ten-fold dilution series of JCV198-transformed wt-BCG::pJV75Amber DNA template starting at 10^5 molecules of genomic DNA/PCR reaction. Lane 19 – 24: Ten-fold dilution series of JCV198+T21Aw-transformed wt-BCG::pJV75Amber DNA template starting at 10^5 molecules of genomic DNA/PCR reaction. C3) MAMA-PCR analysis of wt-BCG::pJV75Amber transformed with V20Iw using GarA2Fm2. Lane 13 – 17: Same DNA template as in C1 & 2. Lane 25 – 30: Ten-fold dilution series of JCV198+V20Iw-transformed wt-BCG::pJV75Amber DNA template starting at 10^5 molecules of genomic DNA/PCR reaction. C4) MAMA-PCR analysis of wt-BCG::pJV75Amber transformed with T21Tw using GarA2Fm3. Lane 13 – 17: Same DNA template as in C1 & 2. Lane 31 – 36: Ten-fold dilution series of JCV198+T21Tw-transformed wt-BCG::pJV75Amber DNA template starting at 10^5 molecules of genomic DNA/PCR reaction. C5) MAMA-PCR analysis of wt-BCG::pJV75Amber transformed with T21Qw using GarA2Fm4. Lane 13 – 17: Same DNA template as in C1 & 2. Lane 37 – 42: Ten-fold dilution series of JCV198+T21Qw-transformed wt-BCG::pJV75Amber DNA template starting at 10^5 molecules of genomic DNA/PCR reaction.

2.2.8 Complementation of wt-BCG with copies of *garA* containing T21A and T21V codon substitutions.

Possible essentiality of the GarA threonine 21 residue is not surprising as over-expression of GarA T21A in *M. smegmatis* resulted in a severe growth defect on LB agar (20). It may be speculated that non-phosphorylatable GarA associates with GOGAT and GDH in an uncontrolled manner, resulting in deregulation of glutamate levels which disrupts normal cellular processes and ultimately affects growth. In order to determine whether the presence of non-phosphorylatable copies of GarA would affect growth of *M. bovis* BCG, wt-BCG cells were transformed with the integrative vectors, pGCgarA3, pGCgarA3-T21A and pGCgarA-T21V (see chapter 5, section 5.4.5). Native *garA*, *garA* with an A61G substitution (T21A amino acid substitution) and *garA* with A61G, C62T and G63T substitutions (T21V amino acid substitution) were expressed under control of the native *garA* promoter from pGCgarA3, pGCgarA3-T21A and pGCgarA-T21V, respectively. A T21V amino acid substitution

was investigated in addition to a T21A substitution as it was reasoned that the slightly larger size of a valine residue may have a different effect on GarA structure than substitution of threonine 21 with alanine. Investigation of both mutants may thus provide more confidence that observed phenotypes are related to loss of the threonine 21 phoshorylation site rather than changes to the structure of GarA. Surprisingly, electro-transformation efficiencies with pGCgarA3 (2.80×10^6 cfu/ml/µg plasmid), pGCgarA3-T21A (2.36×10^6 cfu/ml/µg plasmid) and pGCgarA-T21V (1.84×10^6 cfu/ml/µg plasmid) were similar. In addition, colonies of pGCgarA3-T21A and pGCgarA3-T21V appeared to be larger than colonies of pGCgarA3 transformants (Figure 10). These results suggest that the presence of non-phosphorylatable GarA T21A or T21V copies may not be detrimental to the physiology and growth of *M. bovis* BCG.

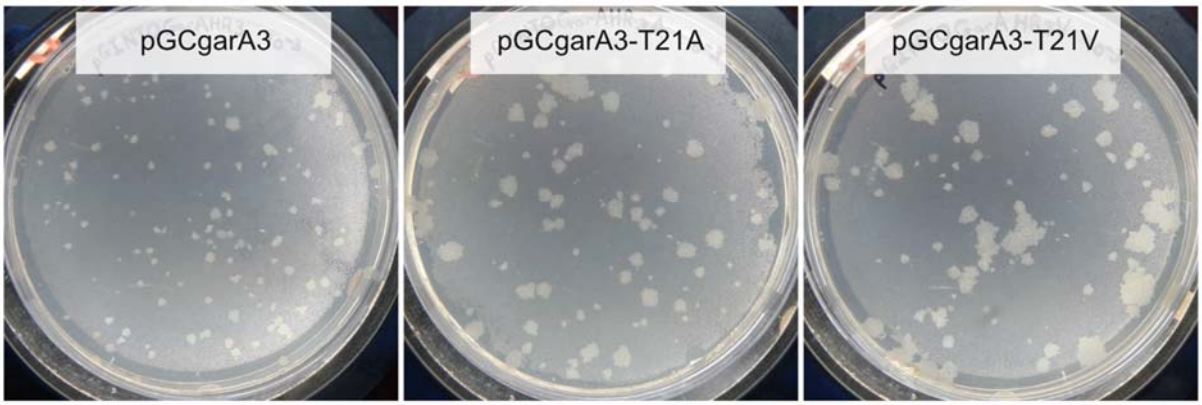

Figure 10: Colonies of *M. bovis BCG attB::*pGCgarA3, *attB::*pGCgarA3-T21A and *attB::*pGCgarA-T21V. *M. bovis* BCG cells were transformed with pGCgarA3, pGCgarA3-T21A and pGCgarA-T21V as described in chapter 5, section 5.4.5, diluted 10-fold to 10^4-fold and plated on 7H11 containing the antibiotic gentamicin (see chapter 5, section 5.2). Shown here are 10^3-dilution factor plates.

2.2.9 Generation of *M. bovis* BCG *garA* T21A or T21V amino acid substitution mutants by method of allelic exchange through homologous recombination.

Successful transformation of wt-BCG with vectors expressing T21A and T21V mutated copies of GarA may indicate that the failure in this study to generate the *M. bovis* BCG *garA* mutant expressing GarA T21A by recombineering is not due to a lethal phenotype conferred by this amino acid substitution. A disadvantage of the recombineering technique to introduce point mutations is the potential variability of the frequency at which mutants are generated which may depend on factors other than the essentiality of the residue being mutated, such as transformation efficiency (143). It may thus be risky to speculate on the essentiality of a nucleotide, amino acid residue or any other small genetic feature studied when even a large amount of colonies are screened without detecting mutants in a recombineering experiment. Therefore, a two-step homologous recombination approach was followed to further investigate the essentiality of the *M. bovis* BCG GarA threonine 21 residue (Figure 11).

Because the expected frequency at which mutants are generated with the two-step homologous recombination technique is theoretically high (one in every two analysed sucrose tolerant, white, kanamycin sensitive, hygromycin sensitive colonies – from here on referred to as putative mutant colonies), a direct sequencing approach was followed to screen putative mutant colonies. Crude DNA extracts were thus prepared from putative mutant colonies (see chapter 5, section 5.5.2.1) and used as DNA template in a high fidelity PCR reaction (see chapter 5, section 5.5.4.2) with the primer set GarA4F and GarA4R (chapter 5, Table 14). These primers were never used before the screening of the colonies occurred and could not anneal to any of the PCR amplicons, cloned fragments or constructs generated throughout the study. Upon completion of thermo cycling, tubes containing amplified product were sent off for post-PCR clean-up and sequencing with the primer GarA3R and were never opened on or near the premises where the study was conducted. A total of 72 putative GarA T21A mutant colonies and 71 putative GarA T21V mutant colonies were analysed by sequencing. Decent quality sequences were obtained for 42 putative GarA T21A and 58 GarA T21V mutant colonies, but no A61G (T21A) or A61G, C62T, and G63T (T21V) substitutions were detected for any of the colonies. In order to provide more evidence

that the GarA threonine 21 residue is essential in *M. bovis* BCG, pAVgarA-T21A-SCO and pAVgarA-T21V-SCO (see chapter 5, Table 14) strains were complemented with copies of *garA*, through integration of the construct pGCgarA3 (see chapter 5, section 5.4.4) at the *attB* site in these strains to generate the *garA*-complemented SCO strains: pAVgarA-T21A-SCO *attB::*pGCgarA3 and pAVgarA-T21V-*SCO attB::*pGCgarA3 (see chapter 5, section 5.4.7). A second SCO event resulting in successful substitution of threonine 21 codon of the native *garA* copy with a threonine or valine codon in the *garA*-complemented SCO strains, but not in the absence of an additional *garA* copy integrated elsewhere in the genome would be strong evidence of the essentiality of the GarA threonine 21 residue (Figure 12).

A total of 40 merodiploid colonies containing both wild type copy of *garA* located at the *attB* site on the bacterial chromosome and a native copy of *garA* which did or did not contain a T21A or T21V amino acid substitution, were obtained and sequenced. Decent quality sequences were obtained for 14 putative merodiploid *garA* T21A *attB::pGCgarA* and 19 putative merodiploid *garA* T21V *attB::*pGCgarA mutant colonies. All of the putative merodiploid *garA* T21A *attB::*pGCgarA or garA T21V *attB::*pGCgarA colonies were found to contain only wild type copies of the native *garA* gene. If the *garA* threonine 21 residue is essential and the expression of *garA* from the integrated copy of the gene at the *attB* site is poor or poorly regulated a *garA* T21A or T21V *attB::*pGCgarA merodiploid strain may be impossible to generate. It thus remains unclear whether failure to generate amino acid substitutions of the *garA* threonine 21 in this study was due to the essentiality of that residue. It could be speculated that the apparent essentiality of *garA* threonine 21 observed in this study is through the effect of molecules of unphosphorylatable GarA on the effectors that it regulates, namely GOGAT and GDH. However, wt-BCG was successfully transformed with integrating vectors containing T21A-codon and T21V-codon mutated versions of *garA* and it would thus appear that *M. bovis* BCG requires phosphorylated molecules of GarA for growth on 7H11. In a previous study GarA phosphorylated by PknG at threonine 21 was used in an affinity purification assay to identify possible binding partners of T21-phosphorylated GarA and none were found (20). It is unclear what the essential functions of T21-phosphorylated GarA are in *M. bovis* BCG.

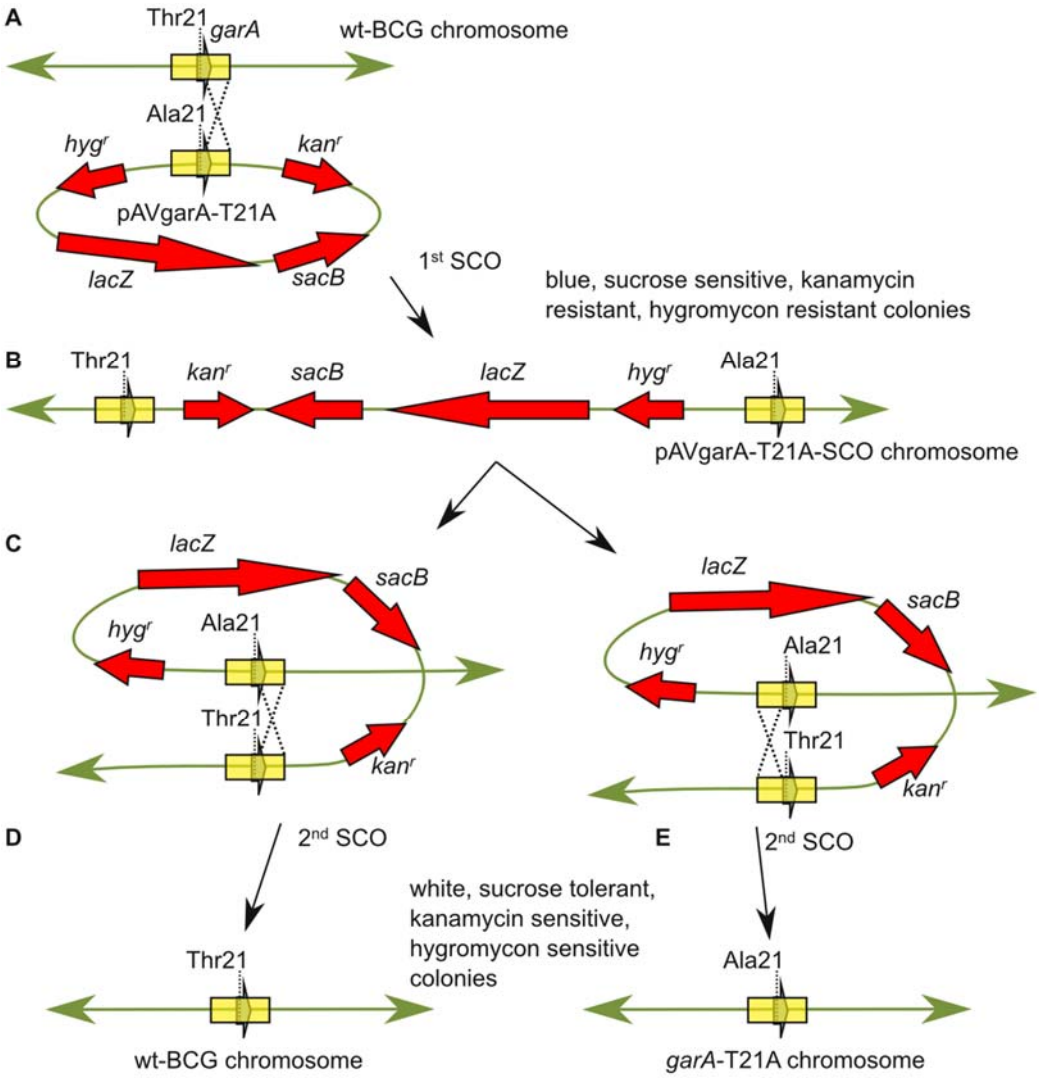

Figure 11: Use of two-step homologous recombination to generate *M. bovis* BCG *garA* T21A and T21V amino acid substitution mutants. A) *M. bovis* BCG was transformed with a suicide plasmid construct (pAVgarA-T21A or pAVgarA-T21V) containing a cloned fragment which flanked a *garA* copy with a T21A (or T21V) amino acid substitution by approximately 1 kb on either side. B) In a first single cross-over (SCO) step pAVgarA-T21A was integrated into the mycobacterial chromosome through homologous recombination upstream (U) or downstream (D) of the threonine 21 encoding codon of *garA* C) pAVgarA-T21A-SCO (or pAVgarA-T21V-SCO) colonies (kanamycin and hygromycin resistant) were isolated and cultured without selective pressure for the retention of pAVgarA-T21A which allowed a second SCO to occur. pAVgarA-T21A which could not replicate episomally was lost during cell divisions subsequent to the second SCO event. D) In the case where the second SCO occurred in the same homologous region that the first SCO event occurred in (downstream of threonine 21 in the figure) colonies with the wild type genotype were produced. E) In the case where the second SCO occurred in the opposite homologous region to the first SCO event (upstream of threonine 21 in the figure) colonies with the *garA* T21A amino acid substitution were produced. *kan*^{r} – kanamycin resistance cassette, *hyg*^{r}

– hygromycin resistance cassette, *sacB* – gene conferring sucrose sensitivity, *lacZ* – β-galactosidase cassette.

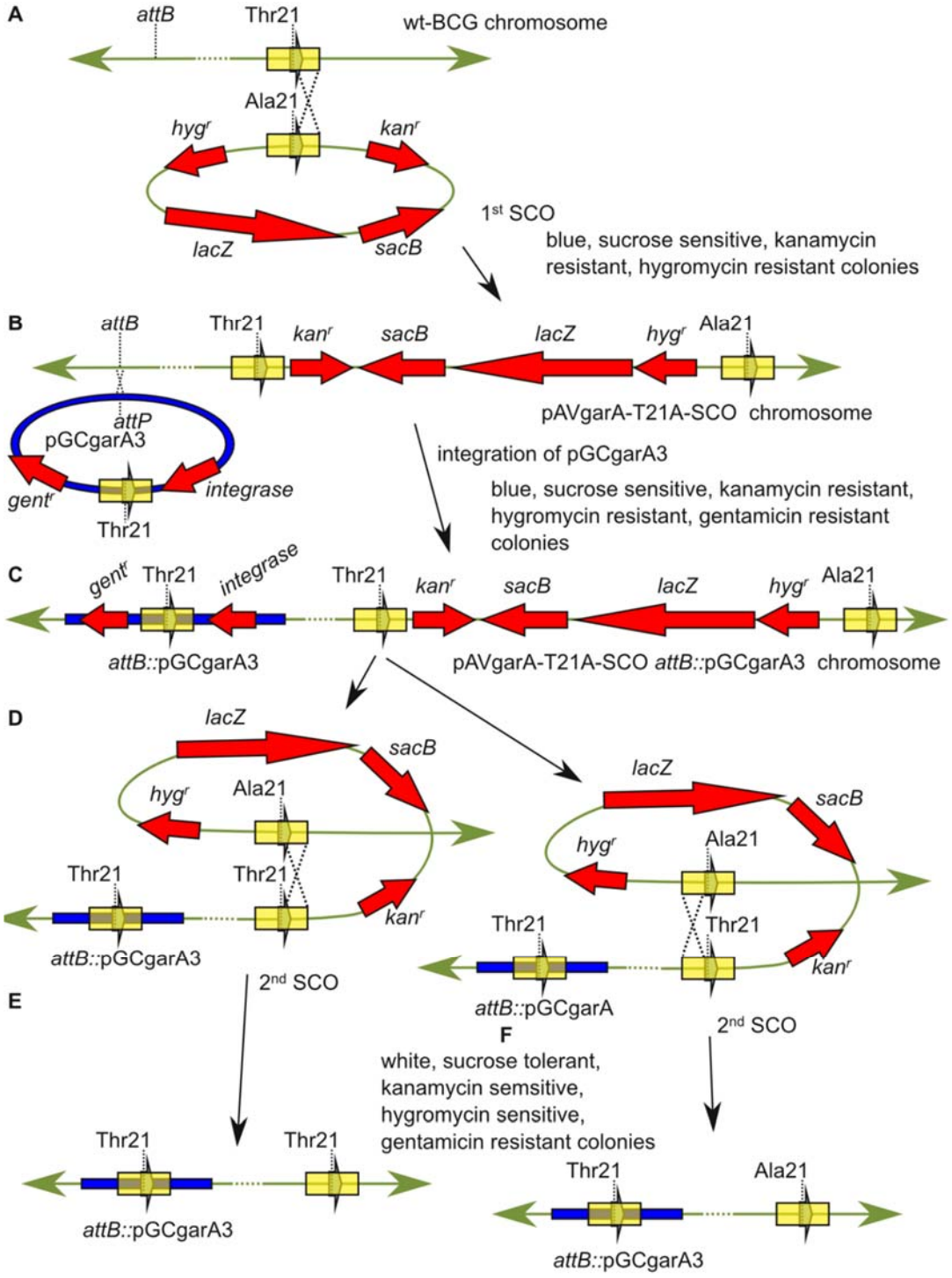

Figure 12: Use of a *garA*-complemented pAVgarA-T21A-SCO and pAVgarA-T21V-SCO strains to test whether the T21A and T21V amino acid substitutions in GarA could be generated in a *garA*-complemented background. A) In a first single cross-over (SCO) step pAVgarA-T21A or pAVgarA-T21V (not shown) was integrated into the mycobacterial chromosome through homologous recombination upstream (U) or downstream (D) of the threonine 21 encoding codon of *garA* B)

pAVgarA-T21A-SCO colonies were obtained and transformed with pGCgarA3 which was integrated at the attB site of the bacterial genome. C) pAVgarA-T21A-SCO *attB::pGCgarA3* colonies (kanamycin, hygromycin and gentamicin resistant) were isolated and cultured with selective pressure (gentamicin) for the retention of pGCgarA3, but without selective pressure for the retention of pAVgarA-T21A (kanamycin and hygromycin) which allowed a second SCO to occur. pAVgarA-T21A which could not replicate episomally was lost during cell divisions subsequent to the second SCO event. D) In the case where the second SCO occurred in the same homologous region that the first SCO event occurred in (downstream of threonine 21 in the figure) colonies with the wild type genotype as well as with a wild type copy of the garA gene integrated at the attB site were produced. E) In the case where the second SCO occurred in the opposite homologous region to the first SCO event (upstream of threonine 21 in the figure) merodiploid colonies with the *garA* Thr21Ala mutation as well as with a wild type copy of the garA gene integrated at the attB site were produced. *kan*^{r} – kanamycin resistance cassette, hyg^r – hygromycin resistance cassette, *sacB* – gene conferring sucrose sensitivity, *lacZ* – β-galactosidase cassette.

2.3 Conclusion

Despite a modest, but clear reciprocal regulation for GS in response to nitrogen limitation and excess, central nitrogen metabolism in *M. bovis* BCG was not regulated in the classical pattern generally observed for *E. coli* (see chapter 1, section 1.2.4.1). It is possible that nitrogen limitation acts as a signal for general nutrient starvation in *M. bovis* BCG, which is a well-documented stimulus for induction of a biochemical cascade of events involved in entry into a dormant growth phase (89, 144–147). The regulation of the enzymes of central nitrogen metabolism has not been investigated in great detail in response to the conditions which induce dormancy phase growth. However, many of the genes involved in the central nitrogen metabolism of *M. tuberculosis* including *glnR*, *garA*, *glnE*, *glnA1*, *gdh* and *gltD* were down-regulated in the Wayne model of dormancy and/or during infection of murine macrophages, while the ammonium transporter gene, *amt*, was up-regulated by these conditions (see Table 1). Down-modulation of general metabolism is a key feature of the dormant bacillus and has been used to explain the resistance of *M. tuberculosis* to chemotherapy during latent infection which requires an extensive duration of antituberculosis treatment often exceeding the disappearance of clinical signs of active disease (88). The regulation of *M. tuberculosis* central nitrogen metabolism is clearly more complex than that of *E. coli* and may be modulated by additional factors to

nitrogen limitation, which may include general nutrient limitation, oxygen limitation, oxidative stress, nitrosative stress, and low pH (12, 146–152).

The *M. bovis* BCG NAD^+-GDH exhibited features associated with an enzyme which plays an anabolic role, such as down-regulation of the enzyme under limiting concentrations of ammonium (see chapter 1, section 1.2.4.1) and very poor affinity of the enzyme for the catabolic reaction substrate glutamate. An anabolic function for NAD^+-GDH may be beneficial to *M. tuberculosis* under conditions where the high energy requirement of GS may be detrimental to cellular homeostasis, such as during latent infection (88, 96). On the other hand the enzyme was not induced by excess nitrogen and its activity was up-regulated in growth media where the catabolic function of the enzyme would be required. Although the remarkably poor affinity for glutamate of the L180 GDH present in the mycobacteria is unique to the genus, a catabolic function was also inferred for the L180 GDH studied in *S. clavuligerus* (56), *Pseudomonas aeruginosa* (59), *Psychrobacter sp.* TAD1 [55] and *Janthinobacterium lividum* (58). An interesting observation is the induction of GDH in *M. bovis* BCG when glutamate was both the sole nitrogen source and carbon source. In a recent TraSH study *gdh* was not detected as required for growth on cholesterol medium (10). However, an almost 30-fold under-representation of *M. tuberculosis* cells with transposon insertions in two sites of the *gdh* gene not required for growth in glycerol containing medium was reported ($p = 0.07$). This may implicate GDH function in carbon metabolism of *M. tuberculosis* during infection. Cholesterol is a preferred carbon source of *M. tuberculosis* in macrophages (118).

Chapter 3

The role of glutamine oxoglutarate aminotransferase and glutamate dehydrogenase in nitrogen metabolism and *ex vivo* growth of *M. bovis* BCG

3.1 Introduction

Maintenance of homeostatic glutamate levels by the effectors GOGAT and GDH may be an important factor of *M. tuberculosis* physiology and could be crucial to survival and growth of the pathogen inside host cells (see chapter 1, section 1.2). Although an exclusive role for GOGAT in the production of glutamate could be inferred from other studies (see chapter 1, section 1.2.2), enzymes such as aspartate aminotransferase and asparagine synthetase also catalyse reactions which result in the formation of glutamate (15–17). The importance of glutamate production by GOGAT in the presence of different nitrogen sources *in vitro* as well as during infection of macrophages remains to be determined. It was shown in chapter 2 (see section 2.2.5) that GDH was induced in *M. bovis* BCG in conditions when the enzyme would be required for its catabolic activity, however owing to the remarkably poor affinity of GDH for glutamate it remains unknown whether the function of the *gdh* protein product is mainly in the deamination or the production of glutamate or both. In addition to their respective roles in central nitrogen metabolism, the maintenance of glutamate homeostasis by GOGAT and GDH may be crucial to efficient functioning of cellular processes such as those involved in central carbon and energy metabolism and resistance to low pH (see chapter 1, section 1.4.2-3). Experimental enquiry is required to delineate the functions of GOGAT and GDH in the physiology of infecting pathogenic mycobacteria, including nitrogen source utilization and adaptation to the host stress responses.

3.2 Results and Discussion

3.2.1 Generation of an *M. bovis* BCG *ΔgltBD* mutant as well as a *ΔgltBD* genetically complemented strain

Recombineering was used to generate an *M. bovis* BCG strain in which the *gltBD* operon, was replaced with a hygromycin cassette (see chapter 5, section 5.4.8 and Figure 13).

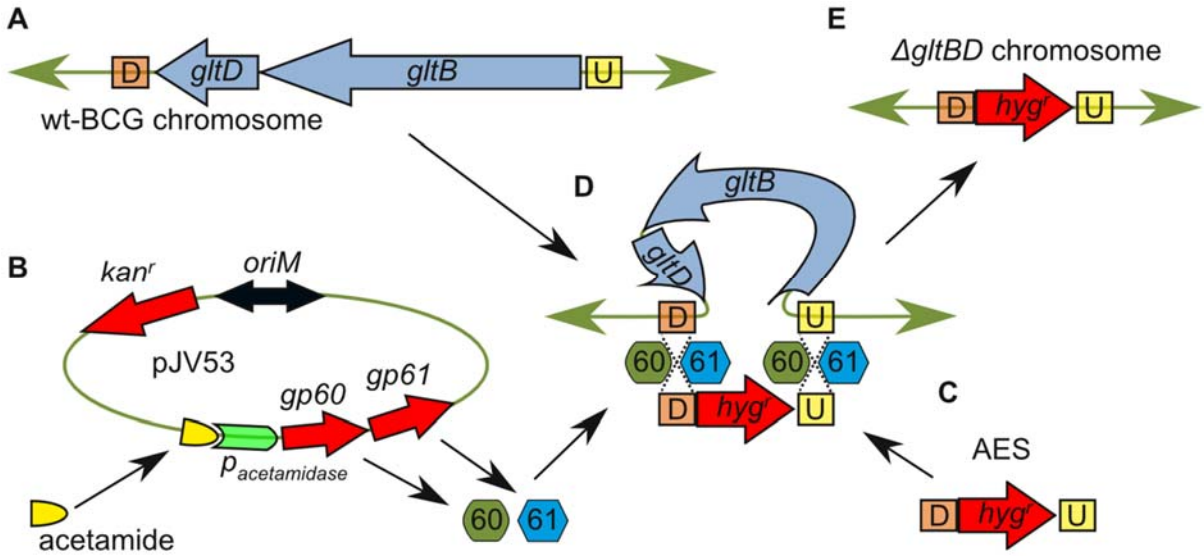

Figure 13: Generation of an *M. bovis* BCG strain in which the *gltBD* operon is replaced with a hygromycin resistance cassette. A) Sequences of approximately 500 bp directly upstream (U) and downstream (D) of the *gtlBD* operon were cloned and used to generate an allelic exchange substrate (AES) in which they flanked a hygromycin resistance cassette (*hyg*^{r}). B) Expression of the Che9c recombineering proteins Gp60 and Gp61 was induced in an *M. bovis* BCG strain carrying the self-replicating recombineering plasmid pJV53 (wt-BCG::pJV53). C) wt-BCG::pJV53 expressing Gp60 and Gp61 were electro-transformed with the AES. D) Homologous recombination between the U and D regions of the *gltBD* operon and the *hyg*^{r} casette in the AES was facilitated by Gp60 and Gp61. E) Hygromycin resistant colonies in which *gltBD* was replaced with the *hyg*^{r} casette, were isolated and analysed.

Hygromycin resistant mutant *ΔgltBD::hyg* (from here on reffered to as *ΔgltBD*) colonies were analysed genotypically by PCR (Figure 14) and by Southern blotting (Figure 15).

When a primer set was used which bound within *gltB*, an amplicon could be generated from wt-BCG template DNA (Figure 14C, lane 1), but not from template DNA prepared from two putative *ΔgltBD* colonies (Figure 14C, lanes 2 and 3). In addition, when a primer set was used to amplify a sequence that spans the *gltBD* operon as well as approximately 500 bp upstream (U) and downstream (D) of it, a 6 – 8 kb fragment (7 kb expected for wt-BCG) was observed when wt-BCG was used as PCR template (Figure 14C, lane 5) and a 2 – 2.5 kb fragment (2.4 kb expected for *ΔgltBD*) was observed when the two putative *ΔgltBD* colonies were used (Figure 14C, lanes 6 and 7).

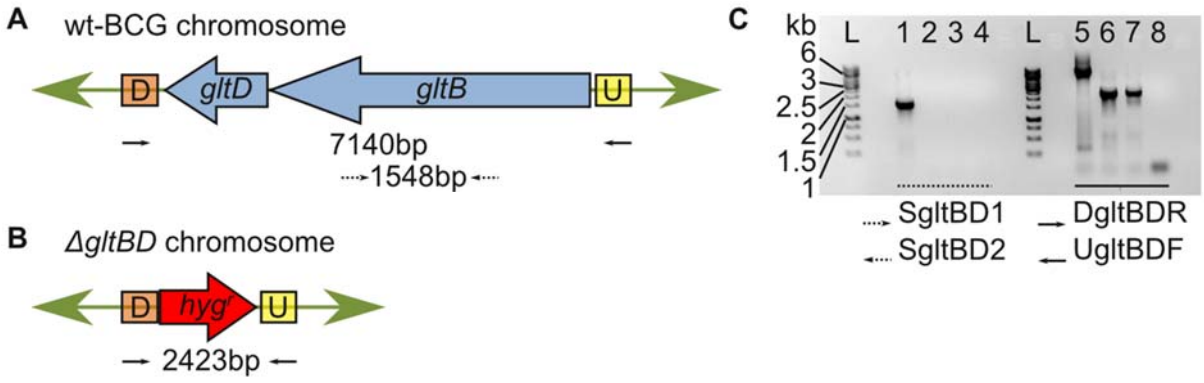

Figure 14: PCR analysis of hygromycin resistant putative *ΔgltBD::hyg* mutant colonies. A) Arrangement of genes in the *gltBD* operon of *M. bovis* BCG. B) Upstream (U) and downstream (D) regions of the *gltBD* operon in wt-BCG flank a hygromycin cassette (hyg^r) in the *ΔgltBD* mutant chromosome. C) Gel image showing differential amplification patterns obtained when PCR was performed using template prepared from wt-BCG and two putative hygromycin resistant *ΔgltBD* cultures and the primer sets indicated below the gel image. L – DNA marker, lanes 1 and 5 – wt-BCG, lanes 2 and 6 – putative *ΔgltBD* colony 1, lanes 3 and 7 – putative *ΔgltBD* colony 2, lanes 4 and 8 – no template controls. See Table 14 for SgltBD1, SgltBD2, DgltBDR and UgltBDF primer sequences.

When probes were used which hybridised in the 1639 bp *SphI* fragment spanning the start codon of *gltB*, or in the 6305 bp *SphI* fragment which spans the 3' portion of *gltB* as well as *gltD*, the corresponding fragments were observed in the Southern blot analysis of wt-BCG (Figure 15C, lanes 1 and 3). Southern blot analysis of genomic DNA prepared from a *ΔgltBD* mutant culture did not reveal either of these fragments, but did reveal a single fragment which corresponded to the 4065 bp *SphI* fragment which was expected for the *gltBD* hygromycin-replacement mutant (Figure 15C, lanes 2 and 4). Interestingly, *gltB* and *gltD* were found to be essential to *in vitro* growth of *M. tuberculosis* in four and three TraSH studies, respectively (see chapter 1, Table 1). The success in the generation of a *ΔgltBD* mutant *M. bovis* BCG strain in this study may indicate a physiological difference between less pathogenic *M. bovis* BCG and virulent *M. tuberculosis* H37Rv. It should be noted however that the *ΔgltBD* colonies were generally smaller than wt-BCG colonies and that growth of the *ΔgltBD* mutant on 7H11, which was used as solid culture medium throughout this study, appeared to be better than on 7H10, which has been the growth medium of preference in the TraSH studies (Figure 16). It is thus possible that *gltB* and *gltD* were determined essential in the TraSH studies because their transposon-insertion mutants were under-represented in the TraSH libraries due to a growth impairment on 7H10 medium.

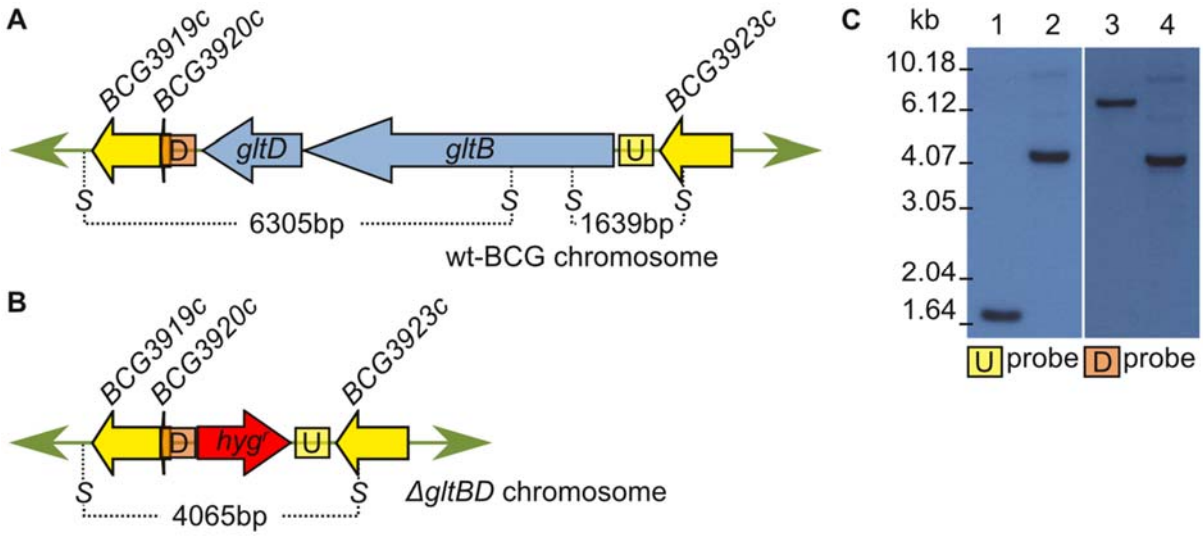

Figure 15: Confirmation of allelic exchange of *gltBD* with a hygromycin cassette (*hyg*^{r}) by Southern blot analysis of genomic DNA prepared from a single putative *ΔgltBD* mutant colony. A) Arrangement of genes in the chromosomal region of *M. bovis* BCG where *gltBD* is located. B) Arrangement of genes in the *ΔgltBD* mutant chromosomal region where the *hyg*^{r} cassette is located. C) Autoradiograph images of differential restriction endonuclease patterns obtained when DNA prepared from wt-BCG or *ΔgltBD* mutant was digested with *SphI* (*S*). Lanes 1 and 3 – wt-BCG, Lanes 2 and 4 – *ΔgltBD*, D – downstream, U- upstream.

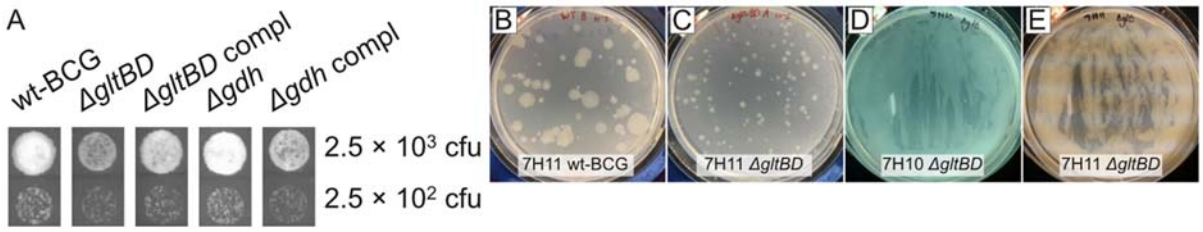

Figure 16: Growth of *ΔgltBD* on 7H10 and 7H11 agar. Bacteria cultured to mid-logarithmic growth phase (OD_{600} = 0.5 – 0.8, see chapter 5, section 5.3) were diluted to OD_{600} = 0.0005, passed 20 times through a 29GA needle (Becton Dickinson, USA), spotted (10 µl) onto 7H11 agar and incubated for 10 days at 37°C before the pictures were taken (A). Frozen stock cultures of wt-BCG and *ΔgltBD* were thawed and diluted 1:10^5 and plated on 7H11 agar (B and C) or streaked (undiluted) onto 7H10 (D) and 7H11 (E) agar plates. The plates in panel B - D were incubated for 25 days at 37°C before the pictures were taken.

The *ΔgltBD* strain was genetically complemented using the integrating vector pGCgltBD as described in chapter 5 (see section 5.4.9). Gentamicin resistant colonies

of the *ΔgltBD* mutant containing pGCgltBD were subjected to PCR analysis (Figure 17). When a primer set was used to amplify a fragment within *gltB*, the PCR amplicon could be detected both for wt-BCG (Figure 17D, lane 1) and for all three putative *ΔgltBD* complement colonies that were tested (Figure 17D, lanes 3 - 5). However, when a primer set was used which amplified a fragment flanking the 3'-portion of *gltD* as well as two genes downstream of *gltD* (not present in the complementation construct pGCgltBD), a PCR amplicon was only detected when wt-BCG was used as template (Figure 17D, lane 7). In addition, a primer which hybridised within the hygromycin cassette together with a primer which hybridised in the gene directly upstream of *gltB*, could generate an amplicon when the *ΔgltBD* strain (Figure 17D, lane 14) and all three putative *ΔgltBD* complement colonies (Figure 17D, lanes 15 - 17) were used as template.

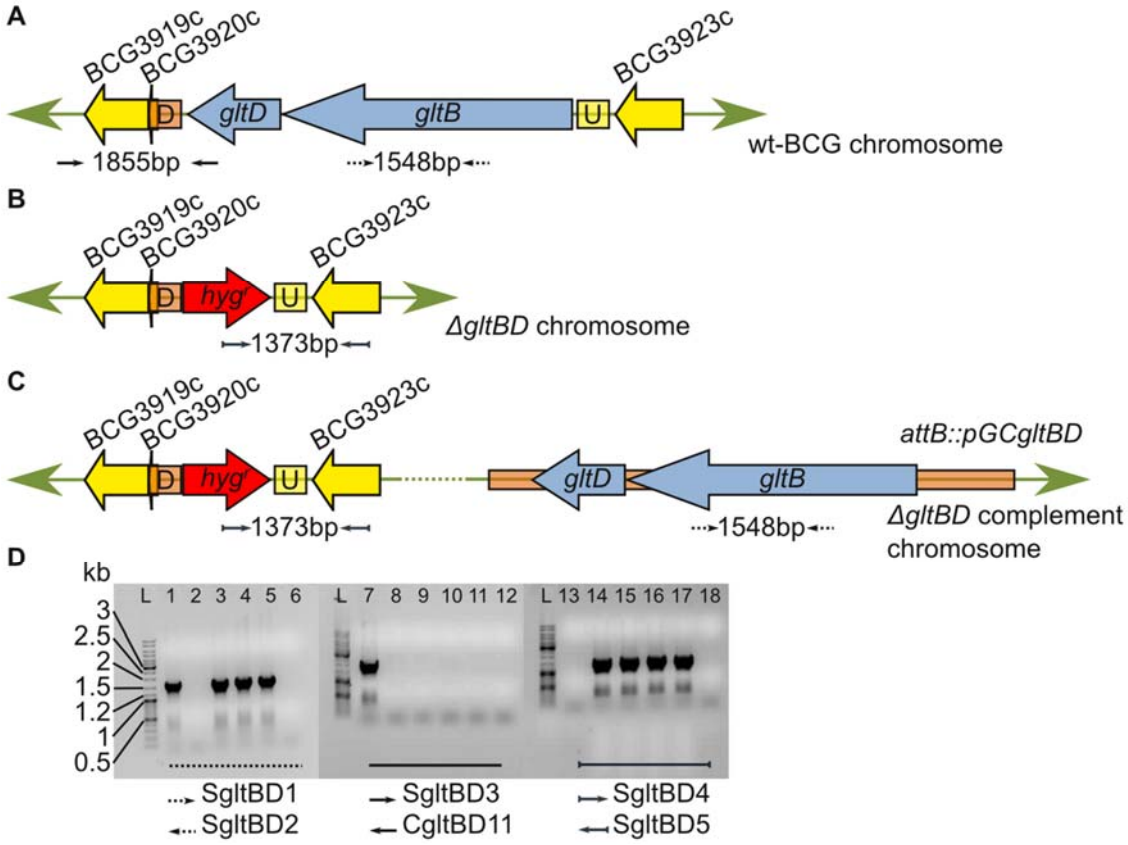

Figure 17. PCR analysis of gentamicin resistant putative *ΔgltBD* complement colonies. A) Arrangement of genes in the chromosomal region of *M. bovis* BCG where *gltBD* is located. B) Arrangement of genes in the *ΔgltBD* mutant chromosomal region where the *hyg*^{r} cassette is located. C) Arrangement of genes in the *ΔgltBD* complement chromosomal region where the *hyg*^{r} cassette is located and at the *attB* locus where pGCgltBD is integrated into the chromosome. D) Gel image showing differential amplification patterns obtained when PCR was performed (see chapter 5, section 5.5.4.2)

using template DNA prepared from wt-BCG, the *ΔgltBD* mutant and three putative gentamicin resistant *ΔgltBD* complement colonies (see chapter 5, section 5.5.2.1) and the primer sets indicated below the gel image. L – DNA marker, lanes 1, 7 and 13 – wt-BCG, lanes 2, 8 and 14 – *ΔgltBD*, lanes 3, 9 and 15 – putative *ΔgltBD* complement colony 1, lanes 4, 10 and 16 – putative *ΔgltBD* complement colony 2, lanes 5, 11 and 17 – putative *ΔgltBD* complement colony 3, lanes 6, 12 and 18 – no template control, D – downstream, U – upstream. See Table 14 for SgltBD1, SgltBD2, SgltBD3, CgltBD11, SgltBD4 and SgltBD5 primer sequences.

3.2.2 Generation of an *M. bovis* BCG *Δgdh* mutant as well as a *Δgdh* genetically complemented strain

The *M. bovis* BCG *gdh* gene was disrupted in a two-step homologous recombination process (see chapter 5, section 5.4.10), which resulted in a deletion of the sequence encoding for the GDH catalytic domains (Figure 18). It was reasoned that deletion of the catalytic domains within the *gdh* sequence would be sufficient to abolish GDH activity without inducing polar effects on the expression of the genes found downstream in an apparent operon with *gdh*, namely, *BCG_2495c* and *BCG_2494c* (http://www.broadinstitute.org/annotation/tbdb/operon/Rv2476c.html). Since L180 GDH was previously characterised in *S. clavuligerus* (56), *M. bovis* BCG *gdh* was compared to the *S. clavuligerus* GDH gene (*SCLAV_2088*) in order to identify the sequences potentially encoding for the catalytic domains of *M. bovis* BCG GDH. A protein blast of *SCLAV_2088* against *gdh* revealed 45% amino acid identity, 61% amino acid similarity (positivity) and 4% gaps for the total protein sequence, while 66% amino acid identity, 80% amino acid similarity and only 2% gaps were observed when only the *SCLAV_2088* sequence containing the GDH subdomain sequences was entered as the query sequence (Table 4). Moreover, it was observed that the *gdh* regions with high similarity to the GDH domain sequences in *SCLAV_2088* were located within an *NruI* fragment, which could be deleted without introducing a frame shift in the *gdh-BCG_2495c-BCG_2494c* reading frame.

White, sucrose tolerant double cross-over (pAVΔgdh-DCO) colonies were analysed genotypically by PCR in order to identify putative *Δgdh* colonies (Figure 19). A single *Δgdh* colony detected by PCR analysis was confirmed to carry a deletion of the *NruI* fragment containing the GDH domain sequences by Southern blotting analysis (Figure 20).

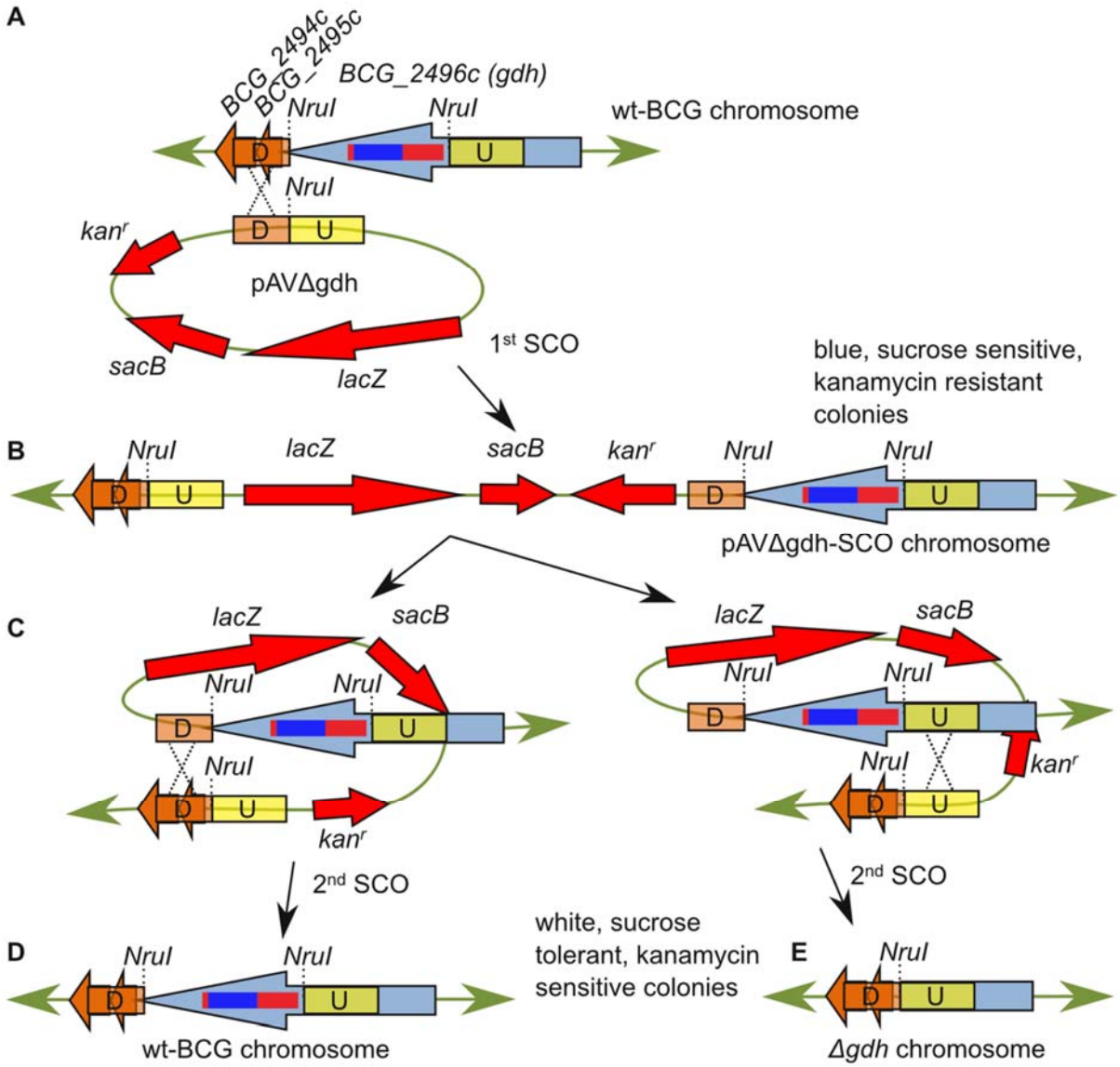

Figure 18: Generation of an *M. bovis* BCG strain with a deletion of the *NruI* fragment spanning the GDH catalytic subdomains in *gdh* by two-step homologous recombination. A) *M. bovis* BCG was transformed with a suicide plasmid construct (pAVΔgdh) containing cloned fragments of approximately 1 kb flanking the *NruI* fragment in *gdh* which contains the GDH catalytic subdomains. B) In a first single cross-over (SCO) step pAVΔgdh was integrated into the mycobacterial chromosome through homologous recombination upstream (U) or downstream (D) of the *NruI* fragment containing the GDH catalytic subdomains (red rectangles represent subdomain I and blue rectangle represents subdomain II). C) pAVΔgdh-SCO colonies (kanamycin resistant) were isolated and cultured without selective pressure for the retention of pAVΔgdh which allowed a second SCO to occur. pAVΔgdh which could not replicate episomally was lost during cell divisions subsequent to the second SCO event. D) In the case where the second SCO occurred in the same homologous region as in the first SCO event (the D region in the figure) colonies with the wild type genotype were produced. E) In the case where the second SCO occurred in the opposite homologous region to the first SCO event (the U region in the

figure) colonies with the *Δgdh* mutant genotype were produced. *kan*^{r} – kanamycin resistance cassette, *sacB* – gene conferring sucrose sensitivity, *lacZ* – β-galactosidase cassette.

Table 4. Alignment of *M. tuberculosis* H37Rv and *M. bovis* BCG *gdh* protein sequences to the GDH catalytic domain sequences for the *S. clavuligerus* gene encoding L_180 GDH which was previously characterized (56).

S. clav	533	LNAELGEERAAELLRRYGAAFPEGYKADPTPRAAVADLVHIEALAGSGRDFALSLYEPVG
H37Rv	498	AAAAG--SVGQADAMHYAAAFSEAYKQAVTPADAIGDIAVITELTDDSVKLVFSERDEQ-
BCG	498	AAAG--SVGQADAMHYAAAFSEAYKQAVTPADAIGDIAVITELTDDSVKLVFSERDEQ-
S. clav	711	QAGSPFSQDYMEDTLRTNVHTTRLLVSLFEARMAPERQ-RAGTELTDGLLEELDGALDQV
H37Rv	672	QAGFPYSQSYIESVLNEHPATVRSLVDLFEALFVPVPSGSASNRDAQAAAAAVAADIDAL
BCG	671	QAGFPYSQSYIESVLNEHPATVRSLVDLFEALFVPVPSGSASNRDAQAAAAAVAADIDAL
S. clav	770	ASLDEDRILRSFLTVIKATLRTNFFQGTTGDGVDGRHGYVSMKFDPQAIPDLPAPRPAYE
H37Rv	732	VSLDTDRILRAFASLVQATLRTNYFVTRQGS--ARCRDVLALKLNAQLIDELPLPRPRYE
BCG	731	VSLDTDRILRAFASLVQATLRTNYFVTRQGS--ARCRDVLALKLNAQLIDELPLPRPRYE
S. clav	830	IWVYSPRVEGVHLRFGKVARGGLRWSDRREDFRTEILGLVKAQMVKNTVIVPVGAKGGFV
H37Rv	790	IFVYSPRVEGVHLRFGPVARGGLRWSDRRDDFRTEILGLVKAQAVKNAVIVPVGAKGGFV
BCG	789	IFVYSPRVEGVHLRFGPVARGGLRWSDRRDDFRTEILGLVKAQAVKNAVIVPVGAKGGFV
S. clav	890	AKQLPDPS----VDRDAWLAEGIACYRTFISALLDITDNMVGG--EVVPPADVVRHDGDD
H37Rv	850	VKRPPLPTGDPAADRDATRAEGVACYQLFISGLLDVTDNVDHATASVNPPPEVVRRDGDD
BCG	849	VKRPPLPTGDPAADRDATRAEGVACYQLFISGLLDVTDNVDHATASVNPPPEVVRRDGDD
S. clav	944	TYLVVAADKGTASFSDIANEVALAYGFWLGDAFASGGSAGYDHKGMGITARGAWESVERH
H37Rv	910	AYLVVAADKGTATFSDIANDVAKSYGFWLGDAFASGGSVGYDHKAMGITARGAWEAVKRH
BCG	909	AYLVVAADKGTATFSDIANDVAKSYGFWLGDAFASGGSVGYDHKAMGITARGAWEAVKRH
S. clav	1004	FRELGHDTQTQDFTVVGVGDMSGDVFGNGMLLSEHIRLVAAFDHRHIFIDPAPDAATSYA
H37Rv	970	FREIGIDTQTQDFTVVGIGDMSGDVFGNGMLLSKHIRLIAAFDHRHIFLDPNPDAAVSWA
BCG	969	FREIGIDTQTQDFTVVGIGDMSGDVFGNGMLLSKHIRLIAAFDHRHIFLDPNPDAAVSWA
S. clav	1064	ERRRLFELPRSSWADYNKELLSAGGGIHPRTAKSIPVNAQVRAALGIEAGIT----KMTP
H37Rv	1030	ERRRMFELPRSSWSDYDRSLISEGGGVYSREQKAIPLSAQVRAVLGIDGSVDGGAAEMAP
BCG	1029	ERRRMFELPRSSWGDYDRSLISEGGGVYSREQKAIPLSAQVRAVLGIDGSVDGGAAEMAP
S. clav	1120	AELMRAILKAPVDLLWNRGIGTYVKASSESNADVGDKANDPIRVNGDELRVKVVGEGGNL
H37Rv	1090	PNLIRAILRAPVDLLFNGGIGTYIKAESESDADVGDRANDPVRVNANQVRAKVIGEGGNL
BCG	1089	PNLIRAILRAPVDLLFNGGIGTYIKAESESDADVGDRANDPVRVNANQVRAKVIGEGGNL
S. clav	1180	GLTQLGRIEFDRNGGKVNTDAIDNSAGVDTSDHEVNIKILLNALVTEGDLTLKQRNILLA
H37Rv	1150	GVTALGRVEFDLSGGRINTDALDNSAGVDCSDHEVNIKILIDSLVSAGTVKADERTQLLE
BCG	1149	GVTALGRVEFDLSGGRINTDALDNSAGVDCSDHEVNIKILIDSLVSAGTVKADERTQLLE
S. clav	1240	QMTDEVGALVLRNNYAQNVALANAVSQSTSLVHAHQRYLRKLVRDGALDRSLEFLPTDRQ
H37Rv	1210	SMTDEVAQLVLADNEDQNDLMGTSRANAASLLPVHAMQIKYLVAERGVNRELEALPSEKE
BCG	1209	SMTDEVAQLVLADNEDQNDLMGTSRANAASLLPVHAMQIKYLVAERGVNRELEALPSEKE

The *S. clavuligerus gdh* glutamate binding-region (sub-domain I) sequences are highlighted in red and the dinucleotide-binding (sub-domain II) sequence is highlighted in pink. Residues identified to form part of the catalytic mechanism of GDH in *S. clavuligerus* are highlighted in yellow. Only two differences exist between the protein sequences of the *M. tuberculosis* H37Rv and *M. bovis* BCG *gdh* homologues (highlighted in green), namely a deletion of the *M. tuberculosis gdh* Ala501 in *M. bovis* BCG and a substitution of the *M. tuberculosis gdh* Ser1041 to a glycine residue in *M. bovis* BCG.

When a primer was used which hybridised upstream of the region in *gdh* homologous to the U region in pAVΔgdh along with a primer which hybridised within the region in *gdh* homologous to the D region in pAVΔgdh, a 4653 bp fragment was amplified using wt-BCG (Figure 19E, lane 1), pAVΔgdh-SCO (Figure 19E, lane 3), pAVΔgdh-DCO colony 1 (Figure 19E, lane 5) or pAVΔgdh-DCO colony 2 (Figure 19E, lane 7) as template, while a 2166 bp fragment was generated when pAVΔgdh-DCO colony 3 was

used as template (Figure 19E, lane 9). When a primer was used which hybridised approximately 1 kb downstream of *gdh* along with a primer which hybridised 163 bp upstream of the central *NruI* site in *gdh* a 4003 bp amplicon was generated from wt-BCG template (Figure 19E, lane 2) or pAVΔgdh-DCO colony 2 (Figure 19E, lane 8) as template, while a 1516 bp amplicon was generated from pAVΔgdh-SCO (Figure 19E, lane 4), pAVΔgdh-DCO colony 1 (Figure 19E, lane 6) or pAVΔgdh-DCO colony 3 template (Figure 19E, lane 10). These results suggested that pAVΔgdh-DCO colony 1 retained the pAVΔgdh-SCO genotype, probably as a result of spontaneous tolerance to sucrose in this strain. A high rate of spontaneous resistance to sucrose was previously observed in a study using the same two-step homologous recombination technique (75). In addition, this PCR analysis revealed the wt-BCG genotype for pAVΔgdh-DCO colony 2 and the *Δgdh* mutant genotype for pAVΔgdh-DCO colony 3.

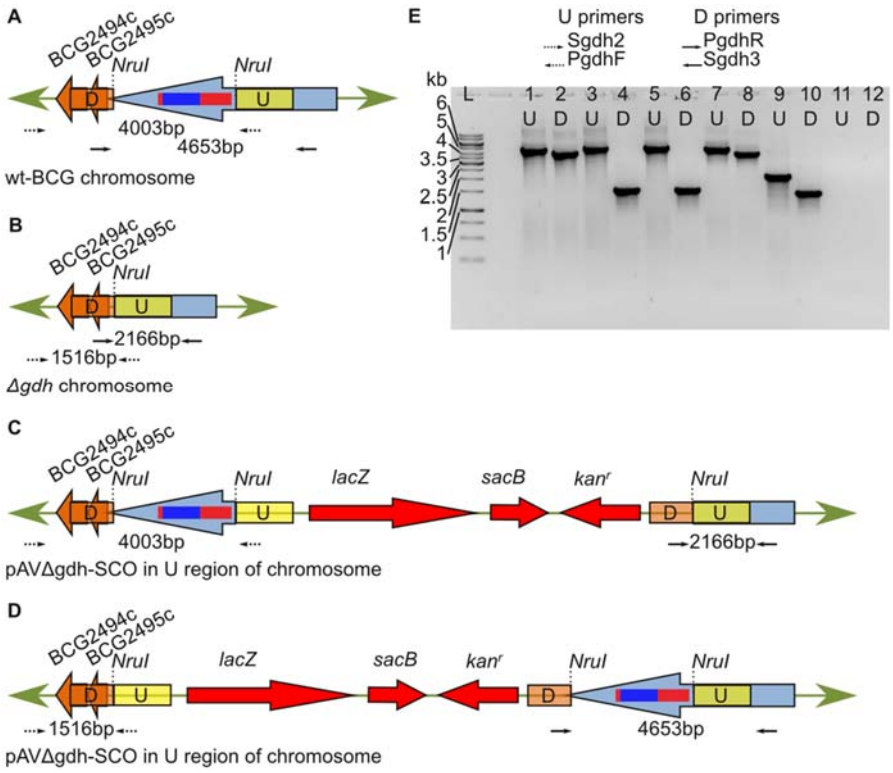

Figure 19: PCR analysis of white, sucrose tolerant, double cross-over (pAVΔgdh-DCO) colonies. A) Arrangement of genes in the chromosomal region of *M. bovis* BCG where *gdh* is located. B) Arrangement of genes in the *Δgdh* mutant chromosomal region where a disrupted version of *gdh* is located. C) Arrangement of genes in the wt-BCG SCO strain where homologous recombination between chromosal DNA and pAVΔgdh occurred in the region upstream (U) of the *NruI* cassette in *gdh* containing the GDH domain sequences. D) Arrangement of genes in the wt-BCG SCO strain where homologous recombination between chromosal DNA and pAVΔgdh occurred in the region downstream

(D) of the *NruI* cassette in *gdh* containing the GDH domain sequences. E) Gel image showing differential amplification patterns obtained when PCR was performed (see chapter 5, section 5.5.4.2) using template prepared from wt-BCG, pAVΔgdh-SCO strain culture and three white, sucrose tolerant putative *Δgdh* colonies (see chapter 5, section 5.5.2.1). L – DNA marker, lanes 1 & 2 – wt-BCG, lanes 3 & 4 – pAVΔgdh-SCO, lanes 5 & 6 – putative pAVΔgdh-DCO 1, lanes 6 & 8 – putative pAVΔgdh-DCO 2, lanes 9 & 10 – putative pAVΔgdh-DCO 3, lanes 11 & 12 – no template controls, D – downstream, U – upstream. See Table 14 for Sgdh2, PgdhF, PgdhR and Sgdh3 primer sequences.

When a probe was used which hybridised in the 6261 bp *KpnI* fragment spanning *gdh*, the corresponding fragment was observed in the Southern blot analysis of wt-BCG (Figure 20C, lane 1), but not of the *Δgdh* strain, in which a 3774 bp fragment was observed (Figure 20C, lane 2). It is noteworthy that *gdh* was found to be essential to *in vitro* growth of *M. tuberculosis* in four TraSH studies (see chapter 1, Table 1). As for the mutant *ΔgltBD* strain of *M. bovis* BCG generated in this study (see section 3.2.1), the success of generating a *gdh* knock-out strain may indicate a physiological difference between pathogenic *M. tuberculosis* and the less pathogenic vaccine *M. bovis* BCG. It appears that GOGAT and GDH are less important to the *in vitro* growth of *M. bovis* BCG than of *M. tuberculosis*. Further evidence of this physiological difference between *M bovis BCG* and *M. tuberculosis* may be found in the regulation of GOGAT and GDH by PknG (see chapter 1, section 1.2.4.3). PknG phosphorylates GarA, thereby abrogating both activation of GOGAT activity and inhibition of GDH activity (Nott *et al*., 2009; O'Hare *et al*., 2008). While deletion of the PknG gene in *M. tuberculosis* led to altered intracellular glutamine and glutamate levels (Cowley *et al*., 2004), no such phenotype was observed in the equivalent *M. bovis* BCG mutant (Nguyen *et al*., 2005).

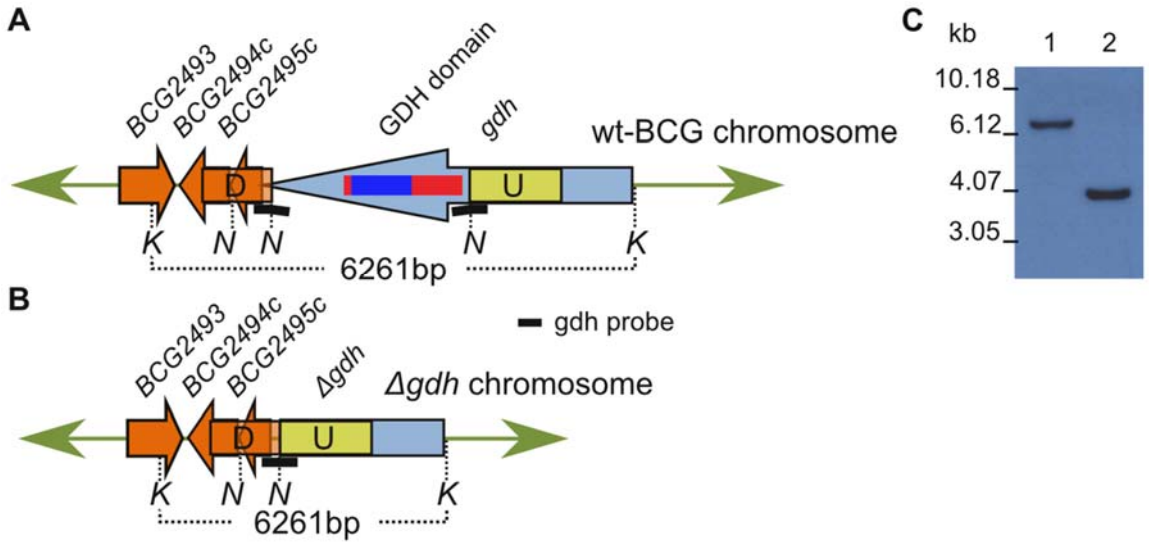

Figure 20: Confirmation of the deletion of the 2487 bp NruI fragment containing the GDH domain sequences by Southern blot analysis of genomic DNA prepared from a single putative *Δgdh M. bovis* BCG colony. A) Arrangement of genes in the chromosomal region of *M. bovis* BCG where *gdh* is located. B) Arrangement of genes in the *Δgdh* mutant chromosomal region where a disrupted version of *gdh* is located. C) Autoradiograph images of differential restriction endonuclease patterns obtained when DNA prepared from wt-BCG or the *Δgdh* mutant was digested with *NruI* (*N*). Note that the probe hybridises partially with the D and U sequences in wt-BCG. Lane 1 – wt-BCG, Lane 2 – *Δgdh*, D – downstream, U – upstream.

The *Δgdh* strain was genetically complemented using the integrative vector pGCgdh as described in section 5.4.9. Gentamicin resistant colonies of the *Δgdh* strain containing pGCgdh were subjected to PCR analysis (Figure 21). When a primer which hybridised 361 bp downstream of *gdh* was used along with a primer which hybridised within the *NruI* fragment containing the GDH domain sequences of *gdh*, a 1029 bp PCR product could be obtained when wt-BCG was used as template (Figure 21D, lane 2), but not when *Δgdh* (Figure 21D, lane 1) or a putative *Δgdh* complement colony (Figure 21D, lane 3) were used as templates. In addition, when the same primer which hybridised 361 bp downstream of *gdh* was used along with a primer which bound 163 bp upstream of the central *NruI* site in *gdh*, a 726 bp fragment could be amplified by PCR from *Δgdh* template (Figure 21D, lane 5) or the putative *Δgdh* complement colony (Figure 21D, lane 7), but not from wt-BCG template (Figure 21D, lane 6). However, when a left primer which bound in the 3'-distal portion of *gdh* was used along with two right primers, one which binds within the *NruI* fragment containing the GDH domain sequences of *gdh* and another which hybridised 163 bp upstream of the central *NruI*

site in *gdh*, a 670 bp PCR product could be obtained from wt-BCG template (Figure 21D, lane 10) or from the putative *Δgdh* complement colony (Figure 21D, lane 11), but not from *Δgdh* template (Figure 21D, lane 9). This produced a 373 bp amplicon which was also visible for the putative *Δgdh* complement colony (Figure 21D, lane 9).

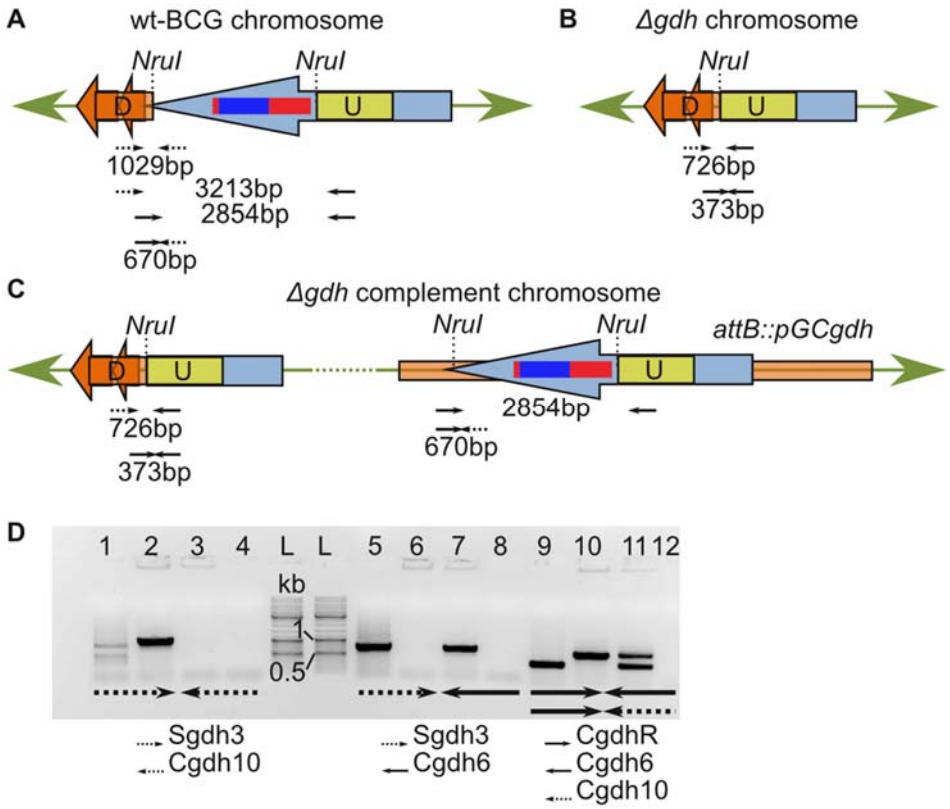

Figure 21: PCR analysis of putative gentamicin resistant *Δgdh* complement colonies. A) Arrangement of genes in the chromosomal region of *M. bovis* BCG where *gdh* is located. B) Arrangement of genes in the *Δgdh* mutant chromosomal region where the disrupted *gdh* is located. C) Arrangement of genes in the *Δgdh* complement chromosomal region where the disrupted *gdh* is located and at the *attB* locus where pGCgdh is integrated into the chromosome. D) Gel image showing differential amplification patterns obtained when PCR was performed using template prepared from wt-BCG, the *Δgdh* strain and one putative gentamicin resistant *Δgdh* complement colony (see chapter 5, section 5.5.2.1). Note that the PCR conditions used (elongation for 1 min) did not allow efficient elongation and amplification of the 3572 bp (wt-BCG) and 3213 bp (wt-BCG and *Δgdh* complement) fragments which may be amplified using the primer set Sgdh3 and Cgdh6 and the primer set CgdhR and Cgdh6, respectively. L – DNA marker, lanes 1, 5 and 9 – *Δgdh*, lanes 2, 6 and 10 – wt-BCG, lanes 3, 7 and 11 – putative *Δgdh* complement colony 1, lanes 4, 8 and 12 – putative *Δgdh* complement colony 2. D – downstream, U – upstream. See Table 14 for Sgdh3, Cgdh10, Sgdh3, Cgdh6, CgdhR, Cgdh6 and Cgdh10 primer sequences.

3.2.3 Enzymatic activity of GOGAT and GDH in the *ΔgltBD* and *Δgdh* mutants, respectively

It was observed that *ΔgltBD* mutant cultures did not grow to an OD_{600} which exceeded 0.60 in 7H9 (see chapter 3, section 3.2.5), therefore GOGAT specific activity was assayed in whole cell lysates prepared from wt-BCG, *ΔgltBD* mutant and *ΔgltBD* complement cultures grown in 7H9 to early exponential growth phase (OD_{600} = 0.3 – 0.5). As for wt-BCG (see chapter 2, section 2.2.2), no specific GOGAT activity was detected above background levels in either *ΔgltBD* or *ΔgltBD* complement strains using two different GOGAT assays (Table 5). It was earlier speculated that a failure to detect GOGAT activity may be due to oxygen sensitivity of the protein and rapid degradation of GOGAT activity during the preparation of whole cell lysates (see chapter 2, section 2.2.2).

It was found in this study that GDH expression may be induced by conditions where *M. bovis* BCG would require the enzyme for its catabolic activity (see chapter 2, section 2.2.5). Therefore, wt-BCG, the *Δgdh* mutant and the *Δgdh* complemented strain were cultured to exponential growth phase (OD_{600} = 0.5 – 0.9) in 7H9 which was supplemented with 10 mM L-Glu and whole cell lysates prepared for GDH specific activity determinations. In two further experiments, cultures of wt-BCG, *Δgdh* mutant and the *Δgdh* complemented strain in exponential growth phase (OD_{600} = 0.5 – 0.9) were either immediately used to prepare whole cell lysates for GDH specific activity measurements or washed twice with medium containing glutamate as sole nitrogen source (-N7H9 + 3 mM L-Glu, see section 5.3), suspended in -N7H9 + 3 mM Glu and incubated at 37°C for 24 hours before whole cell lysates were prepared for GDH specific activity assays. Although some low level GDH activity was detected in whole cell lysates prepared from the *Δgdh* strain cultured with 10 mM excess glutamate, GDH specific activity was effectively undetectable in whole cell lysates prepared form the *Δgdh* strain cultured in 7H9 or exposed to a condition where glutamate was the sole nitrogen source (Table 5). These results indicate that the major GDH activity in *M. bovis* BCG is performed by the protein product of *gdh*. However, GDH activity in whole cell lysates of the *Δgdh* complemented strain was approximately 0.025-fold to 0.100-fold of measurements in wt-BCG whole cell lysates. The low level of GDH specific activity detected in the *Δgdh* complemented strain may be due to low mRNA

expression, which was found to be 0.17-fold to 0.19-fold of wt-BCG in the *Δgdh* complemented strain (see section chapter 3, 3.2.7 and Table 9). It was reasoned that the *gdh* promoter sequences would lie within the 565 bp upstream sequence of *gdh* which was cloned along with the *gdh* open reading frame during the generation of the complementation construct, pGCgdh (see chapter 5, section 5.4.9). However, transcriptional regulators have been found to bind to DNA binding domains up to 1000 bp upstream of the transcription start site in *M. tuberculosis* (153). In addition, because *gdh* is the first gene in the *BCG_2496c – BCG_2494c* operon, it is possible that a termination of transcription sequence for the complete transcript containing the *gdh*-coding sequence is located only near the 3'-end of *BCG_2494c* and that transcription of *gdh* from pGCgdh, which does not contain *BCG_2495c* or *BCG_2494c*, is not efficiently terminated. Intrinsic terminators have been found downstream of several operons in *M. tuberculosis* H37Rv (154).

Table 5: Specific GOGAT or GDH activity in whole cell lysates of wt-BCG, *Δgdh* mutant, *Δgdh* complement, *ΔgltBD* mutant and *ΔgltBD* complement.

Strain	mU/mg protein	
	GOGAT	GDH
7H9		
wt-BCG	0.48 ± 0.31[1]	40.82 ± 6.26
	4.20 ± 8.58[2]	
ΔgltBD	0.52 ± 2.59[1]	
	-4.55 ± 7.88[2]	
ΔgltBD complement	0.84 ± 3.16[1]	
	-4.03 ± 14.76[2]	
*Δgdh****		0.39 ± 0.40
Δgdh complement***		1.06 ± 0.53
7H9 + 10 mM Glu		
wt-BCG		26.57 ± 5.07
*Δgdh****		1.77 ± 0.59
Δgdh complement***		1.22 ± 1.00
-N7H9 + 3 mM Glu		
wt-BCG		13.98 ± 3.12
*Δgdh****		-0.41 ± 0.73
Δgdh complement***		1.28 ± 0.98

Mean specific activity (mU/mg protein) ± standard deviation was calculated from triplicate culture data. Data was analysed by one way ANOVA with Bonferroni post-testing.

1. Meers *et al*. (1970) GOGAT assay (50 mM tris buffer, pH 7.6).....(133)
2. Miller & Stadtman (1972) GOGAT assay (100 mM NaH_2PO_4/K_2HPO_4 buffer, pH 7.0).....(134)

✶✶✶ - significantly different from wt-BCG $p < 0.001$

3.2.4 Growth of wt-BCG in 7H9 containing different nitrogen sources

In order to investigate the *in vitro* growth requirements of the *ΔgltBD* and *Δgdh* mutants, 7H9 (containing 3.4 mM L-Glu and 3.8 mM ammonium sulphate, see chapter 5, section 5.3, Table 11) and -N7H9 (see chapter 5, section 5.3, Table 11) was modified by supplementation with different nitrogen sources (Figure 22 and Table 6). Parameters of wt-BCG growth (A - maximal achieved growth see, R – maximal growth rate and L – lag time, see chapter 5, section 5.10) in the different media used in the study are given in Table 6.

Addition of excess (30 mM) L-aspartate to 7H9 led to an approximately 1.5-fold increase in the maximal growth rate of wt-BCG (Figure 22A, ◇). Although a similar trend was observed when moderate levels of (3 mM) L-aspartate were added to 7H9, this did not test significant (Table 6). Growth of wt-BCG was not different from unmodified 7H9 when excess L-asparagine (Figure 22A, △), L-glutamate (Figure 22A, ▽) or $(NH_4)SO_4$ (Figure 22B, □) was present. In a previous report it was found that *M. tuberculosis* H37Ra growth was suppressed when L-asparagine was added to medium containing glutamate (155). This was attributed to catabolite repression which resulted in inhibition of glutamate utilization by the bacterium. The present results may suggest that the mechanism on which the catabolite repression acts in *M. tuberculosis* is absent in *M. bovis* BCG. The growth of *M. bovis* BCG was also not different from 7H9 in -N7H9 supplemented with L-asparagine at moderate (3 mM; Figure 22D, ×) or excess (30 mM; Figure 22E, □) levels or when these media compositions were further supplemented with 3 mM L-glutamate (Figure 22D, □; Figure 22E, ◇), 4 mM $(NH_4)_2SO_4$ (Figure 22D, ◇; Figure 22E, ▽), 3 mM L-glutamine (Figure 22D, ▽) or 3 mM L-alanine (Figure 22D, △). This is in contrast with a previous report which found that *M. tuberculosis* H37Rv did not grow in medium supplemented with excess asparagine (74).

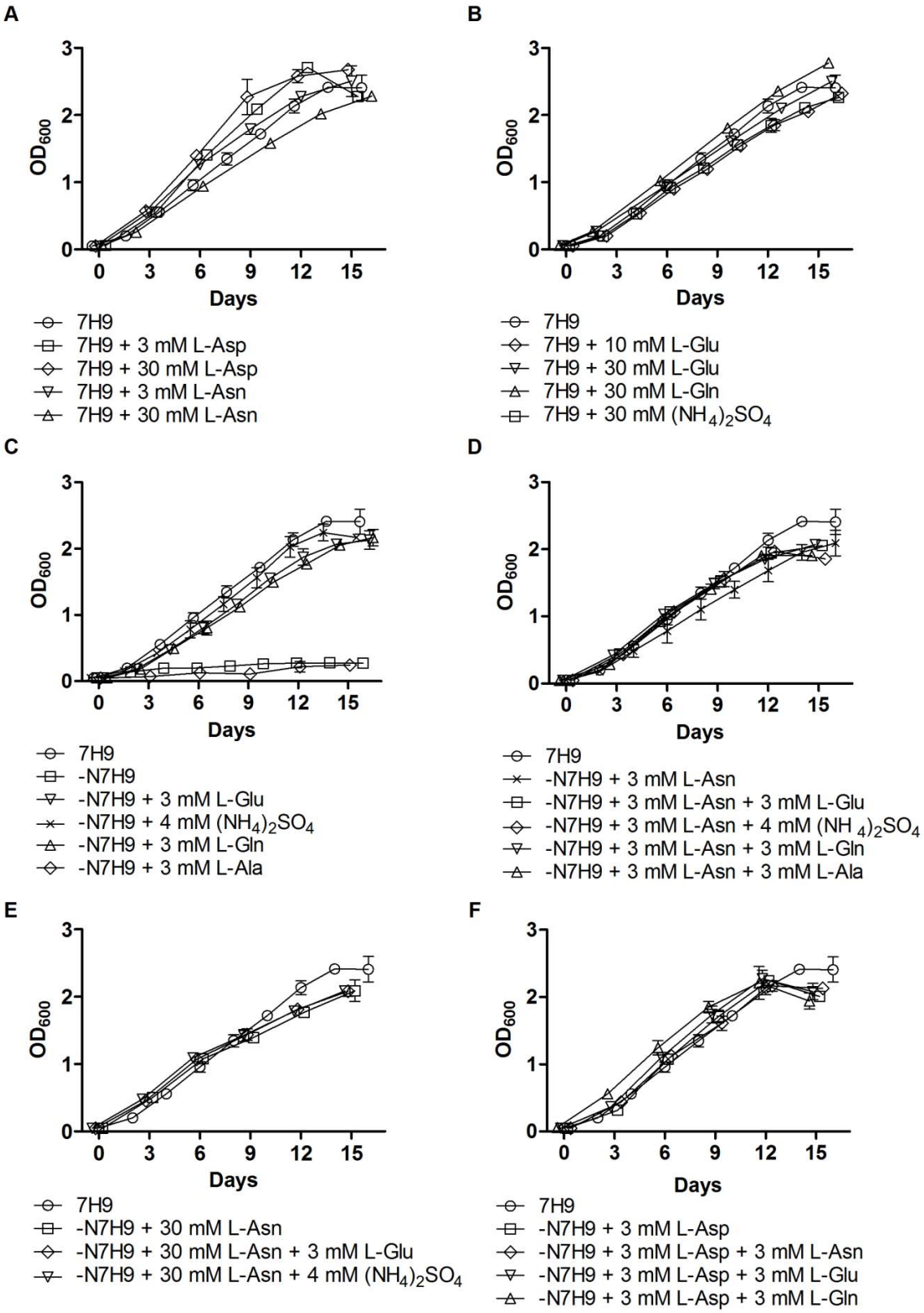

Figure 22: Growth of wt-BCG in 7H9 or nitrogen depleted 7H9 (–N7H9) media supplemented with moderate (3 – 4 mM) or excess (10 – 30 mM) levels of $(NH_4)_2SO_4$, L-glutamate, L-glutamine, L-asparagine, L-aspartate or L-alanine. A) 7H9 supplemented with moderate or excess levels of L-asparagine or L-aspartate. B) 7H9 supplemented with excess $(NH_4)_2SO_4$, L-glutamate or L-glutamine.

C) –N7H9 supplemented with moderate levels of $(NH_4)_2SO_4$, L-glutamate, L-glutamine or L-alanine. D) –N7H9 supplemented with moderate levels of L-asparagine in combination with moderate levels of $(NH_4)_2SO_4$, L-glutamate, L-glutamine, L-asparagine or L-alanine. E) –N7H9 supplemented with excess levels of L-asparagine in combination with moderate levels of $(NH_4)_2SO_4$ or L-glutamate. F) –N7H9 supplemented with moderate levels of L-aspartate in combination with moderate levels of L-asparagine, L-glutamate or L-glutamine. The data presented are the means and standard errors calculated from at least three independent growth curve experiments. In some instances error bars are smaller than the symbols.

Omission of the nitrogen sources present in 7H9 (3.4 mM L-Glu, 3.8 mM $(NH_4)SO_4$, and 0.15 mM ferric ammonium citrate) resulted in a severe growth defect (Figure 22C, □) with maximal growth achieved and maximal growth rate reduced almost 10-fold in comparison to growth in 7H9. Growth in media stripped of any nitrogen source was surprising. Remarkably high intracellular glutamate levels were reported for *M. tuberculosis* cultured in standard 7H9 (112). It could be that such high glutamate levels are also present in *M. bovis* BCG and act as a reservoir of nitrogen to the bacterium when it is completely starved of nitrogen in the extracellular medium.

Addition of $(NH_4)_2SO_4$, the amino acids L-Glu, L-Gln, L-Asn and L-Asp as well as different combinations of these nitrogen sources to –N7H9 restored both maximal achieved growth and maximal growth rate to that observed in 7H9 (Table 6).

Similarly to –N7H9 maximal achieved growth and maximal growth rate was severely affected in medium containing 3 mM L-Ala as sole nitrogen source (Figure 22C, ◇). This result is in line with a previous finding that *M. bovis* BCG cannot utilize alanine as a sole nitrogen source because of a frame-shift mutation in the gene that encodes alanine dehydrogenase (*ald*) and inhibition of GS by non-catabolised alanine (92).

Medium containing L-aspartate as sole nitrogen source (Figure 22F, □) or in combination with L-asparagine (Figure 22F, ◇), L-glutamate (Figure 22F, ▽) or L-glutamine (Figure 22F, △) could support wt-BCG growth comparable to 7H9.

Table 6: Parameters of wt-BCG growth in 7H9 and –N7H9 medium with different nitrogen sources normalized to growth in standard 7H9

	A	R	L
7H9			
unmodified			
+ 30 mM $(NH_4)_2SO_4$	0.95 ± 0.03^{ns}	0.82 ± 0.03^{ns}	0.69 ± 0.12^{ns}
+ 3 mM L-Asp	1.01 ± 0.02^{ns}	1.38 ± 0.06^{ns}	0.76 ± 0.02^{ns}
+ 30 mM L-Asn	1.06 ± 0.05^{ns}	0.78 ± 0.02^{ns}	0.62 ± 0.08^{ns}
+ 10 mM L-Glu	1.08 ± 0.03^{ns}	0.77 ± 0.02^{ns}	0.61 ± 0.03^{ns}
+ 30 mM L-Asp	1.16 ± 0.02^{ns}	1.40 ± 0.24*	0.65 ± 0.32^{ns}
+ 3 mM L-Asn	1.20 ± 0.18^{ns}	0.99 ± 0.06^{ns}	0.45 ± 0.10^{ns}
+ 30 mM L-Glu	1.20 ± 0.03^{ns}	0.83 ± 0.06^{ns}	0.83 ± 0.30^{ns}
+ 30 mM L-Gln	1.22 ± 0.02^{ns}	1.00 ± 0.02^{ns}	1.10 ± 0.23^{ns}
-N7H9			
unmodified	0.12 ± 0.01***	0.17 ± 0.06***	-0.71 ± 0.27***
+ 3 mM L-Ala	0.12 ± 0.06***	0.08 ± 0.03***	-0.28 ± 0.56***
+ 3 mM L-Asn + 3 mM L-Ala	0.73 ± 0.02**	1.02 ± 0.10^{ns}	0.99 ± 0.05^{ns}
+ 3 mM L-Asn + 3 mM L-Glu	0.76 ± 0.02*	0.98 ± 0.08^{ns}	0.66 ± 0.04^{ns}
+ 3 mM L-Asn + 3 mM L-Gln	0.76 ± 0.02*	0.95 ± 0.07^{ns}	0.62 ± 0.03^{ns}
+ 30 mM L-Asn + 3 mM L-Glu	0.80 ± 0.02^{ns}	0.86 ± 0.02^{ns}	0.44 ± 0.04^{ns}
+ 30 mM L-Asn + 4 mM $(NH_4)_2SO_4$	0.80 ± 0.02^{ns}	0.84 ± 0.03^{ns}	0.32 ± 0.01^{ns}
+ 3 mM L-Asn + 4 mM $(NH_4)_2SO_4$	0.80 ± 0.01^{ns}	0.97 ± 0.11^{ns}	0.58 ± 0.09^{ns}
+ 30 mM L-Asn	0.81 ± 0.04^{ns}	0.80 ± 0.03^{ns}	0.27 ± 0.08^{ns}
+ 3 mM L-Asn	0.85 ± 0.06^{ns}	0.77 ± 0.02^{ns}	0.85 ± 0.10^{ns}
+ 3 mM L-Asp + 3 mM L-Gln	0.86 ± 0.08^{ns}	1.19 ± 0.11^{ns}	0.65 ± 0.07^{ns}
+ 3 mM L-Asp	0.88 ± 0.02^{ns}	1.22 ± 0.05^{ns}	1.01 ± 0.05^{ns}
+ 3 mM L-Asn + 3 mM L-Asp	0.89 ± 0.05^{ns}	1.02 ± 0.10^{ns}	0.67 ± 0.12^{ns}
+ 3 mM L-Gln	0.87 ± 0.06^{ns}	0.82 ± 0.03^{ns}	0.88 ± 0.10^{ns}
+ 3 mM L-Asp + 3 mM L-Glu	0.90 ± 0.04^{ns}	1.21 ± 0.12^{ns}	0.92 ± 0.05^{ns}
+ 3 mM L-Glu	0.89 ± 0.07^{ns}	0.87 ± 0.03^{ns}	0.92 ± 0.16^{ns}
+ 4 mM $(NH_4)_2SO_4$	0.93 ± 0.04^{ns}	0.99 ± 0.04^{ns}	1.28 ± 0.02^{ns}

Data presented are the means and standard errors calculated from growth parameters estimated by modelling growth curve data from three independent experiments. Comparisons made between conditions were analysed by one-way ANOVA with Bonferroni post-testing. ✶ - $p < 0.05$, ✶✶ - $p < 0.01$, ✶✶✶ - $p < 0.001$, ^{ns} non-significant, A – maximal attained growth, R – maximal growth rate, L – lag time (see chapter 5, section 5.10)

3.2.5 *In vitro* growth phenotypes of the *ΔgltBD* mutant

Growth parameters of *ΔgltBD* in 7H9 or nitrogen depleted 7H9 (–N7H9) supplemented with different nitrogen sources are given in Table 7.

The maximal growth attained by the *ΔgltBD* mutant was approximately 20% of wt-BCG levels in standard 7H9 (Figure 23A, ▽), which contains 3.4 mM L-glutamate and 3.8

mM $(NH_4)_2SO_4$, suggesting that glutamate production by the *gltBD* protein product is important for growth even when exogenous glutamate is supplied.

Maximal growth achieved or maximal growth rate remained significantly lower than wt-BCG levels in 7H9 medium supplemented with moderate (3 mM) levels of L-asparagine (Figure 26B, ▽) or L-aspartate (Figure 23C, ▽) and excess (30 mM) levels of L-asparagine (Figure 26A, ▽). Since GDH can catalyse the reductive amination of 2-oxoglutarate to produce glutamate, it was hypothesised that excess ammonium would complement glutamate auxotrophy through GDH activity. However, supplementation of 7H9 with 30 mM $(NH_4)_2SO_4$ (Figure 23B, ▽) did not ameliorate the poor growth of the mutant, suggesting that GDH does not play a role in the fixation of ammonium or the production of glutamate in *M. bovis* BCG. Interestingly, the maximal growth rate of the *ΔgltBD* complemented strain was increased by 32% relative to wt-BCG in 7H9 supplemented with excess L-asparagine (Figure 26A, ◇) and maximal growth achieved was increased by almost 50% relative to wt-BCG in -N7H9 containing excess L-asparagine (Figure 26F, ◇). This observation may be a result of differential expression of the *gltBD* gene products from the *gltBD* complementation construct, pGCgltBD, and may implicate regulation of the *gltBD* gene product in the rate at which asparagine is metabolised in *M. bovis* BCG.

Both maximal growth achieved and maximal growth rate of *ΔgltBD* was not significantly different from that of wt-BCG in 7H9 supplemented with 10 mM (Figure 23F, ▽) or 30 mM L-glutamate (Figure 23D, ▽) or 30 mM L-aspartate (Figure 23E, ▽). Interestingly, while maximal growth of the *ΔgltBD* mutant was approximately 60% of wt-BCG levels in 7H9 supplemented with 3 mM L-aspartate (Figure 23C, ▽) compared to only 30% of wt-BCG levels in –N7H9 supplemented with 3 mM L-glutamate, maximal growth achieved of the mutant was not significantly different from wt-BCG in –N7H9 supplemented with 3 mM L-aspartate. It thus appears that while growth of the *ΔgltBD* mutant was better in medium containing both aspartate and glutamate than when glutamate was the sole nitrogen source, growth was best when aspartate was the sole nitrogen source. It could be speculated that the extracellular L-glutamate in 7H9 inhibits efficient uptake of L-aspartate which may explain why only a partial increase in maximal growth achieved relative to wt-BCG levels was seen when this medium was supplemented with additional L-aspartate. The presence of three

genes putatively encoding for aspartate aminotransferases in the *M. tuberculosis* genome (see Chapter 1, Table 1) illustrates the close relationship between aspartate and glutamate metabolism in this organism. A protein blast revealed that homologues to *aspB*, *aspC* and *Rv3722c* are present in *M. bovis* BCG (http://blast.ncbi.nlm.nih.gov/Blast.cgi). In addition, it was illustrated that *ansP1* encodes an aspartate permease in *M. tuberculosis* (see chapter 1, section 1.3.2). It is possible that the glutamate present in 7H9 has an inhibitory effect on the uptake of L-aspartate by AnsP1. It was found that a high affinity aspartate tranporter in *E. coli* is weakly inhibited by L-glutamate (156).

Both maximal growth achieved and maximal growth rate of the *ΔgltBD* mutant were less than 10% of wt-BCG levels in –N7H9 medium containing 4 mM $(NH_4)_2SO_4$ as sole nitrogen source (Figure 23H). Moreover, cfu determination showed that *ΔgltBD* growth was static in this medium (Figure 25B, ▽). Full chemical complementation determined by cfu determination was achieved at 3 mM (Figure 25B, □) or 10 mM (Figure 25B, ○) L-glutamate levels, but not at 0.3 mM (Figure 25B, △). Interestingly, this was not reflected at a spectrophotometric level where maximal growth achieved and maximal growth rate of the *ΔgltBD* mutant cultured with 3 mM L-glutamate (Figure 25A, □) was approximately 50% of 10 mM L-glutamate culture levels (Figure 25A, ○, Table 8). This may have been due to bacterial clumping, which is characteristic of the mycobacteria or it may have been related to the morphology of the bacteria in response to the stress of nutrient limitation. Although morphology of the bacteria was not investigated at the time of the growth curve determinations it was observed with Ziehl-Neelsen staining and microscopy (see chapter 5, section 5.3) of frozen stock cultures of the *ΔgltBD* mutant that the bacilli appeared to be shorter rods compared to wt-BCG (Figure 24). It was previously shown that *M. tuberculosis* bacilli become shorter as they enter stationary phase and may thus act as a morphological marker of stresses encountered during stationary phase growth such as nutrient limitation (157).

Table 7: *ΔgltBD* mutant and complemented strain growth characteristics normalized to wt-BCG

	ΔgltBD			*ΔgltBD* complement		
	A	**R**	**L**	**A**	**R**	**L**
7H9 (4 mM $(NH_4)_2SO_4$ + 3 mM L-Glu)						
unmodified	$0.25 \pm 0.05^{***}$	0.65 ± 0.31^{ns}	0.33 ± 0.14^{ns}	1.03 ± 0.09^{ns}	1.01 ± 0.15^{ns}	0.93 ± 0.07^{ns}
+ 30 mM $(NH_4)_2SO_4$	$0.29 \pm 0.05^{***}$	$0.66 \pm 0.19^{*}$	0.47 ± 0.23^{ns}	1.01 ± 0.23^{ns}	0.96 ± 0.15^{ns}	0.70 ± 0.11^{ns}
+ 3 mM L-Asn	$0.40 \pm 0.14^{**}$	0.84 ± 0.24^{ns}	0.34 ± 0.78^{ns}	0.93 ± 0.22^{ns}	1.27 ± 0.21^{ns}	1.44 ± 1.18^{ns}
+ 3 mM L-Asp	$0.56 \pm 0.09^{**}$	$0.54 \pm 0.05^{***}$	$0.21 \pm 0.47^{*}$	0.97 ± 0.09^{ns}	1.05 ± 0.05^{ns}	1.06 ± 0.11^{ns}
+ 30 mM L-Asn	$0.63 \pm 0.18^{**}$	0.92 ± 0.16^{ns}	0.08 ± 1.06^{ns}	0.81 ± 0.32^{ns}	$1.32 \pm 0.26^{**}$	0.84 ± 0.37^{ns}
+ 30 mM L-Glu	0.88 ± 0.08^{ns}	1.12 ± 0.17^{ns}	0.51 ± 0.68^{ns}	0.86 ± 0.37^{ns}	1.21 ± 0.32^{ns}	0.38 ± 0.06^{ns}
+ 30 mM L-Asp	0.91 ± 0.53^{ns}	0.77 ± 0.25^{ns}	0.84 ± 0.43^{ns}	0.75 ± 0.23^{ns}	1.12 ± 0.30^{ns}	1.09 ± 0.41^{ns}
+ 10 mM L-Glu	0.98 ± 0.10^{ns}	1.01 ± 0.11^{ns}	1.07 ± 0.31^{ns}	1.01 ± 0.06^{ns}	1.01 ± 0.16^{ns}	0.87 ± 0.73^{ns}
-N7H9						
unmodified	$0.31 \pm 0.08^{**}$	0.57 ± 0.40^{ns}	1.57 ± 0.96^{ns}	1.05 ± 0.11^{ns}	1.18 ± 0.25^{ns}	1.03 ± 0.65^{ns}
+ 4 mM $(NH_4)_2SO_4$	$0.05 \pm 0.03^{***}$	$0.08 \pm 0.01^{***}$	0.43 ± 3.63^{ns}	1.03 ± 0.09^{ns}	0.96 ± 0.16^{ns}	0.84 ± 0.23^{ns}
+ 3 mM L-Gln	$0.15 \pm 0.04^{***}$	$0.18 \pm 0.02^{***}$	$-0.20 \pm 0.46^{*}$	1.11 ± 0.24^{ns}	0.97 ± 0.28^{ns}	0.74 ± 0.97^{ns}
+ 3 mM L-Asn	$0.25 \pm 0.07^{***}$	0.74 ± 0.05^{ns}	0.46 ± 0.32^{ns}	1.17 ± 0.31^{ns}	0.95 ± 0.22^{ns}	0.77 ± 1.05^{ns}
+ 3 mM L-Glu	$0.30 \pm 0.13^{***}$	0.61 ± 0.39^{ns}	0.36 ± 0.37^{ns}	0.97 ± 0.15^{ns}	1.01 ± 0.29^{ns}	0.91 ± 0.50^{ns}
+ 30 mM L-Asn	$0.56 \pm 0.06^{*}$	0.81 ± 0.06^{ns}	-0.19 ± 1.02^{ns}	$1.49 \pm 0.74^{*}$	1.05 ± 0.13^{ns}	1.64 ± 0.59^{ns}
+ 3 mM L-Asp	0.74 ± 0.29^{ns}	0.67 ± 0.36^{ns}	1.02 ± 0.18^{ns}	1.09 ± 0.20^{ns}	1.10 ± 0.47^{ns}	1.00 ± 0.10^{ns}
+ 3 mM L-Asp + 3 mM L-Gln	1.10 ± 0.26^{ns}	$0.67 \pm 0.16^{*}$	$2.58 \pm 0.36^{**}$	1.17 ± 0.31^{ns}	0.93 ± 0.26^{ns}	1.05 ± 0.39^{ns}

Data presented are the means and standard errors calculated from growth parameters estimated by modelling growth curve data from three independent experiments. Comparisons made between strains were analysed by one-way ANOVA with Bonferroni post-testing. ✶ - $p < 0.05$, ✶✶ - $p < 0.01$, ✶✶✶ - $p < 0.001$, ns - non-significant, A – maximal attained growth, R – maximal growth rate, L – lag time (see chapter 5, section 5.10)

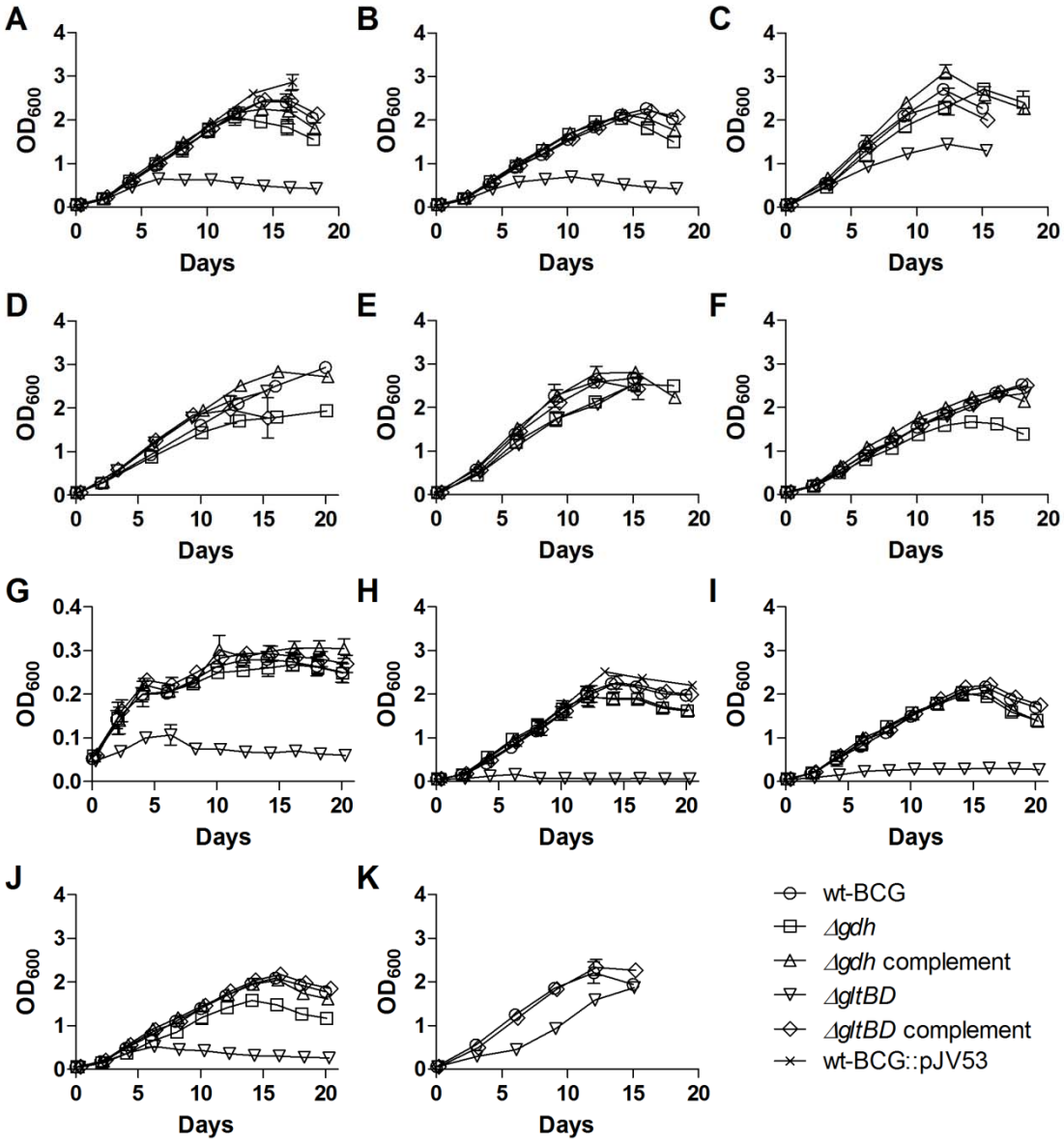

Figure 23: Growth of the *ΔgltBD* and *Δgdh* mutant and complemented strains in 7H9 or nitrogen depleted 7H9 (–N7H9) media supplemented with nitrogen sources in which the growth of the *ΔgltBD* mutant was poorest relative to wt-BCG growth. A) 7H9. B) 7H9 + 30 mM $(NH_4)_2SO_4$. C) 7H9 + 3 mM L-Asp. D) 7H9 + 30 mM L-Glu. E) 7H9 + 30 mM L-Asp. F) 7H9 + 10 mM L-Glu. G) –N7H9. H) –N7H9 + 4 mM $(NH_4)_2SO_4$. I) –N7H9 + 3 mM L-Gln. J) –N7H9 + 3 mM L-Asn. K) –N7H9 + 3 mM L-Gln + 3 mM L-Asp. The data presented are the means and standard errors calculated from at least three independent growth curve experiments. In some instances error bars are smaller than the symbols.

Maximal growth achieved by the *ΔgltBD* mutant was 30%, 25% and 15% of wt-BCG levels when L-glutamine (Figure 23I, ▽), L-asparagine (Figure 23J, ▽) or L-glutamate (Figure 26D, ▽) were the sole nitrogen sources, respectively. Interestingly, while a more than two-fold increase in lag-time and more than 30% reduction in maximal

growth rate relative to wt-BCG were observed for the *ΔgltBD* mutant in -N7H9 supplemented with L-glutamine and L-aspartate, maximal growth achieved was not different between the *ΔgltBD* mutant and wt-BCG. Glutamate synthesis from glutamine could be catalysed by the asparagine synthetase encoded by *asnB*, but this would require aspartate as a substrate which may explain the suppression of the *ΔgltBD* mutant's growth when L-glutamine is the sole nitrogen source and the chemical complementation of further supplementation with L-aspartate.

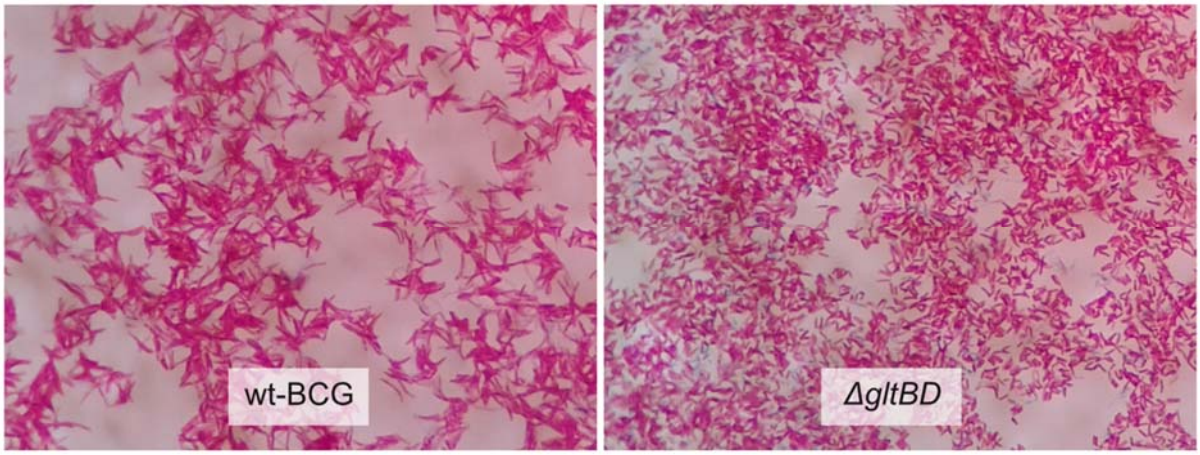

Figure 24: Microscopic view of Ziehl-Neelsen stained wt-BCG and *ΔgltBD* cells. Frozen stock cultures were thawed, stained according to the Ziehl-Neelsen method (see chapter 5, section 5.3) and viewed under a light microscope at 400×.

While the other strains investigated in this study grew exponentially for a short duration when cultured in 7H9 media stripped of all nitrogen sources, growth of the *ΔgltBD* mutant (Figure 23G, ▽) was inhibited, suggesting that glutamate production by GOGAT may support some growth under these conditions. Interestingly, in an earlier study of *M. tuberculosis* growth as a function of the nutrient ammonium's availability, marginal growth (measured by OD) was observed in the total absence of ammonium (158). It was speculated earlier that the marginal growth of wt-BCG in the absence of nitrogen sources may be explained by the high intracellular glutamate levels which has been reported in *M. tuberculosis* (see section 3.2.4), which may act as a reservoir nitrogen source. It is possible that in the absence of glutamate production by GOGAT in the *ΔgltBD* mutant the intracellular glutamate pool is more rapidly depleted under conditions of nitrogen starvation and not even the marginal growth observed for the other strains investigated in this study could be achieved.

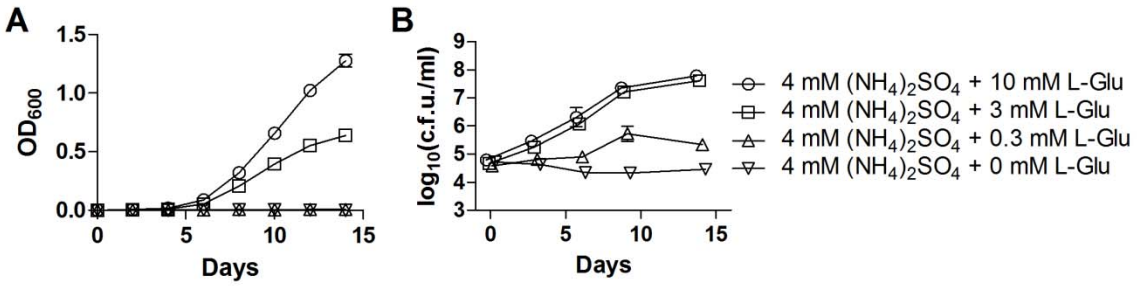

Figure 25: Chemical complementation of *ΔgltBD* by L-glutamate. A) Growth of *ΔgltBD* in –N7H9 + 4 mM $(NH_4)_2SO_4$ supplemented with increasing concentrations of L-glutamate as measured by optical density (OD) readings. B) Growth of *ΔgltBD* in –N7H9 + 4 mM $(NH_4)_2SO_4$ supplemented with increasing concentrations of L-glutamate as measured by cfu determinations. Data was analysed by repeated measures two-way ANOVA with Bonferroni post-testing. -N7H9 + 4 mM $(NH_4)_2SO_4$ + 10 mM Glu was different from -N7H9 + 4 mM $(NH_4)_2SO_4$ + 0 mM Glu at every time point after and including 3 days ($p < 0.001$). -N7H9 + 4 mM $(NH_4)_2SO_4$ +3 mM Glu was different from -N7H9 + 4 mM $(NH_4)_2SO_4$ + 0 mM Glu at 3 days ($p < 0.01$) and every following time point ($p < 0.001$). -N7H9 + 4 mM $(NH_4)_2SO_4$ + 0.3 mM Glu was different from -N7H9 + 4 mM $(NH_4)_2SO_4$ + 0 mM Glu at 6 days ($p < 0.01$) and every following time point ($p < 0.001$). The data presented are the means and standard errors calculated from three independent growth curve experiments. In some instances error bars are smaller than the symbols.

Table 8. Growth of *ΔgltBD* in -N7H9 + 4 mM $(NH_4)_2SO_4$ + 3 mM L-Glu relative to growth in -N7H9 + 4 mM $(NH_4)_2SO_4$ + 10 mM L-Glu.

A	R	L
0.47 ± 0.02**	0.52 ± 0.02***	0.92 ± 0.04^{ns}

Data presented are the means and standard errors calculated from growth parameters estimated by method of modelling growth curve data from three independent experiments. Comparisons made between the conditions were analysed by unpaired two-tailed t-test. ✶✶ - $p < 0.01$, ✶✶✶ - $p < 0.001$ ^{ns} non-significant, A – maximal attained growth, R – maximal growth rate, L – lag time (see chapter 5, section 5.10)

It was reasoned that the phenotypic observations for the *ΔgltBD* mutant may have been due to a residual effect of the recombineering proteins expressed from pJV53. It was previously observed that acetamidase promoter activity is leaky in *M. tuberculosis* (159). However, there is evidence that this is not the case in *M. bovis* BCG (160, 161). The pJV53 vector may be passaged out of *ΔgltBD* by serial culture, but a concern was that serial culture may result in suppressor mutations which may obscure possible phenotypes that may otherwise be observed for the mutant. Therefore, the growth of the progenitor strain of *ΔgltBD*, wt-BCG::pJV53, was also investigated in 7H9 and in –N7H9 supplemented with 4 mM $(NH_4)_2SO_4$ as sole nitrogen source. All the growth

parameters of wt-BCG::pJV53 were comparable to those of wt-BCG in these media (Figure 23A & H, ×, Table 9).

Table 9: wt-BCG::pJV53 growth characteristics normalized to wt-BCG

	wt-BCG::pJV53		
	A	**R**	**L**
7H9	1.10 ± 0.07^{ns}	1.23 ± 0.29^{ns}	0.86 ± 1.00^{ns}
-N7H9	1.11 ± 0.11^{ns}	1.15 ± 0.08^{ns}	0.99 ± 0.50^{ns}

Data presented are the means and standard errors calculated from growth parameters estimated by method of modelling growth curve data from three independent experiments. Comparisons made between wt-BCG::pJV53 and wt-BCG as well as the other strains investigated in this study (see sections 3.2.1 and 3.2.2) were analysed by one-way ANOVA with Bonferroni post-testing. ns - non-significant, A – maximal attained growth, R – maximal growth rate, L – lag time (see chapter 5, section 5.10)

3.2.6 *In vitro* growth phenotypes of the *Δgdh* mutant

The growth parameter data of the *Δgdh* mutant are listed in Table 10.

The maximum growth achieved by the *Δgdh* mutant was 15% lower than wt-BCG in standard 7H9 (Figure 23A, □). However, it should be remarked that where differences in maximum growth achieved and growth rate were smaller than 20%, significance should be interpreted with caution due to the small data sets used to model growth in this study. Growth of the *Δgdh* mutant was severely affected in medium containing L-glutamate as sole nitrogen source (Figure 26D, □) where the maximal growth achieved and maximal growth rate of the mutant were reduced relative to wt-BCG by 5-fold and 3-fold, respectively. This result supports a physiological role for the *gdh* protein product in the catabolism of L-glutamate. While addition of 1 mM (Figure 27A & B, □) and 4 mM $(NH_4)_2SO_4$ (Figure 27A & B, ○) resulted in more than 4-fold increase in the maximal growth achieved relative to growth in –N7H9 + 3 mM L-Glu, addition of 0.1 mM $(NH_4)_2SO_4$ (Figure 27A & B, △) led to only a 2-fold increase in maximal growth achieved (Table 11). Addition of 0.1 mM, 1 mM and 4 mM $(NH_4)_2SO_4$ resulted in a more than 2-fold increase in maximal growth rate of the *Δgdh* mutant relative to growth in -N7H9 + 3 mM L-Glu. It could be speculated that the deamination of glutamate by GDH provides ammonium for assimilation by GS in the production of glutamine and that GDH in this way provides the major route for utilization of glutamate as a sole nitrogen source.

The maximal growth achieved by the *Δgdh* mutant in –N7H9 + 3 mM L-Glu relative to wt-BCG was improved by the addition of 3 mM L-asparagine (Figure 26J, □) and to a lesser extent by addition of 3 mM L-aspartate (Figure 26H, □), while the maximal growth rate of the *Δgdh* mutant in –N7H9 + 3 mM L-Glu relative to wt-BCG was only improved by additional supplementation with L-asparagine. Deamination of L-asparagine by L-asparaginase may provide ammonium for assimilation by GS, while utilization of aspartate as a nitrogen source probably depends on its inter-conversion to glutamate which would require the activity of GDH for the acquisition of ammonium (16, 17). Although a nearly 3-fold increase in lag time relative to wt-BCG was observed for the *Δgdh* mutant in -N7H9 supplemented with L-asparagine and L-aspartate as nitrogen sources (Figure Figure 26L, □), maximal growth achieved and maximal growth rate of the mutant in this medium was not significantly different to wt-BCG. Growth of the *Δgdh* mutant was also no different to wt-BCG when –N7H9 + 3 mM L-Asn was supplemented with L-glutamine or L-alanine (see Table 7).

The maximal growth achieved and the maximum growth rate of the *Δgdh* mutant when excess L-asparagine was added to –N7H9 on its own (Figure 26F, □), supplemented with 3 mM L-Glu (Figure 26G, □), or supplemented with 4 mM $(NH_4)_2SO_4$ (Figure 26E, □) were both reduced by more than 2-fold relative to wt-BCG. This effect of excess L-asparagine on growth of the *Δgdh* mutant was even more pronounced in 7H9 where the maximal growth achieved of the mutant was reduced to 25% of wt-BCG levels. It was previously observed that L-asparagine has a repressive effect on *M. tuberculosis* H37Ra growth when glutamate is also present in growth media (155), while in a more recent report it was observed that *M. tuberculosis* H37Rv growth is inhibited by excess (30 mM) L-asparagine. It is noteworthy that a repressive effect of L-asparagine on *M. bovis* BCG growth in this study was only observed in a GDH-deficient mutant, which may suggest that GDH activity is repressed in *M. tuberculosis* under the same culturing conditions in comparison to wt-BCG. It was previously observed that intracellular glutamate and glutamine levels were unaffected in a PknG-deficient *M. bovis* BCG mutant which were contradictory to earlier observations in the corresponding *M. tuberculosis* mutant (81, 139). PknG controls GDH activity through phosphorylation of GarA, which ameliorates inhibition of GDH by this protein (20, 78). It could be speculated that the higher sensitivity of *M. tuberculosis* for catabolite repression by L-asparagine corresponds with a difference in the regulation of

glutamate levels by GDH between the two organisms. Interestingly, it is characteristic of the L180 class of GDHs to be allosterically activated by L-asparagine and L-aspartate (56–59).

The repressive effect of L-asparagine was less severe when moderate levels (3 mM) of the amino acid was added to –N7H9 (Figure 26B, □), -N7H9 + 3 mM L-Glu (Figure 26J, □) or –N7H9 + 4 mM $(NH_4)_2SO_4$ (Figure 26K, □) and only led to marginal although significant decreases in maximal growth achieved by the mutant while maximum growth rate was not different from wt-BCG. Addition of 3 mM L-Asn to 7H9 had no significant effect on maximum growth achieved or maximum growth rate, but resulted in a more than 4-fold increase in lag time relative to wt-BCG. In addition, no similar effect on *Δgdh* growth to that of excess L-asparagine was observed when 7H9 was supplemented with an excess of L-aspartate (Figure 23E, □), $(NH_4)SO_4$ (Figure 23B, □) or L-glutamine which actually slightly stimulated *Δgdh* maximal growth rate relative to wt-BCG (Figure 26C, □).

Table 10: *Δgdh* mutant and complemented strain growth characteristics normalized to wt-BCG

	Δgdh			***Δgdh* complement**		
	A	**R**	**L**	**A**	**R**	**L**
7H9 (4 mM $(NH_4)_2SO_4$ + 3 mM L-Glu)						
unmodified	0.85 ± 0.11*	0.99 ± 0.31^{ns}	0.87 ± 0.27^{ns}	0.95 ± 0.06^{ns}	1.05 ± 0.12^{ns}	0.75 ± 0.53^{ns}
+ 30 mM L-Asn	0.25 ± 0.01***	0.43 ± 0.12***	0.06 ± 0.94^{ns}	0.83 ± 0.10^{ns}	1.11 ± 0.13^{ns}	1.26 ± 0.65^{ns}
+ 30 mM L-Glu	0.59 ± 0.03**	0.96 ± 0.13^{ns}	0.91 ± 0.42^{ns}	0.94 ± 0.08^{ns}	1.31 ± 0.06^{ns}	1.12 ± 0.75^{ns}
+ 10 mM L-Glu	0.65 ± 0.23**	0.94 ± 0.25^{ns}	1.10 ± 0.44^{ns}	0.87 ± 0.16^{ns}	1.23 ± 0.05^{ns}	0.99 ± 0.22^{ns}
+ 3 mM L-Asn	0.77 ± 0.13^{ns}	0.86 ± 0.26^{ns}	4.56 ± 3.14***	0.92 ± 0.11^{ns}	1.20 ± 0.09^{ns}	1.49 ± 0.66^{ns}
+ 30 mM L-Asp	0.77 ± 0.21^{ns}	0.81 ± 0.08^{ns}	0.89 ± 0.32^{ns}	0.78 ± 0.35^{ns}	1.21 ± 0.40^{ns}	1.23 ± 0.61^{ns}
+ 30 mM $(NH_4)_2SO_4$	0.88 ± 0.24^{ns}	1.14 ± 0.02^{ns}	1.06 ± 0.29^{ns}	0.95 ± 0.16^{ns}	1.10 ± 0.09^{ns}	0.81 ± 0.22^{ns}
+ 30 mM L-Gln	0.98 ± 0.15^{ns}	1.25 ± 0.10*	0.90 ± 0.13^{ns}	0.98 ± 0.15^{ns}	1.18 ± 0.11^{ns}	0.89 ± 0.41^{ns}
+ 3 mM L-Asp	1.08 ± 0.39^{ns}	0.81 ± 0.23^{ns}	1.01 ± 0.62^{ns}	1.11 ± 0.15^{ns}	1.15 ± 0.13^{ns}	1.09 ± 0.71^{ns}
-N7H9						
unmodified	0.94 ± 0.02^{ns}	1.08 ± 0.51^{ns}	0.90 ± 0.63^{ns}	1.13 ± 0.13^{ns}	1.02 ± 0.22^{ns}	1.11 ± 0.51^{ns}
+ 3 mM L-Glu	0.19 ± 0.11***	0.31 ± 0.38**	-0.79 ± 2.11^{ns}	0.91 ± 0.03^{ns}	1.14 ± 0.32^{ns}	0.79 ± 0.14^{ns}
+ 30 mM L-Asn + 4 mM $(NH_4)_2SO_4$	0.41 ± 0.02***	0.43 ± 0.08**	0.71 ± 1.51^{ns}	0.78 ± 0.01***	1.03 ± 0.23^{ns}	1.87 ± 0.76^{ns}
+ 30 mM L-Asn	0.42 ± 0.09**	0.38 ± 0.18***	0.32 ± 2.07^{ns}	0.75 ± 0.05^{ns}	1.02 ± 0.34^{ns}	3.10 ± 4.72^{ns}
+ 30 mM L-Asn + 3 mM L-Glu	0.42 ± 0.08***	0.39 ± 0.15**	0.41 ± 1.15^{ns}	0.79 ± 0.04**	1.03 ± 0.25^{ns}	1.33 ± 0.50^{ns}
+ 3 mM L-Asp + 3 mM L-Glu	0.65 ± 0.16**	0.29 ± 0.13**	1.01 ± 0.54^{ns}	0.82 ± 0.05^{ns}	1.18 ± 0.05^{ns}	0.97 ± 0.18^{ns}
+ 3 mM L-Asp	0.74 ± 0.32^{ns}	0.32 ± 0.04***	0.27 ± 0.16***	0.90 ± 0.06^{ns}	1.20 ± 0.24^{ns}	1.04 ± 0.27^{ns}
+ 3 mM L-Asn	0.77 ± 0.15*	0.88 ± 0.23^{ns}	1.25 ± 0.48^{ns}	1.07 ± 0.07^{ns}	0.95 ± 0.17^{ns}	0.58 ± 0.74^{ns}
+ 3 mM L-Asn + 3 mM L-Glu	0.83 ± 0.05*	0.83 ± 0.19^{ns}	1.55 ± 0.65^{ns}	0.99 ± 0.15^{ns}	1.08 ± 0.09^{ns}	0.98 ± 0.25^{ns}
+ 3 mM L-Asn + 4 mM $(NH_4)_2SO_4$	0.83 ± 0.05**	0.94 ± 0.07^{ns}	2.09 ± 1.02^{ns}	0.94 ± 0.08^{ns}	1.16 ± 0.19^{ns}	1.27 ± 0.93^{ns}
+ 3 mM L-Asn + 3 mM L-Asp	0.85 ± 0.08^{ns}	0.78 ± 0.08^{ns}	2.83 ± 2.72**	0.91 ± 0.13^{ns}	1.13 ± 0.08^{ns}	1.26 ± 0.64^{ns}
+ 3 mM L-Asn + 3 mM L-Gln	0.92 ± 0.08^{ns}	1.01 ± 0.18^{ns}	1.11 ± 0.49^{ns}	1.09 ± 0.06*	1.21 ± 0.13^{ns}	1.03 ± 0.16^{ns}
+ 4 mM $(NH_4)_2SO_4$	0.93 ± 0.11^{ns}	0.92 ± 0.22^{ns}	0.60 ± 0.17^{ns}	0.94 ± 0.16^{ns}	0.91 ± 0.13^{ns}	0.61 ± 0.16^{ns}
+ 3 mM L-Gln	0.95 ± 0.07^{ns}	1.09 ± 0.07^{ns}	0.81 ± 0.78^{ns}	0.99 ± 0.06^{ns}	0.97 ± 0.13^{ns}	0.56 ± 0.62^{ns}
+ 3 mM L-Asn + 3 mM L-Ala	1.01 ± 0.07^{ns}	1.10 ± 0.15^{ns}	0.86 ± 0.11^{ns}	0.97 ± 0.05^{ns}	0.97 ± 0.10^{ns}	0.95 ± 0.08^{ns}

Data presented are the means and standard errors calculated from growth parameters estimated by modelling of growth curve data from three independent experiments. Comparisons made between strains were analysed by one-way ANOVA with Bonferroni post-testing. ‡ AS - $(NH_4)_2SO_4$, ✶ - $p < 0.05$, ✶✶ - $p < 0.01$, ✶✶✶ - $p < 0.001$, ns - non-significant, A – maximal attained growth, R – maximal growth rate, L – lag time (see chapter 5, section 5.10)

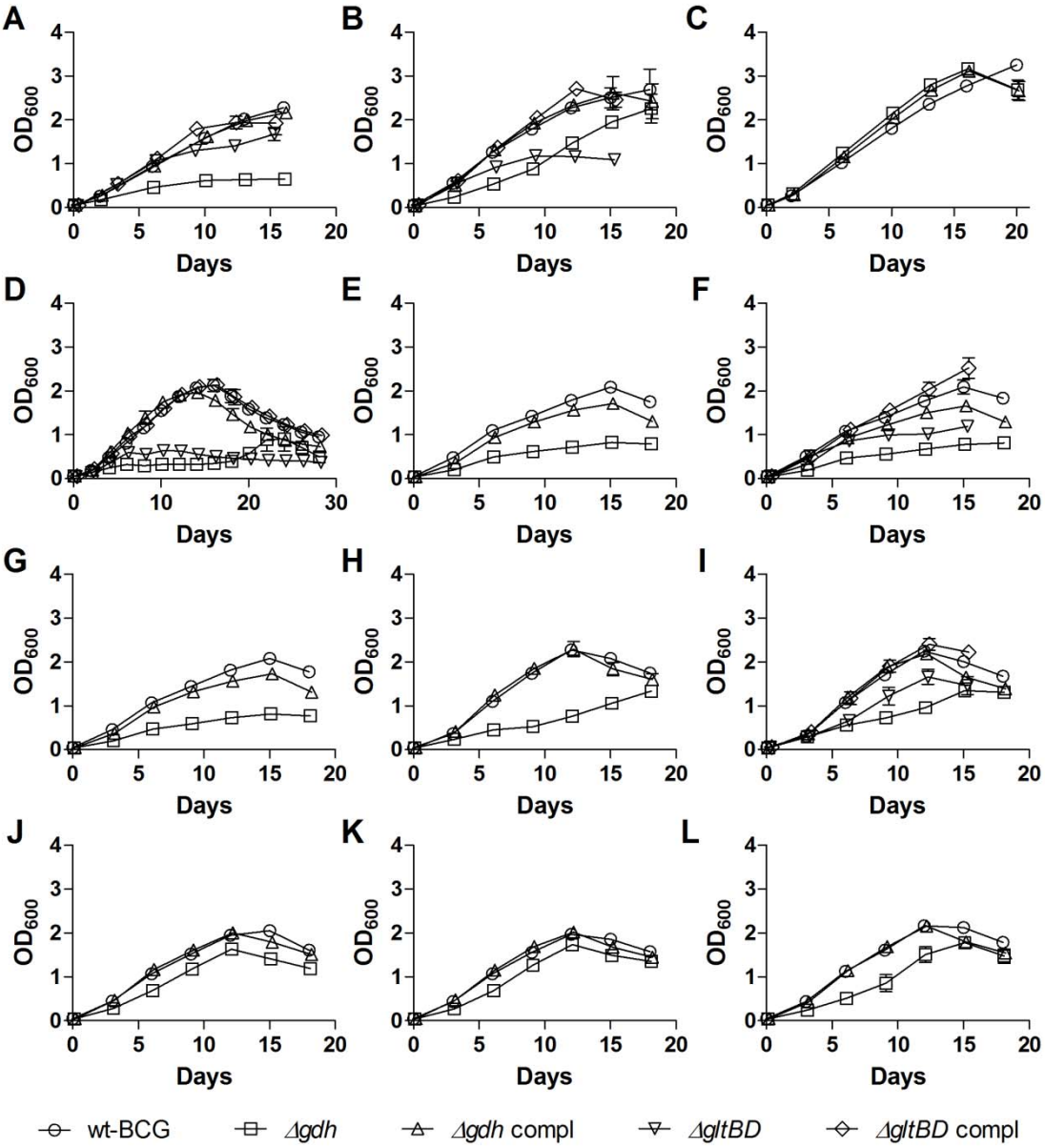

Figure 26: Growth of the *ΔgltBD* and *Δgdh* mutant and complemented strains in 7H9 or nitrogen depleted 7H9 (–N7H9) media supplemented with nitrogen sources in which the growth of the *Δgdh* mutant was poorest relative to wt-BCG growth. A) 7H9 + 30 mM L-Asn. B) 7H9 + 3 mM L-Asn. C) 7H9 + 30 mM L-Gln. D) -N7H9 + 3 mM L-Glu. E) -N7H9 + 30 mM L-Asn + 4 mM $(NH_4)_2SO_4$. F) -N7H9 + 30 mM L-Asn. G) –N7H9 + 30 mM L-Asn + 3 mM L-Glu. H) –N7H9 + 3 mM L-Asp + 3 mM L-Glu. I) –N7H9 + 3 mM L-Asp. J) –N7H9 + 3 mM L-Asn + 3 mM L-Glu. K) -N7H9 + 3 mM L-Asn + 4 mM $(NH_4)_2SO_4$. L) –N7H9 + 3 mM L-Asn + 3 mM L-Asp. The data presented are the means and standard errors calculated from at least three independent growth curve experiments. In some instances error bars are smaller than the symbols.

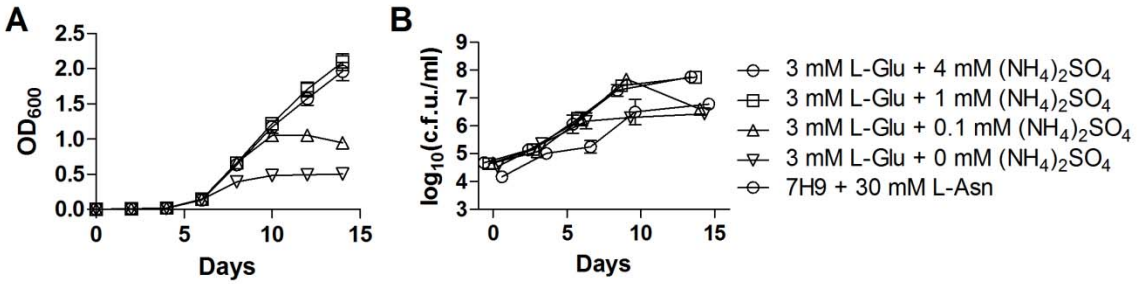

Figure 27: Chemical complementation of *Δgdh* cultured in nitrogen depleted medium (–N7H9) containing L-glutamate as sole nitrogen source with $(NH_4)_2SO_4$. A) Growth of *ΔgltBD* in –N7H9 + 4 mM $(NH_4)_2SO_4$ supplemented with increasing concentrations of L-glutamate as measured by optical density (OD) readings. B) Growth of *ΔgltBD* in –N7H9 + 4 mM $(NH_4)_2SO_4$ supplemented with increasing concentrations of L-glutamate as measured by cfu determinations. Data was analysed by two-way ANOVA with Bonferroni post-testing. cfu measurements of the *Δgdh* mutant in -N7H9 + 3 mM L-Glu was significantly different from -N7H9 + 3 mM L-Glu supplemented with 1 mM or 4 mM $(NH_4)_2SO_4$ at day 9 and 14 ($p < 0.01$), but was only significantly different from –N7H9 + 3 mM L-Glu supplemented with 0.1 mM L-Glu at day 9 ($p < 0.001$). cfu measurements of the *Δgdh* mutant in 7H9 + 30 mM L-Asn was significantly different from –N7H9 + 3 mM L-Glu supplemented with 1 or 4 mM $(NH_4)_2SO_4$ at day 6, 9 and 14 ($p < 0.05$), from –N7H9 + 3 mM L-Glu supplemented with 0.1 mM $(NH_4)_2SO_4$ at day 6 and 9 ($p < 0.001$) and from –N7H9 + 3 mM L-Glu at day 6 ($p < 0.01$). The data presented are the means and standard errors calculated from three independent growth curve experiments. In some instances error bars are smaller than the symbols.

Table 11. Growth of the *Δgdh* mutant in -N7H9 + 3 mM L-Glu supplemented with increasing $(NH_4)_2SO_4$ concentrations relative to growth in -N7H9 + 3 mM L-Glu.

	A	R	L
-N7H9 + 3 mM L-Glu + 4 mM AS	4.26 ± 0.10^{ns}	2.07 ± 0.03^{ns}	1.21 ± 0.02^{ns}
-N7H9 + 3 mM L-Glu + 1 mM AS	$4.47 \pm 0.02^{***}$	2.45 ± 0.34^{ns}	1.27 ± 0.05^{ns}
-N7H9 + 3 mM L-Glu + 0.1 mM AS	$2.08 \pm 0.11^{***}$	$2.50 \pm 0.16^{***}$	$1.20 \pm 0.02^{**}$

Data presented are the means and standard errors calculated from growth parameters estimated by modelling of growth curve data from at least two independent experiments. Data was analysed with one-way ANOVA with Bonferroni post-tests. ✶ - $p < 0.05$, ✶✶ - $p < 0.01$, ✶✶✶ - $p < 0.001$, ns - non-significant, A – maximal attained growth, R – maximal growth rate, L – lag time (see chapter 5, section 5.10)

The maximal growth achieved by the *Δgdh* mutant was also reduced relative to wt-BCG in 7H9 supplemented with 10 mM (Figure 23F, □) or 30 mM (Figure 23D, □) L-Glu. It could be speculated that the absence of GDH activity in the *Δgdh* mutant results in a disturbance of intracellular glutamate pools which is particularly emphasised when glutamate is present at high levels in growth medium or when excess L-asparagine is

present which may lead to a rapid flux into aspartate through the activity of asparaginase (162 - 164) and subsequently to glutamate through the activity of aspartate aminotransferases (15, 165).

Interestingly, after approximately 3 weeks of culture in medium containing 3 mM L-Glu as only nitrogen source, the optical density of *Δgdh* cultures started to increase (Figure 23D, □). Contaminating micro-organisms as a source of the increase in turbidity were not detected by Ziehl-Neelsen staining or by testing for growth on blood agar plates (see chapter 5, section 5.3). When a volume of the cultures were washed twice with –N7H9 and used to inoculate fresh cultures of –N7H9 + 3 mM L-Glu as well as standard 7H9 no difference in growth was observed (Figure 28A). In addition, aliquots of the 3 week old -N7H9 + 3 mM L-Glu *Δgdh* cultures were spread onto 7H11 plates and single colonies obtained. The single colonies were grown in 7H9 to mid-log phase before they were used for growth curve determinations in -N7H9 + 3 mM L-Glu (Figure 28B1). Out of thirteen colonies analysed, eight had similar growth profiles to that of wt-BCG (Figure 28B1, ▽, ○, ◇; Figure 28B2, ▽, ○, ◇, □; Figure 28B3, △, □). These colonies grew in 7H9 + 30 mM L-Asn (Figure 28C1) but not in –N7H9 + 3 mM L-Ala (Figure 28C2). It was speculated that the suppressor mutation could have occurred in the alanine dehydrogenase gene, *ald*. Sequencing of the *ald* gene using the primers aldF and aldR (see chapter 5, section 5.5.4.2, Table 14) revealed no mutations. The colonies were also analysed by PCR to exclude wt-BCG and the *Δgdh* complement strain as contaminating sources of the increase in OD observed (Figure 29). A primer set which was expected to amplify a 726bp product from the *Δgdh* mutant DNA template (Figure 29D2, lane 2) also amplified in the *Δgdh* suppressor mutant colonies (Figure 29D2, lanes 4 - 10). Moreover, primer sets which were expected to amplify 1029bp and 670bp products from wt-BCG (Figure 29D1, lane 1) and *Δgdh* complement DNA template (Figure 29D3, lane 3), respectively, but not from *Δgdh* mutant DNA template (Figure 29D3, lane 2) also did not amplify from any of the *Δgdh* suppressor mutant colonies analysed ate (Figure 29D1&3, lanes 4 - 10). These results suggest that a currently unknown genetic adaptation compensates for the loss of GDH activity in these colonies.

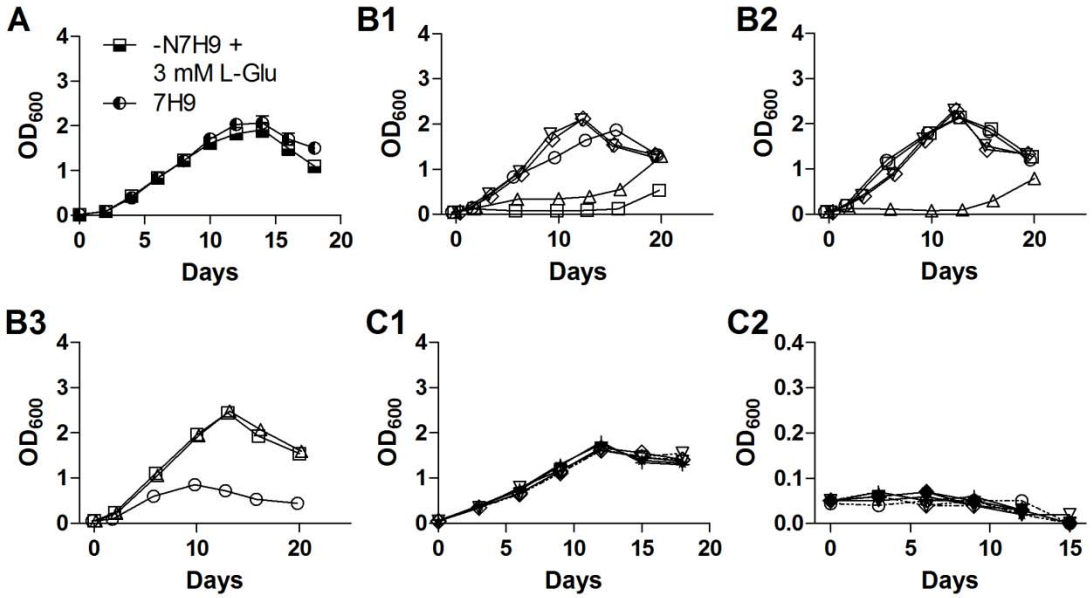

Figure 28: Growth curve analysis of *Δgdh* suppressor mutant colonies obtained from 3-week old *Δgdh* mutant –N7H9 + 3 mM L-glutamate cultures. A) Sub-cultured 3-week old *Δgdh* mutant -N7H9 + 3mM L-Glu culture. Bacteria (1 ml) were washed twice and used to inoculate fresh 7H9 or -N7H9 + 3 mM L-Glu. Data presented are the means and standard errors calculated from three independent growth curve experiments. B1-3) Growth of putative *Δgdh* suppressor mutant colonies, obtained from three independent –N7H9 + 3 mM L-Glu growth curve experiments, in fresh –N7H9 + 3 mM L-Glu. B1) colonies obtained from the first experiment. B2) colonies obtained from the second experiment. B3) colonies obtained from the third experiment. C1&2) Growth curves of putative *Δgdh* suppressor mutant colonies (as listed in heading B) in 7H9 + 30 mM L-Asn (C1) or –N7H9 + 3 mM L-Ala (C2).

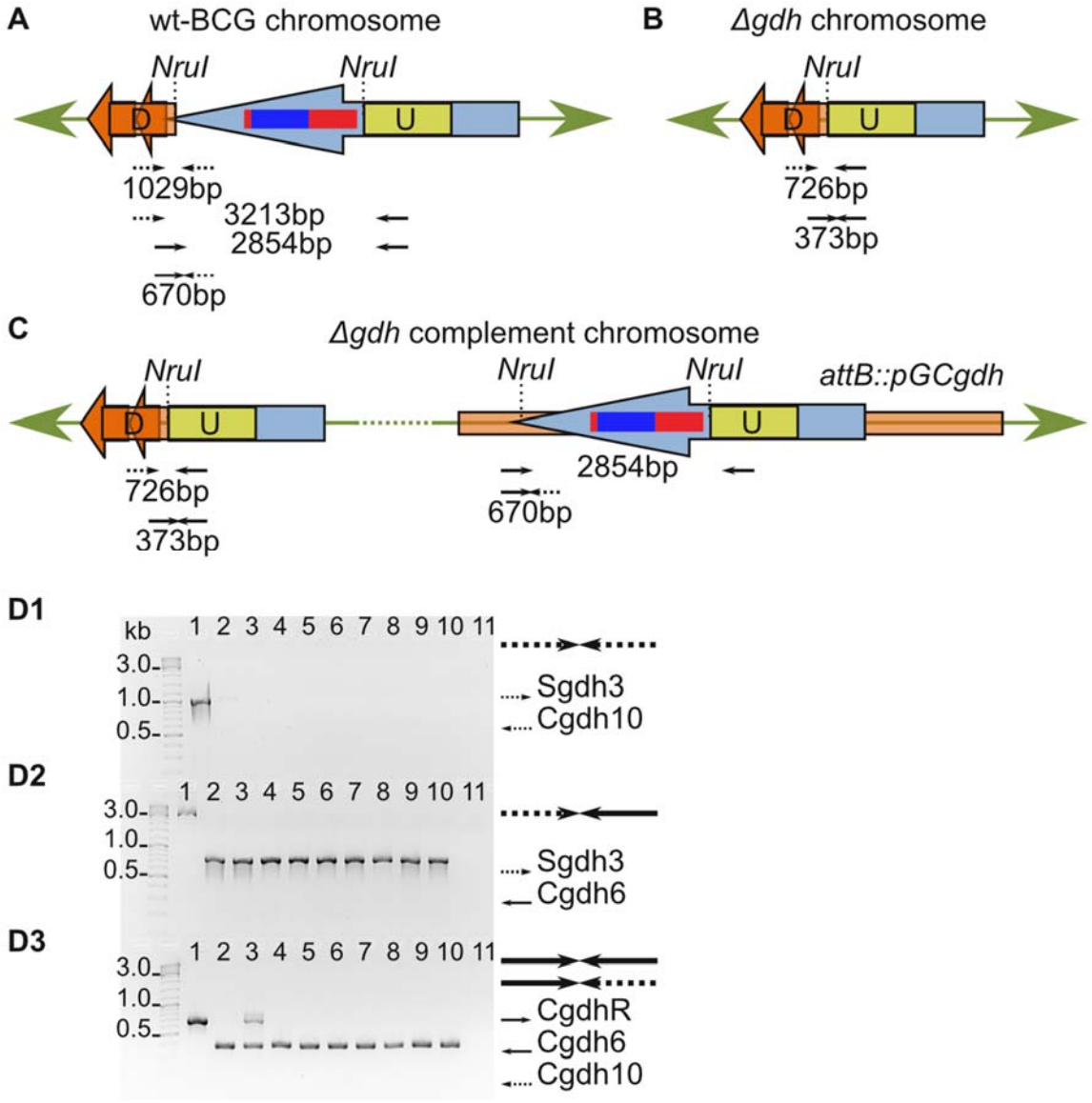

Figure 29: PCR analysis of potential *Δgdh* suppressor mutant colonies. A) Arrangement of genes in the chromosomal region of *M. bovis* BCG where *gdh* is located. B) Arrangement of genes in the *Δgdh* mutant chromosomal region where the disrupted *gdh* is located. C) Arrangement of genes in the *Δgdh* complement chromosomal region where the disrupted *gdh* is located and at the *attB* locus where pGCgdh is integrated into the chromosome. D) Gel image showing differential amplification patterns obtained when PCR was performed using template prepared from wt-BCG, the *Δgdh* strain and seven colonies obtained from *Δgdh* –N7H9 + 3 mM L-glutamate cultures which underwent an apparent suppressor mutation after 3 weeks of culture (see chapter 5, section 5.5.2.1). Note that the PCR conditions used (elongation for 1 min) did not allow efficient elongation and amplification of the 3572 bp (wt-BCG) and 3213 bp (wt-BCG and *Δgdh* complement) fragments which may be amplified using the primer set Sgdh3 and Cgdh6 and the primer set CgdhR and Cgdh6, respectively. L – DNA marker, lane 1 – wt-BCG, lane 2 – *Δgdh*, lane 3 – *Δgdh* complement, lane 4 – colony A1, lane 5 – colony A2, lane 6 – colony B1, lane 7 – colony B2, lane 8 – colony C1, lane 9 – colony C2, lane 10 – colony C3, lane 11

– no template control. D – downstream, U – upstream. See Table 14 for Sgdh3, Cgdh10, Sgdh3, Cgdh6, CgdhR, Cgdh6 and Cgdh10 primer sequences.

3.2.7 Gene expression in the *Δgdh* mutant

Relative gene expression analysis on RNA extracted from wt-BCG, the *Δgdh* mutant and the *Δgdh* complemented strain grown in 7H9 to mid-exponential growth phase (OD_{600} = 0.5 – 0.7), washed twice with –N7H9 and transferred to 7H9, 7H9 + 30 mM L-Asn or –N7H9 + 3 mM L-Glu for 24 hours is listed in Table 12.

The gene encoding for GS, *glnA1*, as well as *pknG* was upregulated in the *Δgdh* mutant relative to wt-BCG in medium that contained L-glutamate as sole nitrogen source (-N7H9 + 3 mM L-Glu). This indicates that the *Δgdh* mutant initiates a nitrogen limitation response when glutamate is the sole nitrogen source which supports the theory that GDH is required when L-glutamate is the only source of nitrogen for the deamination of L-glutamate to produce ammonium for assimilation by GS in the production of L-glutamine (see chapter 3, section 3.2.6). The induction of PknG may indicate that the lack of GDH activity in the *Δgdh* mutant under a condition where this activity is required elicits a response to ameliorate inhibition of GDH activity.

Compellingly, genes encoding for asparaginase, *asnB*, asparagine synthetase, *ansA*, the α-subunit of GOGAT, *gltB* and PknG were upregulated in the *Δgdh* mutant in comparison to wt-BCG when excess L-asparagine was added to 7H9. Upregulation of L-asparaginase could be explained by the role of this enzyme in the deamidation of L-asparagine to produce L-aspartate (162, 163). However, upregulation of asparagine synthetase is unexpected as this enzyme is involved in the ATP-dependent production of asparagine and may be an indication of deregulation of asparagine metabolism in the *Δgdh* mutant. This deregulation in asparagine metabolism may underlie the poor growth phenotype of the *Δgdh* mutant in 7H9 supplemented with an excess of L-asparagine. Similarly, the upregulation of *gltB* in the *Δgdh* mutant relative to wt-BCG in this condition may be an indication of a deregulation of glutamate metabolism in this strain. Theoretically, rapid metabolism of L-asparagine which was observed in a previous study on *M. tuberculosis* (164) may indirectly result in an increase in intracellular glutamate levels through the activity of aspartate aminotransferase and

the absence of GDH in the *Δgdh* mutant. Interestingly, *gltB* was also upregulated in the *Δgdh* complemented strain in comparison to wt-BCG 7H9 + 30 mM L-Asn. Notably, *gdh* transcript levels were approximately 20% of wt-BCG levels in the *Δgdh* complement under all the conditions tested. Upregulation of *gltB* in the *Δgdh* complement may indicate that deregulation of metabolism may not be fully complemented as a likely result of the low presence of *gdh* transcript, which was also shown to be accompanied by nearly undetectable enzymatic activity in the whole cell lysate (chapter 3, see section 3.2.3).

Table 12: Relative gene expression in the *Δgdh* mutant and *Δgdh* complement normalized to wt-BCG.

	Δgdh normalized to wt-BCG		
	7H9	-N7H9 + 3 mM L-Glu	7H9 + 30 mM L-Asn
gdh			
aspB	1.11 ± 0.40^{ns}	2.00 ± 0.39^{ns}	1.45 ± 0.14^{ns}
BCG3782c	1.44 ± 0.42^{ns}	1.10 ± 0.18^{ns}	1.59 ± 0.11^{ns}
asnB	1.44 ± 0.43^{ns}	1.19 ± 0.22^{ns}	1.72 ± 0.12*
ansA	0.97 ± 0.13^{ns}	1.12 ± 0.03^{ns}	1.37 ± 0.22*
gltD	1.17 ± 0.24^{ns}	1.15 ± 0.07^{ns}	1.68 ± 0.30**
glnA1	1.18 ± 0.18^{ns}	1.37 ± 0.03*	1.44 ± 0.25^{ns}
garA	1.00 ± 0.19^{ns}	1.30 ± 0.21^{ns}	1.32 ± 0.16^{ns}
pknG	1.02 ± 0.06^{ns}	1.91 ± 0.15**	1.73 ± 0.20**
	Δgdh complement normalized to wt-BCG		
	7H9	-N7H9 + 3 mM L-Glu	7H9 + 30 mM L-Asn
gdh	0.18 ± 0.02**	0.17 ± 0.02*	0.19 ± 0.03**
aspB	0.86 ± 0.12^{ns}	0.88 ± 0.12^{ns}	1.04 ± 0.18^{ns}
BCG3782c	1.09 ± 0.09^{ns}	0.96 ± 0.10^{ns}	1.42 ± 0.21^{ns}
asnB	1.10 ± 0.08^{ns}	0.96 ± 0.10^{ns}	1.32 ± 0.21^{ns}
ansA	0.89 ± 0.04^{ns}	0.89 ± 0.03^{ns}	1.10 ± 0.14^{ns}
gltD	1.01 ± 0.07^{ns}	0.97 ± 0.10^{ns}	1.48 ± 0.17*
glnA1	1.13 ± 0.08^{ns}	1.11 ± 0.06^{ns}	1.37 ± 0.22^{ns}
garA	1.02 ± 0.05^{ns}	0.98 ± 0.19^{ns}	1.21 ± 0.06^{ns}
pknG	0.97 ± 0.08^{ns}	0.96 ± 0.13^{ns}	1.31 ± 0.10^{ns}

Data presented are means ± standard errors of 16S-normalized gene expression in the *Δgdh* mutant or *Δgdh* complemented strain relative to 16S-normalized gene expression in wt-BCG calculated for three independent experiments. 16S-normalised expression in the *Δgdh* mutant or *Δgdh* complemented strain compared to 16S-normalized expression of genes of interest in wt-BCG were analysed with two-way ANOVA with Bonferroni post-testing. ✶ - $p < 0.05$, ✶✶ - $p < 0.01$, ns - non-significant ($p > 0.05$).

3.2.8 Growth phenotypes of the *Δgdh* and *ΔgltBD* mutants in murine bone marrow-derived macrophages

Change in $\log_{10}$(cfu/well) data between the investigated strains and wt-BCG are presented in Table 13. The intracellular growth profile of the *ΔgltBD* mutant did not differ appreciably from wt-BCG at day 2 or 4, but was 0.26 $\log_{10}$(cfu/well) lower than wt-BCG at day 6 (Figure 30, ▽). This difference was not observed between the *ΔgltBD* complement strain and wt-BCG (Figure 30, ◇). The *Δgdh* mutant cfu/well count was 0.18 $\log_{10}$(cfu/well) lower than wt-BCG 3 hours post infection of the macrophages, suggesting that uptake of this strain was marginally poorer than that of wt-BCG. Moreover, growth of the *Δgdh* mutant in the macrophages was poor in comparison to wt-BCG over the course of the experiment and the cfu counts for this strain were almost 0.7 $\log_{10}$(cfu/well) below wt-BCG at days 4 and 6 (Figure 30, □). However, a similar profile was observed for the *Δgdh* complement which had cfu counts of approximately 0.5 $\log_{10}$(cfu/well) lower than wt-BCG at days 4 and 6 (Figure 30, △). The cfu/well counts of the *Δgdh* complement strain were however approximately 0.2 $\log_{10}$(cfu/well) higher than the mutant strain at day 2 ($p < 0.05$), 4 ($p < 0.01$) and 6 ($p < 0.05$) compared to the mutant strain. A similar marginal complementation was not observed for any of the *in vitro* assays. However, it could be speculated that the poor expression of GDH in the complemented strain which was observed both in relative expression analysis (see chapter 3, section 3.2.7) and at enzymatic activity level (see chapter 3, section 3.2.3) correlated with the poor intracellular growth phenotype.

Table 13: Change in log(cfu/well) relative to wt-BCG.

Δgdh	*Δgdh* compl	*ΔgltBD*	*ΔgltBD* compl	wt-BCG::pJV53
-0.18 ± 0.08*	-0.07 ± 0.05^{ns}	0.01 ± 0.03^{ns}	0.08 ± 0.04^{ns}	0.03 ± 0.03^{ns}
-0.47 ± 0.10***	-0.28 ± 0.03***	0.08 ± 0.02^{ns}	0.07 ± 0.06^{ns}	0.13 ± 0.07^{ns}
-0.69 ± 0.04***	-0.48 ± 0.15***	-0.07 ± 0.10^{ns}	0.03 ± 0.07^{ns}	0.08 ± 0.05^{ns}
-0.69 ± 0.04***	-0.51 ± 0.03***	-0.26 ± 0.04***	-0.02 ± 0.01^{ns}	-0.11 ± 0.02^{ns}

Data presented are the mean $\log_{10}$(cfu/well) change to wt-BCG ± standard error calculated from three independent experiments. Data were analysed with repeated measure two-way ANOVA with Bonferroni post-tests. ✶ - $p < 0.05$, ✶✶ - $p < 0.01$, ✶✶✶ - $p < 0.001$, ns - non-significant ($p > 0.05$).

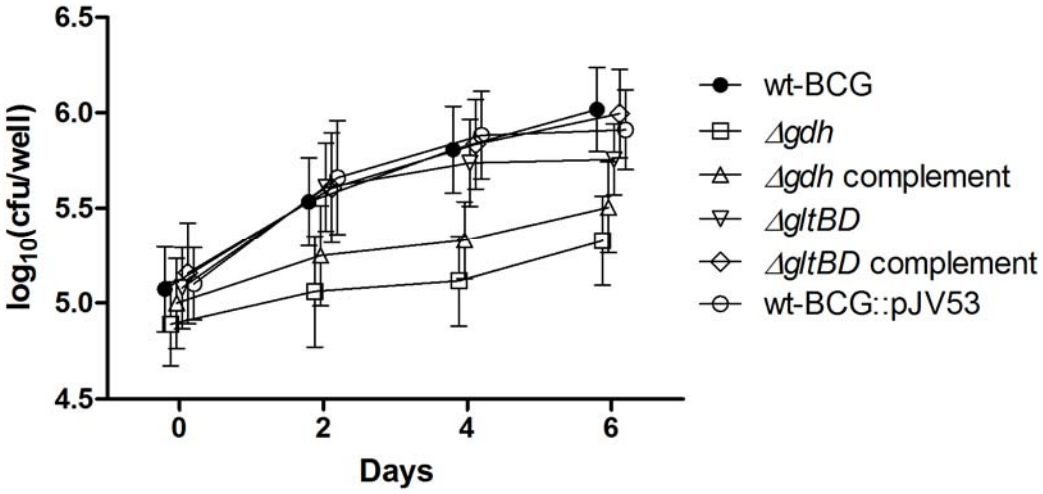

Figure 30: Growth of wt-BCG, the *Δgdh* and *ΔgltBD* mutant, the complemented strains of the mutants and the recombineering proficient *M. bovis* BCG strain (wt-BCG::pJV53) in bone marrow-derived macrophages. Means and standard errors were calculated from three independent experiments each in which a different mouse was used.

3.2.9 Growth phenotypes of *Δgdh* and *ΔgltBD* in *in vitro* conditions which may resemble the macrophage phagosome.

The poor complementation of the *Δgdh* complemented strain in macrophages was further investigated in *in vitro* systems which may model certain aspects of the intracellular environment. As acidification of the phagosome is a known host defence mechanism against infection (123), the effect of pH on *in vitro* bacterial growth was investigated. Interestingly, while wt-BCG, *ΔgltBD* and both complemented strains exhibited an extensive lag phase before exponential growth, the growth profile of *Δgdh* remained a flat line at pH = 5.0 (Figure 31A, □). While the extensive lag phase observed for the strains disappeared at pH = 6.0 (Figure 31B), the growth profile of *Δgdh* remained poorer than all other investigated strains (Figure 31B, □). These results clearly imply a role for GDH in adaptation to an acidic environment. It may be speculated that by its deaminating activity GDH releases ammonium ions into the medium which may neutralise the acidic environment. Interestingly, at neutral pH, the growth profile of the *Δgdh* mutant (Figure 31C, □) was similar to that of wt-BCG (Figure 31C, ○), however, in this condition the growth of the *ΔgltBD* mutant was poorer than that of the other strains, suggesting that glutamate import is less efficient at neutral pH than at lower pH environments. It was observed in *Streptococcus lacti* and

C. glutamicum that the pH optimum for glutamate import was in the neutral to high pH range, where the amino acid was mostly in its deprotonated anionic form, and glutamate uptake was poor at pH values lower than 6, where the amino acid was mostly in its protonated neutral form (166, 167). However, the current results suggest that in *M. tuberculosis* the protonated neutral form of glutamate is more efficiently imported into the cell, which may reflect an adaptation in this facultative intracellular pathogen to import glutamate in the low pH environment of the macrophage cell (122, 123). Alternatively, increased import of deprotonated glutamate in the *ΔgltBD* mutant under neutral growth conditions may result in an alteration of intracellular pH, which may underlie the observed growth defect.

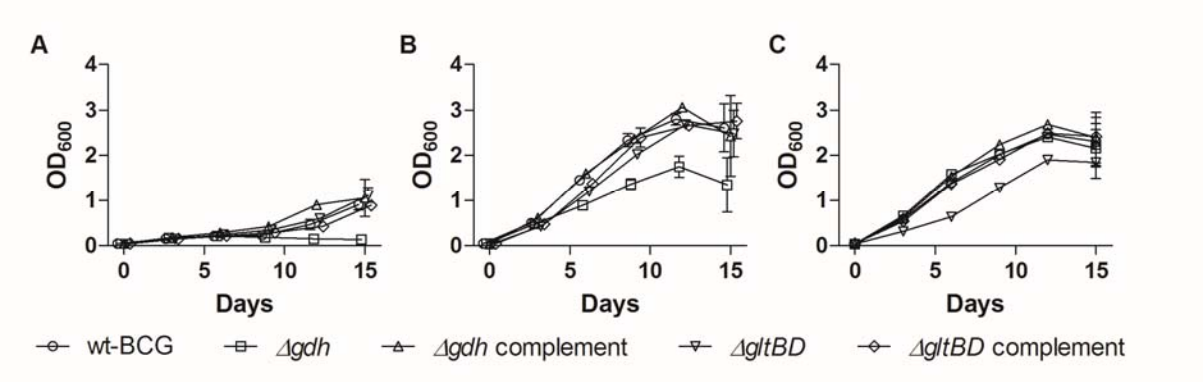

Figure 31: Growth of wt-BCG, the *Δgdh* mutant, the *Δgdh* complement strain, *ΔgltBD* mutant and the *ΔgltBD* complement strain in 7H9 medium supplemented with 20 mM L-glutamate, 5 mM L-aspartate, 5 mM L-glutamine and 1 mM L-asparagine. Amino acid concentrations were based on previously determined intracellular amino acid levels in the macrophage-like human cell line, THP-1 cells (36). pH was adjusted to A) 5.0. B) 6.0. C) 7.0. Data presented are means and standard errors calculated from two independent experiments.

A role for GDH in central carbon metabolism was possibly implicated in a recent TraSH study (see chapter 1, section 1.4.2). Therefore, the growth of wt-BCG, the *Δgdh* mutant, the *Δgdh* complement, the *ΔgltBD* mutant and the *ΔgltBD* complement was investigated in medium containing glutamate as sole nitrogen and sole carbon source (-N7H9 in which glycerol was omitted and Tween80 was replaced with Tyloxapol (Sigma, Germany)). While growth of wt-BCG (Figure 32, ○) in this condition was poor in comparison to wt-BCG growth in 7H9 (Figure 22A, ○), no growth was observed for the *Δgdh* mutant (Figure 32, □) or for the *Δgdh* complemented strain (Figure 32, ◇). The lack of complementation for the *gdh* deletion in the genetically complemented

Δgdh strain makes it impossible to discount that the *gdh* gene product may not have a direct function in the utilization of glutamate as a sole carbon and nitrogen source. However, these phenotypes for the *Δgdh* mutant and *Δgdh* complemented strain correspond with the phenotypes observed for these strains in BMDM cells (see chapter 3, section 3.2.8) and may be evidence of a requirement for glutamate as a nitrogen and carbon source by *M. bovis* BCG during infection of macrophage cells. This result illustrates the importance of glutamate both as a nitrogen and carbon source to mycobacteria during infection of macrophages.

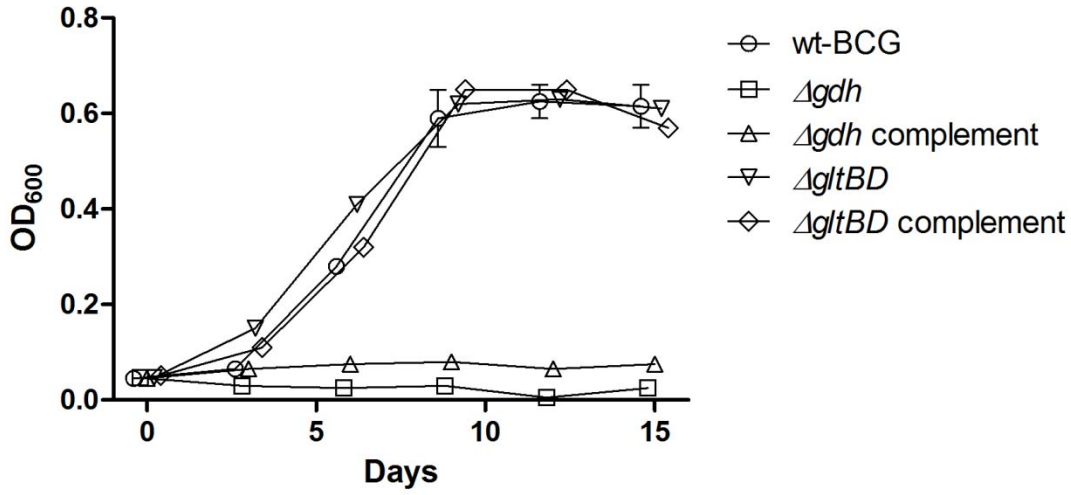

Figure 32: Growth of wt-BCG, the *Δgdh* mutant, the *Δgdh* complement strain, *ΔgltBD* mutant and the *ΔgltBD* complement strain in -N7H9 medium in which the glycerol was omitted, the Tween80 replaced with Tyloxapol and the sole nitrogen and carbon source was L-glutamate (5 g/L). Data presented are the means and standard errors calculated from two independent experiments, except for the *ΔgltBD* mutant and complemented strains which are from a single experiment.

3.3 Conclusion

As both genes in the *gltBD* operon and *gdh* were identified to be essential to *in vitro* growth of *M. tuberculosis*, successful generation of the *ΔgltBD* and *Δgdh M. bovis* BCG in this study is a compelling result, especially taking into consideration the high degree of genomic similarity between the two organisms as well as the difference in virulence between them. Interestingly, in *C. glutamicum*, which like *M. tuberculosis* and *M. bovis* BCG lack an anabolic GDH, but does possess a catabolic member of the L180 class of GDH enzymes, GOGAT-deficient mutants, like the GOGAT mutant *M.*

bovis BCG strain generated and investigated in this study, did not grow when ammonium was the sole nitrogen source and required supplementation with glutamate or amino acids which could be transaminated or catabolised to produce glutamate, such as asparagine and glutamine (168). This highlights the uniqueness of *M. tuberculosis* in which *gltB* and *gltD* insertion mutants are not obtained on 7H10 medium, which is supplemented with a reasonably high amount of L-glutamate (3 mM). Moreover, results from this study indicate that GDH may be an important factor for survival of *M. bovis* BCG in host macrophage cells and that this requirement for GDH in the intracellular milieu may have to do with its role in the utilization of glutamate as a nitrogen and carbon source within infected macrophages. This scenario may very likely be the same in *M. tuberculosis*, where the *gdh* gene is already required for growth on the standard mycobacterial culture medium 7H10. The *M. tuberculosis* GDH is structurally and functionally different from the GDH found in humans as well as in the human intestinal flora, which may make this enzyme a potential specific target for antituberculosis drug intervention (56).

Chapter 4

Study conclusions and future considerations

4.1. Study conclusions

Central nitrogen metabolism is regulated differently in *M. bovis* BCG to other bacteria, such as *E. coli*, *C. glutamicum* and *M. smegmatis* (see chapter 2, section 2.3), which is in line with major differences in the genes encoding for effectors and regulators of nitrogen metabolism between the organisms (61, 62). However, GS expression in *M. bovis* BCG was less affected by nitrogen limitation than previous reports for *M. tuberculosis*, which may suggest that a potent response to nitrogen limitation is important for pathogenicity. This is not surprising taking into account the well documented importance of GS in the pathogenicity of *M. tuberculosis*. *M. bovis* BCG NAD^+-GDH expression was induced by conditions where this enzyme would be required for its catabolic function. This is in contrast to previous observations which suggested a major role for NAD^+-GDH in the production of glutamate as opposed to the degradation of the amino acid (see chapter 1, section 1.2.3).

Despite the essentiality of *gltB*, *gltD,* and *gdh* to *in vitro* growth of *M. tuberculosis* (see chapter 1, section 1.2), a gene replacement mutant of the entire *gltBD* operon as well as an unmarked deletion mutant of *gdh* were successfully generated in *M. bovis* BCG in this study. It is shown that *gdh* is important for growth of *M. bovis* BCG under conditions where the catabolic activity of a GDH enzyme may be required. This is the first study to show that a member of the L180 class of GDHs is required for optimal growth of an organism when L-glutamate is the sole nitrogen source. Interestingly, it was previously reported that supplementation of Sauton medium containing L-glutamate as nitrogen source with L-asparagine resulted in an increase in extracellular glutamate concentration and decreased growth of *M. tuberculosis* H37Ra (155). However, while no such repressive effect was observed for wt-BCG in this study, growth of the *gdh*-deletion mutant *M. bovis* BCG strain was severely impeded by high levels of asparagine, suggesting that GDH is important in the metabolism of asparagine in *M. bovis* BCG. Activation of L180 GDH activity by L-asparagine and/or L-aspartate was shown for *S. clavuligerus* and *P. aeruginosa* and L-Asp enhanced the activity of *J. lividum* L180 GDH by more than 1,700% (56, 58, 59). These findings suggest that glutamate catabolism by L180 GDH is promoted when asparagine/aspartate are utilized as nitrogen sources. Results from this study indicate that the *gdh* protein product is required for optimal growth of *M. bovis* BCG cells in

macrophages and that this may be related to a dependency of intracellular mycobacteria on L-glutamate as a nitrogen and carbon source. This is the first study to implicate glutamate as an important nutrient in the intracellular milieu as well as GDH as an important effector of metabolism of infecting mycobacteria.

Results from this study highlight the importance of GOGAT and GDH to glutamate metabolism of *M. bovis* BCG. As the genes encoding for these enzymes were found to be essential to the *in vitro* growth of *M. tuberculosis* (see chapter 1, section 1.2), it is possible that these enzymes are required for the growth and survival of pathogenic mycobacteria in their host organisms. There is no gene encoding for GOGAT in the human genome (see chapter 1, section 1.2.2) and the *M. tuberculosis* GDH is structurally and functionally different from the GDH found in humans and does not have homologues in the bacteria of the human intestine (see chapter 3, section 3.3), which may make these enzymes potential targets for novel antituberculosis chemotherapeutic intervention.

4.2. Future considerations

Although the relative contributions of GOGAT and GDH in homeostasis of glutamate were determined in *M. bovis* BCG in this study, the roles of these enzymes in carbon and energy metabolism remain imprecisely defined. In future studies the *in vitro* responses of the strains generated in this study to a range of carbon sources, such as glucose and glycerol which enter glycolysis and cholesterol, succinate and gluconeogenic amino acids which enter the TCA cycle, should be investigated. To more accurately define metabolic responses within the strains generated in this study continuous fermentation culture at a range of constant growth rates may be considered over batch culture. Also stable isotope labelling (of substrates such as glutamate, glucose or succinate) may provide valuable insight on central nitrogen, carbon and energy metabolism in the different strains generated in this study. Differences in the essentiality of *gdh* and *gltBD* between *M. bovis* BCG and *M. tuberculosis* may necessitate experimental enquiry to elucidate the functions of GOGAT and GDH in maintenance of glutamate homeostasis in *M. tuberculosis*. Generation of conditional mutants of the GOGAT and GDH genes in *M. tuberculosis* may allow investigation of their function, despite their *in vitro* essentiallity (169).

Chapter 5

Materials and methods

5.1. Ethical statement

Ethical approval for this study was granted by the Stellenbosch University Faculty of Medicine and Health Sciences (US-FMHS) Human Health Research ethics committee (project number: N08/08/205). Ethical approval for the use of bone marrow-derived macrophages obtained from mice in this study was granted by the Stellenbosch University Research Ethics Committee (project number: 11GH_PIE01). Mice were procured from the University of Cape Town where they were bred under specific pathogen free conditions and kept, also under specific pathogen free conditions, at the US-FMHS animal facility where procedures to obtain the bone marrow from the mice occurred. The procedures used to kill the mice and in the isolation of bone marrow cells were according to The South African National Standard for the Care and Use of Animals for Scientific Purpose (SANS 10386:2008).

5.2. Bacterial strains, plasmids, and primers

Bacterial strains, plasmids and oligonucleotides used in this study are listed and described in Table 14.

Table 14: Bacterial Strains, plasmids, and oligonucleotides used in this study.

Strains/ plasmids/ oligonucleotides:	Description:	Source/reference:
Strains:		
***E. coli*:**		
DH5α	ATCC 53868	Laboratory collection
***M. bovis* BCG:**		
wt-BCG	Wild type *M. bovis* BCG str. *Pasteur 1743P2*, progenitor strain of all other *M. bovis* BCG strains in the study	Laboratory collection
wt-BCG::pJV75	wt-BCG strain carrying pJV75Amber; recombineering proficient strain used for point mutagenesis	This study
wt-BCG::pJV53	wt-BCG strain carrying pJV53; recombineering proficient strain used to make allelic replacement mutants	This study
ΔgltBD::*hyg* (referred to simply as *ΔgltBD*)	gene replacement of *gltBD* operon with a hygromycin cassette, carries recombineering plasmid pJV53, *hyg*^{r}, *kan*^{r}	This study

ΔgltBD attB::pGCgltBD	complemented strain of *ΔgltBD*::*hyg*, carries pGCgltBD and pJV53, *hyg*^{r}, *kan*^{r}, *gent*^{r}	This study
Δgdh	*Δgdh*, deletion of 2487bp *NruI* fragment spanning the GDH domain within the *gdh* gene.	This study
Δgdh attB::pGCgdh	complemented strain of *Δgdh*, carries pGCgdh, *gent*^{r}	This study
attB::pGCgarA	wt-BCG strain complemented with an additional copy of *garA*, carries pGCgarA, *gent*^{r}	This study
attB::pGCgarA-T21A	wt-BCG strain complemented with an additional copy of *garA*, carries pGCgarA-T21A, *gent*^{r}	This study
attB::pGCgarA-T21V	wt-BCG strain complemented with an additional copy of *garA*, carries pGCgarA-T21V, *gent*^{r}	This study
pAVgarA-T21A-SCO	pAVgarA-T21A integrated into wt-BCG chromosome by single cross over, *kan*^{r}, *hyg*^{r}	This study
pAVgarA-T21V-SCO	pAVgarA-T21V integrated into wt-BCG chromosome by single cross over, *kan*^{r}, *hyg*^{r}	This study
pAVgarA-T21A-SCO *attB*::pGCgarA	pGCgarA integrated into pAVgarA-T21A-SCO chromosome at *attB* site, *kan*^{r}, *hyg*^{r}, *gent*^{r}	This study
pAVgarA-T21A-SCO *attB*::pGCgarA	pGCgarA integrated into pAVgarA-T21V-SCO chromosome at *attB* site, *kan*^{r}, *hyg*^{r}, *gent*^{r}	This study

Plasmids:

General cloning:

pGEM-T easy	*E. coli* vector for cloning PCR products, *amp*^{R}	Promega

Point mutagenesis of *garA* by recombineering:

pJV75Amber	Expresses the Che9c mycobacterio-phage enzymes Gp60 and Gp61 under acetamide induction, *oriC*, *oriM*, *kan*^{r}, *hyg*^{r} disrupted with two amber stop codons - D15*, D16*	(140)

Genetic complementation of wt-BCG with copies of *garA* containing T21A and T21V amino acid substitutions:

pGCgarA3	1035 bp garA3 PCR product from wt-BCG genomic DNA as template blunt-end cloned into pGINTO linearized with *ScaI*	This study
pGCgarA3-T21A	1035 bp garA3 PCR product from pAVgarA-T21A as template blunt-end cloned into pGINTO linearized with *ScaI*	This study

pGCgarA3-T21V	1035 bp garA3 PCR product from pAVgarA-T21V as template blunt-end cloned into pGINTO linearized with *ScaI*	This study
Generation of *M. bovis* BCG pAVgarA-T21A-SCO and pAVgarA-T21V-SCO strains:		
p2NilgarA-T21A	p2Nil containing a 2069 bp *KpnI* fragment with a mutant *garA* gene (A61G)	This study
p2NilgarA-T21V	p2Nil containing a 2069 bp *KpnI* fragment with a mutant *garA* gene (A61G, C62T, and G63T)	This study
pGOAL19	*amp*^{r}, *hyg*^{r}, *lacZ*, *sacB*, *oriE*	(170)
pAVgarA-T21A	*PacI* fragment from pGOAL19 containing the *hyg*^{r,} *sacB* and *lacZ* cassettes cloned into the single *PacI* site of p2NilGarAHRA	This study
pAVgarA-T21V	*PacI* fragment from pGOAL19 containing the *hyg*^{R,} *sacB* and *lacZ* cassettes cloned into the single *PacI* site of p2NilGarAHRV	This study
Generation of the *ΔgltBD* mutant and the *ΔgltBD* genetically complemented strain:		
pJV53	Expresses the Che9c mycobacterio-phage enzymes Gp60 and gp61 under acetamide induction, *oriC*, *oriM*, *kan*^{r}	(159)
pMNFhyg	Hygromycin cassette TA-cloned into the pGEM-T Easy vector (Promega), *hyg*^{R}	Newton-Foot *et al.*, unpublished data
pMNFhygU	UgltBD PCR product TA cloned into pGEM-T Easy, excised with *SphI-NcoI* and ligated to pMNFhyg which was linearised with *SphI* and *NcoI*.	This study
pAVΔgltBD	DgltBD PCR product TA cloned into pGEM-T Easy, excised with *SpeI-PstI* and ligated to pMNFgltU which was linearised with *SpeI* and *PstI*.	This study
pGINTO	*integrase*, *attP*, *gent*^{r}	(171)
pGCgltBD	6662 bp CgltBD PCR product blunt-end cloned into pGINTO linearized with *ScaI*	This study
Generation of the *Δgdh* mutant and the *Δgdh* genetically complemented strain:		
p2Nil	*kan*^{r}, *oriE*	(170)
pGOAL17	*amp*^{r}, *lacZ*, *sacB*, *oriE*	(170)
pGEMgdh	4624 bp gdh1 PCR amplicon T/A cloned into pGEM-T Easy	This study
pGEMΔgdh	2487 bp GDH domain spanning NruI fragment deleted from pGEMgdh	This study
p2NilΔgdh	*KpnI* fragment from pGEMΔgdh containing *Δgdh* sequence cloned into the single *KpnI* site of p2Nil.	This study

pAVΔgdh	*PacI* fragment from pGOAL17 containing the *sacB* and *lacZ* cassettes cloned into the single *PacI* site of p2NilΔgdh.	This study
pGCgdh	5439 bp Cgdh PCR product blunt-end cloned into pGINTO linearized with *ScaI*	This study

Oligonucluotides:

qRT-PCR:

qPCR_sigAF	5'-CATGGTCGAGGTGATCAACAA-3'	This study
qPCR_sigAR	5'-GGGTGATGTCCATCTCTTTGG-3'	This study
qPCR_16SSF	5'-CCGGAATTACTGGGCGTAAA-3'	This study
qPCR_16SR	5'-AGTACTCTAGTCTGCCCGTATC-3'	This study
qPCR_gdhF	5'-CGACAACGAAGATCAGAACGA-3'	This study
qPCR_gdhR	5'-CGCTCAGCCACCAAATACT-3'	This study
qPCR_aspBF	5'-CTGGCCTTCTGCTCAAAGT-3'	This study
qPCR_aspBR	5'-GGCAAACGATATCCGAACAAAC-3'	This study
qPCR_BCG3782cF	5'-CATACCCTGACGCTGGATTT-3'	This study
qPCR_BCG3782cR	5'-CCTAACGATCCACCGAAGAAG-3'	This study
qPCR_asnBF	5'-GGTGGCCAGTGAGAAGAAAT-3'	This study
qPCR_asnBR	5'-TACTGCAGGACGGTGTAGT-3'	This study
qPCR_ansAF	5'-ATCACTACTGGAGGGACAATCT-3'	This study
qPCR_ansAR	5'-TACTTCGATGTCGGAGTCCAT-3'	This study
qPCR_gltDF	5'-CATCAGGCGATGGAGTTTCT-3'	This study
qPCR_gltDR	5'-GACGACCTTCTTGCCCTTT-3'	This study
qPCR_glnA1F	5'-CGGCCAAGACGCTGAATA-3'	This study
qPCR_glnA1R	5'-CAGTGCTGATCAGGTAGTTCTC-3'	This study
qPCR_garAF	5'-CATCCCGACAGCGACATATT-3'	This study
qPCR_garAR	5'-CCGACATCGACGACATTGAA-3'	This study
qPCR_pknGF	5'-CGGCTACATCGTGATGGAATA-3'	This study
qPCR_pknGR	5'-TAGACCAAGCCGATGGAATG-3'	This study

Point mutagenesis of *garA* threonine codon 21 by recombineering:

T21Aw	5'-AAGTCTGCGCGGAAGACGGAGGT CGCCTCTACCGTGACTTCATCGGAG GTC-3'	This study
T21Ac	5'-GACCTCCGATGAAGTCACGGTAG AGGCGACCTCCGTCTTCCGCGCAGA CTT-3'	This study
V20Iw	5'-AAGTCTGCGCGGAAGACGGAGGT GGTATTTACCGTGACTTCATCGGAG GTC-3'	This study
T21Tw	5'-AAGTCTGCGCGGAAGACGGAGGT GGTCTCTACCGTGACTTCATCGGAG GTC-3'	This study
T21Qw	5'-AAGTCTGCGCGGAAGACGGAGGT CTGCTCTACCGTGACTTCATCGGAG GTC-3'	This study
JCV198	5'-CCCTGTTACTTCTCGACCGTATTG ATTCGGATGATTCCTACGCGAGCCT GCGGAACGACCAGG-3'	(140)
GarAF	5'-GGACATGAACCCGGATATTG-3'	This study

GarAR	5'-TCGTTTGACTACCAGCAACG-3'	This study
GarA1F	5'-CACGAGAAAGTAGTAAGGGCGA-3'	This study
GarA1Fm	5'-CCGATGAAGTCACGGTAGATG-3'	This study
GarA1R	5'-GACGTAGGTGCCGTTGAGAC-3'	This study
GarA2F	5'-AGCCCGTCAAGTGAACTAGC-3'	This study
GarA2Fm1	5'-CCGATGAAGTCACGGTAGATG-3'	This study
GarA2Fm2	5'-CCGATGAAGTCACGGTAAGT-3'	This study
GarA2Fm3	5'-CGATGAAGTCACGGTAGAGAAC-3'	This study
GarA2Fm4	5'-CCGATGAAGTCACGGTAGATCA-3'	This study
GarA2FmamaWT	5'-CCGATGAAGTCACGGTAGATA-3'	This study
GarA2R	5'-TGGAGATGGTGACATCAGGA-3'	This study
Generation of *M. bovis* BCG *attB*::pGCgarA3, *attB*::garA-T21A, *attB*::garAT21V, pAVgarA-T21A-SCO, pAVgarA-T21V-SCO, pAVgarA-T21A-SCO *attB*::pGCgarA3 and pAVgarA-T21V-SCO *attB*::pGCgarA3 strains:		
GarAHR1F	5'-GGTACCATCCAGATCAACGATGCACA-3'	This study
GarAHR1AR	5'-ACGGAGGTCGCCTCTACCGT-3'	This study
GarAHR1VR	5'-ACGGAGGTAACCTCTACCGT-3'	This study
GarAHR2AF	5'-ACGGTAGAGGCGACCTCCGT-3'	This study
GarAHR2VF	5'-ACGGTAGAGGTTACCTCCGT-3'	This study
GarAHR2R	5'-GGTACCAATCTGGGCAATCAGGTC-3'	This study
GarA3F	5'-GGTACCTCGTTTTCGTTCAGCTACCC-3' *KpnI* recognition site on 5' end.	This study
GarA3R	5'-GGTACCTCATCAGCTCACGGGCCCCCGGTAC-3' *KpnI* recognition site on 5' end.	This study
GarA4F	5'-GTAGCGCCTGAGGTGATGAT-3'	This study
GarA4R	5'-GACTTGATCAGCGACGTGTG-3'	This study
pJet1.2F	5'-CGACTCACTATAGGGAGAGCGGC-3'	Fermentas
pJet1.2R	5'-AAGAACATCGATTTTCCATGGCAG-3'	Fermentas
Generation of *ΔgltBD* mutant and genetically complemented strain:		
UgltBDF	5'-GCATGCCCGACCAATATCGTCCC-3', *SphI* recognition sequence on 5' end	This study
UgltBDR	5'-CCTAGGCGATAGGCTGTCCGTCAA-3', *NcoI* recognition sequence on 5' end	This study
DgltBDF	5'-ACTAGTAGCTCCGAGGTGTCTAATG-3', *SpeI* recognition sequence on 5' end	This study
DgltBDR	5'-CTGCAGATTTCGCCGAGGATGA-3', *PstI* recognition sequence on 5' end	This study
SgltBD1	5'-CCTTTGCCGACGTAGTCATT-3'	This study
SgltBD2	5'-GTTCAACCCGGAGACTGTGT-3'	This study
SgltBD3	5'-AATCCATCGACAGCTTGGAG-3'	This study
SgltBD4	5'-GCGTAGGAATCATCCGAATC-3'	This study
SgltBD5	5'-TCTTTCCCACACCTCCTTTG-3'	This study

T7_promoter	5'-TAATACGACTCACTATAGGG-3'	Central analytical facility (Stellenbosch University)
SP6	5'-TATTTAGGTGACACTATAG-3'	Central analytical facility (Stellenbosch University)
CgltBDF	5'-P-CCCTTTTAGTATCGCGCAAA--3'	This study
CgltBDR	5'-P-GAAGCCCACATCGACTCATT-3'	This study
CgltBD2	5'-GTTGCCATGGTTGTGGACAT-3'	This study
CgltBD3	5'-CGGTTCTCCACGAACACTTT-3'	This study
CgltBD4	5'-CTCCGATGAGGAGATCAAGG-3'	This study
CgltBD5	5'-GAGGAAATGGCTCCGATACC-3'	This study
CgltBD6	5'-GTTCAACCCGGAGACTGTGT-3'	This study
CgltBD7	5'-TAAAGAACGCCAATCCATCC-3'	This study
CgltBD8	5'-AGGCGCATAAGCTGGATCT-3'	This study
CgltBD9	5'-GTAACTTTGCGGCGGGTAT-3'	This study
CgltBD10	5'-CGGAATGGAACGATCTGGT-3'	This study
CgltBD11	5'-GGCAAGAAGGTCGTCATCAT-3'	This study
Generation of *Δgdh* mutant and genetically complemented strain:		
gdhF	5'-GGTACCGCTTCGTCGGGCTCTTC-3', *KpnI* recognition site on 5' end.	This study
gdhR	5'-GGTACCAGGCATCCGTTGTGGC-3', *KpnI* recognition site on 5' end.	This study
PgdhF	5'-TGCTGCTCCGTGCCTAC-3'	This study
PgdhR	5'-ACGAACCCGACGCTCA-3'	This study
Sgdh1	5'-AAAGCTGTGTCGCCGTCTAT-3'	This study
Sgdh2	5'-ATCCGGAAATGAACCATCCT-3'	This study
Sgdh3	5'-TCATCAGCTCACGGGCCCCCGGTAC-3'	This study
gdh4F	5'-GAATCACCTTGGGCACTCAT-3'	This study
CgdhF	5'-P-GTCTCGGACGGTCTGGACTA-3'	This study
CgdhR	5'-P-GCTCACCCCGAGATTCC-3'	This study
Cgdh2	5'-AGGAGCGGGAAAATTGAATC-3'	This study
Cgdh3	5'-AGGCCTGGATGCACGTAG-3'	This study
Cgdh4	5'-CTTCGTCGGGCTCTTCAG-3'	This study
Cgdh5	5'-ATTACGCTGCCGCCTTCT-3'	This study
Cgdh6	5'-GTTCAACCCGGAGACTGTGT-3'	This study
Cgdh7	5'-GGTGAAGAACGCCGTCAT-3'	This study
Cghd8	5'-GACCACCGCCACATCTTC-3'	This study
Cgdh9	5'-GAGTCAATGACCGACGAGGT-3'	This study
Cgdh10	5'-CGGAATGGAACGATCTGGT-3'	This study
aldF	5'-CGAGTCTTGTGTTCCGTTGA-3'	This study
aldR	5'-AACAACTTCACTCGCCTGCT-3'	This study

5.3. Cultivation of bacteria

All bacterial strains used are listed in Table 14 and all culture media used are listed in Table 15. *E. coli* was cultured with shaking at 200 r.p.m. in Lysogeny Broth (LB) and on LB agar at 37ºC. *M. bovis* BCG was cultured without agitation in 7H9 in 25 cm^2 (5 - 10 ml) and 75 cm^2 (30 ml) cell culture flasks (Nunc, Denmark) and on 7H10 or 7H11 plates. Frozen bacterial stocks (1 ml aliquots) of *E coli* were maintained in LB containing 15% glycerol and of *M. bovis* BCG in 7H9 also containing 15% glycerol at -80°C.

In order to investigate growth of bacteria in the presence of different nitrogen sources modified Middlebrook 7H9 medium lacking a nitrogen source (-N7H9) was prepared and subsequently supplemented with different nitrogen sources as is indicated in the text. Bacteria were washed once with –N7H9 before they were used to inoculate 7H9 media with different nitrogen compositions. In order to investigate the response of *M. bovis* BCG to nitrogen limitation or excess (see section 2.2.1, Figure 3A), modified Kirchner's Broth lacking a nitrogen source (-NKB) was prepared and subsequently supplemented with a limiting concentration (0.1 mM) or excess concentration (60 mM) of $(NH_4)_2SO_4$. *M. bovis* BCG cultures were routinely tested for contaminating microorganisms by method of Ziehl-Neelsen staining and microscopy as previously described (172) or by by spreading out a 100 µl volume of the cultures on blood agar plates (Becton Dickinson, USA) and monitoring for growth for 2 – 7 days. Antibiotic concentrations for *M. bovis* BCG were as follows: hygromycin, 50 µg/ml on solid medium and 25 µg/ml in liquid medium; kanamycin, 20 µg/ml; and gentamycin, 2.5 µg/ml. Antibiotic concentrations for *E. coli* were: ampicillin, 50 µg/ml; hygromycin, 100 µg/ml; kanamycin, 50 µg/ml; and gentamicin, 5 µg/ml.

Table 15: Media used in this study and their compositions.

Medium	Composition*
Lysogeny Broth (LB)	NaCl, 10 g/L; yeast extreact powder, 5g/L; pancreatic digest of casein, 10 g/L
LB agar	NaCl, 10 g/L; yeast extreact powder, 5g/L; pancreatic digest of casein, 10 g/L; bacteriological agar, 15 g/L
SOC medium	tryptone, 2% w/v; yeast extract, 0.5% w/v; NaCl, 10 mM; KCl, 2.5 mM; $MgCl_2$, 10 mM; $MgSO_4$, 10 mM; D-glucose, 20 mM

Albumin dextrose catalase (ADC)	bovine serum albumin fraction V, 50 g/L; D-glucose, 20 g/L; catalase, 15 mg/L
oleic acid albumin dextrose catalase (OADC)◇	oleic acid, 0.06% v/v; bovine serum albumin fraction V, 50 g/L; D-glucose, 20 g/L; catalase, 30 mg/L; NaCl, 8.5 g/L
7H9○	$(NH_4)_2SO_4$, 0.5 g/L; L-glutamate, 0.5 g/L; sodium citrate, 0.1 g/L; pyridoxine, 1 mg/L; biotin, 0.5 mg/L; disodium phosphate, 2.5 g/L; monopotassium phosphate, 1 g/L; ferric ammonium citrate, 40 mg/L; magnesium sulphate, 50 mg/L; $CaCl_2$, 0.5 mg/L; $ZnSO_4$, 1 mg/L; $CuSO_4$, 1 mg/L; glycerol, 0.2% v/v; Tween80, 0.05% v/v; ADC, 10% v/v
-N7H9	sodium citrate, 0.1 g/L; pyridoxine, 1 mg/L; biotin, 0.5 mg/L; disodium phosphate, 2.5 g/L; monopotassium phosphate, 1 g/L; ferric citrate, 40 mg/L; magnesium sulphate, 50 mg/L; $CaCl_2$, 0.5 mg/L; $ZnSO_4$, 1 mg/L; $CuSO_4$, 1 mg/L; glycerol, 0.2% v/v; Tween80, 0.05% v/v; ADC, 10% v/v
7H10▽	$(NH_4)_2SO_4$, 0.5 g/L; monosodium glutamate, 0.5 g/L; sodium citrate, 0.4 g/L; pyridoxine, 1 mg/L; biotin, 0.5 mg/L; disodium phosphate, 1.5 g/L; monopotassium phosphate, 1.5 g/L; ferric ammonium citrate, 40 mg/L; magnesium sulphate, 25 mg/L; $CaCl_2$, 0.5 mg/L; $ZnSO_4$, 1 mg/L; $CuSO_4$, 1 mg/L; malachite green, 0.25 mg/L; agar, 15 g/L; glycerol, 0.5% v/v; Tween80, 0.05% v/v; ADC, 10% v/v
7H11△	pancreatic digest of casein, 1 g/L; $(NH_4)_2SO_4$, 0.5 g/L; monosodium glutamate, 0.5 g/L; sodium citrate, 0.4 g/L; pyridoxine, 1 mg/L; biotin, 0.5 mg/L; disodium phosphate, 1.5 g/L; monopotassium phosphate, 1.5 g/L; ferric ammonium citrate, 40 mg/L; magnesium sulphate, 50 mg/L; $CaCl_2$, 0.5 mg/L; $ZnSO_4$, 1 mg/L; $CuSO_4$, 1 mg/L; malachite green, 0.25 mg/L; agar, 13.5 g/L; glycerol, 0.5% v/v; Tween80, 0.05% v/v; ADC, 10% v/v
Kirchners Broth lacking a nitrogen source (-NKB)	disodium phosphate, 3 g/L; monopotassium phosphate, 4 g/L; magnesium sulphate heptahydrate, 1.07 g/L; sodium citrate, 2.5 g/L; glycerol, 2% v/v; Tween80, 0.05% v/v

✶ - chemicals were either obtained from Sigma (Germany) or Merck (Germany), ◇ - Middlebrook OADC was obtained from Becton Dickinson (USA), ○ - Middlebrook 7H9 powder was obtained from Becton Dickinson (USA), ▽ - Difco Middlebrook 7H10 agar powder was obtained from Becton Dickinson (USA), △ - BBL 7H11 agar base powder was obtained from Becton Dickinson (USA).

5.4. Genetic manipulation of bacteria

5.4.1. Preparation of electrocompetent *E. coli* cells and transformation

Tetracycline resistant *E. coli DH5α* was streaked out on an LB plate containing tetracycline (50 µg/ml). A single colony was picked and used to inoculate 50 ml LB medium (50 µg/ml tetracycline) which was incubated overnight at 37°C with shaking at 200 r.p.m. Two Erlenmeyer flasks containing 250ml LB medium (50µg/ml tetracycline) each were incubated overnight at 37°C before they were inoculated with

25ml of the starter culture. These were incubated at 37°C for approximately 2 hours with shaking until the OD_{600} was between 0.7 and 0.8. The cultures were decanted into 50 ml centrifuge tubes and placed on ice for 10 minutes before centrifugation (3000 × g, 4°C, 10 minutes). After centrifugation the supernatants were discarded and the cell-pellets gently, but thoroughly re-dissolved in 50 ml ice cold 10% glycerol. These suspensions were centrifuged again and the supernatants discarded (first wash). After another wash the cell pellets in each 50 ml tube were re-dissolved in 1 ml ice cold 10% glycerol, pooled together in a single 50 ml tube (total volume ≈ 10 ml) and centrifuged. The supernatant was discarded and the pellet gently, but thoroughly re-suspended in 1 ml ice cold 10% glycerol. Aliquots (50µl each) were made of the washed cells in 1.5ml microcentrifuge tubes. The aliquots were subsequently snap frozen in liquid nitrogen and stored at -80°C before use. For electro-transformation of *E. coli* an aliquot of electrocompetent *E. coli* cells was thawed on ice, 45 µl thereof transferred to a sterile 1.5 ml microcentrifuge tube (Axygen, USA) containing 1-10µl salt-free plasmid solution (see chapter 5, section 5.5.1) or ligation mixture (see chapter 5, section 5.5.7), mixed gently and transferred to a 2mm-gap sterile electroporation cuvette (Bio-Rad, USA) which was precooled on ice. Electro-transformation followed immediately and was performed using a Bio-Rad Gene Pulser II electroporator and the following settings: 200Ω, 25µF, 2.5kV. After electroporation cells were immediately suspended in 1ml SOC medium (see Table 15), transferred to a sterile 2ml microcentrifuge tube (Axygen, USA) and incubated without agitation at 37°C for 1 hour. Electro-transformed bacteria were diluted appropriately and spread on LB agar containing antibiotic (as indicated in the section 1.2: cultivation of bacteria).

5.4.2. Preparation of electrocompetent *M. bovis* BCG cells and transformation

Two 100 ml *M. bovis* BCG cultures were grown to an OD_{600} between 0.5 and 0.7 in 175cm^2 cell culture flasks (PAA, Austria). Glycine was then added to each culture (final concentration of 1.5% (w/v)) and the cultures incubated overnight. Addition of glycine to mycobacterial cultures has been shown to increase electro-transformation efficiency (173–175). Cells were subsequently pelleted by centrifugation (2000 × g, 10 minutes, 37°C) and the supernatant discarded. The cell pellets were re-suspended in a solution (80 ml) of 10% (v/v) glycerol and 0.05% (v/v) tween80 (GlycTw) which was pre-warmed to 37°C. Cells were again pelleted by centrifugation and the supernatant

discarded (first wash). The cells were washed similarly two more times, but with decreasing volumes of GlycTw (2nd wash: 40 ml, 3rd wash: 20 ml). After the final wash the pellet of electrocompetent cells was re-suspended in 5 ml GlycTw. For electro-transformation 400µl electrocompetent *M. bovis* BCG cell suspension was added to 10µl salt-free plasmid solution in a 1.5ml sterile microcentrifuge tube (Axygen, USA), mixed gently and transferred to a 2mm-gap sterile electroporation cuvette (Bio-Rad, USA). Electro-transformation was performed at room temperature with a Bio-Rad Gene Pulser II electroporator (Bio-Rad, USA) using the following settings: 1000Ω, 25µF, 2.5kV. Electro-transformation of slow growing mycobacteria at elevated temperatures as opposed to at 4°C was also previously shown to increase electro-transformation efficiency (175, 176). Following electroporation cells were immediately suspended in 5ml 7H9, transferred to a 25cm^2 cell culture flask and incubated without agitation at 37°C overnight. Electro-transformed bacteria were diluted appropriately and spread on 7H11 containing antibiotic (as indicated in the section 1.2: cultivation of bacteria).

5.4.3. Generation of recombineering proficient *M. bovis* BCG strains

Recombineering proficient strains of *M. bovis* BCG were generated by electro-transformation of wt-BCG (see Table 14) with the plasmids pJV53 or pJV75Amber. The mycobacteriophage Che9c genes *gp60* and *gp61* are expressed under the control of an acetamide-inducible promoter from pJV53. Che9c gp60 and gp61 are homologous to the *E. coli* Rac prophage RecE and RecT proteins, respectively and together act to increase homologous recombination efficiency in mycobacteria (159). wt-BCG::pJV53 (see Table 14) could subsequently be used to generate gene replacement mutants upon transformation of the strain with an appropriate allelic exchange substrate (AES). The AES for gene replacement is a linear fragment of dsDNA usually containing a selectable marker (e.g. hygromycin) flanked by approximately 500bp sequences homologous to the regions up- and down-stream of the genomic sequence targeted for replacement with the marker. Che9c *gp61* is expressed under the control of an acetamide-inducible promoter from pJV75Amber and facilitates strand invasion at the replication fork during replication of DNA of an ssDNA oligonucleotide (approximately 50bp in length) complementary to a genomic sequence targeted for mutation to introduce point mutations and small (1-2bp)

insertions/deletions (140). In addition pJV75Amber contains a hygromycin marker with two consecutive amber stop codon mutations conferring sensitivity to hygromycin (*hyg*$^{r-}$). Co-transformation with the ssDNA oligonucleotide JCV198 (see Table 14) which targets the *hyg*$^{r-}$ mutations in the hygromycin cassette of pJV75Amber and restores hygromycin resistance was used as a control for recombineering efficiency.

5.4.4. Point mutagenesis of *M. bovis* BCG *garA* codon T21 by method of recombineering

All oligonucleotides used are listed in Table 14. A 6ml starter culture of wt-BCG::pJV75Amber was prepared in a 25cm^2 cell culture flask and incubated at 37°C without agitation. When the starter culture reached an OD_{600} = 0.5 - 0.7, it was used to inoculate 100 ml induction medium (Middlebrook 7H9 supplemented with 0.05% (v/v) Tween80, 20 µg/ml kanamycin, and 0.2% (w/v) succinate) to an OD_{600} = 0.05 in a 175cm^2 cell culture flask. When this culture reached an OD_{600} of approximately 0.5, acetamide was added to a final concentration of 0.2% (w/v) and the culture incubated for another 24 hours. Cells were made electro-competent and transformed as described elsewhere (see section 1.3.2) with some modifications. Briefly, 100µl electrocompetent cells were mixed with 1µl (100 or 500 ng) oligonucleotide (T21Ac, T21Aw, V20Iw, T21Tw or T21Qw) and 1µl (100 ng) JCV198. Following electro-transformation cells were immediately suspended in 1ml 7H9 supplemented with 10% (v/v) OADC and 0.05% Tween80, transferred to a sterile 2 ml microcentrifuge tube and incubated without agitation at 37°C for 3 days. After the 3 days incubation period bacteria were diluted appropriately and spread on 7H11 containing 50 µg/ml hygromycin. Hygromycin resistant colonies were screened for mutations as described in the text (see chapter 2, sections 2.2.6 and 2.2.7).

5.4.5. Complementation of wt-BCG with a copy of *garA* containing a T21A or T21V codon substitution.

All oligonucleotides and plasmids used are listed in Table 1 and all molecular cloning procedures were carried out as previously described (177). *M. bovis* BCG was complemented with a *garA* copy harbouring the A61G (Thr21Ala) mutation, a *garA* copy harbouring the A61G, C62T, and G63T (Thr21Val) mutations and a wild type

garA copy using the integrating vector pGINTO. Briefly, the *garA* gene, along with a 526bp region upstream of the gene was amplified by PCR using Phusion High Fidelity PCR polymerase (FinnZymes, Finland), the specific oligonucleotides GarA3F and GarA3R, and pAVgarA-T21A and pAVgarA-T21V or purified wild type *M. bovis* BCG DNA as template (see chapter 5, section 5.4.6, Table 14). GarA3, GarA3-T21A and GarA3-T21V were each cloned into pJet1.2 (Fermentas, USA) using the manufacturer's recommendations, subsequently excised using the restriction endonuclease, *Asp718I* (Roche, Germany) according to the manufacturer's recommendations and cloned into the *Asp718I* site of pGINTO to produce the constructs: pGCgarA3, pGCgarA3-T21A, and pGCgarA3-T21V, respectively. Electro-competent *M. bovis* BCG cells were transformed with pGCgarA3, pGCgarA3-T21A, and pGCgarA3-T21V (see chapter 5, section 5.4.2). All sequences generated by PCR within pGCgarA3, pGCgarA3-T21A, and pGCgarA3-T21V were subjected to sequencing with the primers GarAF, GarAR, pJet1.2F, pJet1.2R, GarA3F, and GarA3R to confirm that no mutations were introduced by the polymerases.

5.4.6. Generation of *M. bovis* BCG pAVgarA-T21A-SCO and pAVgarA-T21V-SCO strains

All oligonucleotides and plasmids used are listed in Table 14 and all molecular cloning procedures were carried out as previously described (177). Briefly, single joint PCR and the oligonucleotides GarAHR1F, GarAHR1AR, GarAHR2AF, and GarAHR2R were used as decribed in chapter 5, section 5.5.4.2, to generate a 2kb fragment (GarAHRA) spanning approximately 1kb on either side of A61 of the *garA* sequence with the substitution A61G which resulted in a T21A alteration of the GarA polypeptide sequence. Similarly, using single joint PCR and substituting the oligonucleotides GarAHR1AR and GarAHR2AF for GarAHR1VR and GarAHR2VF were used to generate a similar 2kb fragment (GarAHRV) but with the nucleotide substitutions of *garA*: A61G, C62T, and G63T which resulted in a T21V alteration of the GarA polypeptide sequence. GarAHRA and GarAHRV were each cloned into pJet1.2 (Fermentas, USA) using the manufacturer's recommendations, subsequently excised using the restriction endonuclease, *KpnI* (Promega, USA) using the manufacturer's recommendations and cloned into the *KpnI* site of p2Nil to produce the constructs: p2NilgarA-T21A and p2NilgarA-T21V. The entire GarAHRA and GarAHRV fragments

within pJet1.2 were subjected to sequencing using the primers GarAR, pJet1.2F, and pJet1.2R to confirm that no mutations were introduced by the polymerase. The *PacI* fragment from pGOAL19 containing *lacZ*, *sacB*, and *hyg*^{R} was subsequently cloned into the *PacI* sites of p2NilgarA-T21A and p2NilgarAT21V to produce pAVgarA-T21A and pAVgarA-T21V, respectively. Exponentially growing *M. bovis* BCG cells (OD_{600} 0.5-0.8) were made electro-competent and transformed with the pAVgarA-T21A and pAVgarA-T21V constructs as was previously described (see chapter 5, section 5.4.2). The pAVgarA-T21A and pAVgarA-T21V constructs were treated with 100 mJ UV irradiation prior to electro-transformation into *M. bovis* BCG which was previously shown to increase homologous recombination efficiency (178). Bacteria in which pAVgarA-T21A and pAVgarA-T21V was integrated into the chromosome by homologous recombination were resistant to kanamycin and to hygromycin and turned blue in the presence of 50 µg/ml 5-bromo-4-chloro-indolyl-β-D-galactopyranoside (X-gal). Hence, blue, kan^R colonies were transferred to liquid culture without antibiotics, grown to mid-exponential phase (OD_{600} = 0.5 – 0.8) and plated on 7H11 supplemented with 2% sucrose and 50 µg/ml X-gal. Bacteria in which pAVgarA-T21A and pAVgarA-T21V were lost from the chromosome due to a second homologous recombination event were resistant to sucrose and remained white in the presence of X-gal. The genotype of white, *suc*^{R}, double cross-over (DCO) colonies was assayed by MAMA-PCR (see chapter 5, section 5.5.4.4).

5.4.7. Genetic complementation of *M. bovis* BCG pAVgarA-T21A-SCO and pAVgarA-T21V-SCO strains with a wild type copy of *garA*

The *M. bovis* BCG pAVgarA-T21A-SCO and pAVgarA-T21V-SCO strains were complemented with a wild type *garA* gene using the integrating vector pGCgarA3 (see chapter 5, section 5.4.5, Table 14). Electro-competent pAVgarA-T21A-SCO and pAVgarA-T21V-SCO cells were transformed with pGCgarA3 (see chapter 5, section 5.4.2). Gentamicin, kanamycin and hygromycin resistant colonies were subsequently isolated (see chapter 2, section 2.2.9, Figure 12).

5.4.8. Generation of a *ΔgltBD* strain of *M. bovis* BCG

All oligonucleotides and plasmids used are listed in Table 14. All molecular cloning procedures were carried out as previously described (177). The mycobacterial recombineering method was used to replace the *gltBD* operon with a hygromycin cassette (159). Briefly, the specific oligonucleotides UgltBDF and UgltBDR, harbouring *SphI* and *NcoI* restriction endonuclease recognition sites respectively, were used to generate a 499bp PCR fragment of the region directly upstream of the *gltBD* operon. The PCR fragment was cloned into pGEM-T Easy, which was subsequently digested with *SphI* and *NcoI* to obtain a restriction fragment of the upstream (U) region. The restriction fragment was directionally cloned into the *SphI-NcoI* sites of pMNFhyg to obtain pMNFhygU. Next the specific oligonucleotides DgltBDF and DgltBDR, harbouring *SpeI* and *PstI* restriction endonuclease recognition sites respectively, were used to generate a 511bp PCR fragment of the region directly downstream (D) of the *gltBD* operon. The PCR fragment was cloned into pGEM-T Easy, and subsequently digested with *SpeI* and *PstI* to obtain a restriction fragment of the D region. The restriction fragment was directionally cloned into the *SphI-NcoI* sites of pMNFhygU to produce pAVgltBD. The linear allelic exchange substrate was obtained from pAVgltBD in a double restriction digestion with *SphI* and *PstI*. *M. bovis* BCG carrying the pJV53 recombineering plasmid (see Table 1) was cultured in Middlebrook 7H9 supplemented with 0.05% (v/v) Tween80 and 0.2% (w/v) succinate to approximately 0.5 OD_{600} and acetamide was added to a final concentration of 0.2% w/v (159). The culture was incubated for 16 hours at 37°C without agitation before it was used to make electrocompetent cells (see chapter 5, section 5.4.2) which were subsequently transformed with the linear allelic exchange substrate. Hygromycin resistant colonies were subjected to PCR and Southern blot analysis (see chapter 3, section 3.2.1). The U and D sequences in pGEM-T Easy were subjected to sequencing (see chapter 5, section 5.5.7) using the primers T7_promoter and SP6 to confirm that no mutations were introduced by the polymerase.

5.4.9. Generation of a genetically complemented *M. bovis* BCG *ΔgltBD* strain

Briefly, the *gltBD* operon, along with a 525bp region upstream of the gene, which is likely to contain the native promoter of the operon, was amplified by PCR using Phusion High Fidelity PCR polymerase (FinnZymes, Finland) and the specific oligonucleotides CgltBDF and CgltBDR. The CgltBD fragment was ligated to pGINTO that was linearized with *ScaI* to produce pGCgltBD. Electro-competent *ΔgltBD* mutant cells were transformed with pGCgltBD (see chapter 5, section 5.4.2). The entire CgltBD fragment within pGCgltBD was subjected to sequencing using the primers CgltBDF, CgltBD2 – CgltBD11, and CgltBDR to confirm that no mutations were introduced by the polymerases. Gentamicin resistant complemented colonies were assayed by PCR to confirm integration of the plasmid (see chapter 3, section 3.2.1). Although there is evidence that expression from the acetamidase promoter is supressed in *M. bovis* BCG when cultured in the absence of acetamide (160, 161), the progenitor strain of *ΔgltBD*, wt-BCG::pJV53 was included in analyses (as indicated in the text) to control for residual effects of the recombineering plasmid.

5.4.10. Generation of a *Δgdh* strain of *M. bovis* BCG

All oligonucleotides and plasmids used are listed in Table 1 and all molecular cloning procedures were carried out as previously described (177). The *gdh* gene was disrupted by allelic-exchange using the plasmids p2Nil and pGOAL17 (75). Briefly, a fragment that spans the GDH domain of *gdh*, as well as approximately 1 kb of the 5' and 3' sequences flanking the GDH domain, was amplified by PCR with long PCR enzyme mix (Fermentas, USA) using the specific oligonucleotides gdhF and gdhR. The resulting PCR amplicon was cloned into the pGEM-T Easy vector to generate pGEMgdh. The central in-frame *NruI* fragment spanning the GDH domain was subsequently excised to obtain vector pGEMΔgdh containing adjacent 5' and 3' flanking sequences of the GDH domain. The entire Δgdh fragment within pGEMΔgdh was subjected to sequencing using the primers T7_promoter, gdh4, PgdhF, PgdhR, gdh3, and SP6 to confirm that no mutations were introduced by the polymerase. The *KpnI* fragment containing the GDH domain flanking regions was excised from pGEMΔgdh and cloned into the *KpnI* site of p2Nil to produce p2NilΔgdh. Finally, a *PacI* cassette containing the genes *sacB* and *lacZ* from pGOAL17 (170) was excised

and cloned into the *PacI* site of p2NilΔgdh to produce pAVΔgdh. The pAVΔgdh deletion construct was treated with 100 mJ UV irradiation prior to electro-transformation (see chapter 5, section 5.4.6) *M. bovis* BCG was made electro-competent and electro-transformed with pAVΔgdh as described elsewhere (see chapter 5, section 5.4.2). Bacteria in which pAVΔgdh was integrated into the chromosome by homologous recombination were resistant to kanamycin (kan^R) and turned blue in the presence of 50 µg/ml 5-bromo-4-chloro-indolyl-β-D-galactopyranoside (X-gal). Hence, blue, kan^R colonies were transferred to liquid culture without antibiotics, grown to mid-exponential phase (OD_{600} = 0.5 – 0.8) and plated on 7H11 supplemented with 2% sucrose and 50 µg/ml X-gal. Bacteria in which pAVΔgdh was lost from the chromosome by a second homologous recombination were resistant to sucrose (suc^R) and remained white in the presence of X-gal. White, suc^R colonies were subjected to PCR and Southern blot analysis (see chapter 3, section 3.2.2).

5.4.11. Generation of a genetically complemented *M. bovis* BCG *Δgdh* strain

The *Δgdh* mutant strain was complemented with a functional *gdh* gene using the integrating vector pGINTO (Table 14). Briefly, the *gdh* gene, along with a 565bp region upstream of the gene was amplified by PCR using Phusion High Fidelity PCR polymerase (FinnZymes, Finland) and the specific oligonucleotides CgdhF and CgdhR (Table 14). The Cgdh fragment was ligated to *ScaI*-linearized pGINTO to produce pGCgdh (Table 14). Electro-competent *Δgdh* mutant cells were transformed with pGCgdh (see chapter 5, section 5.4.2). The entire Cgdh fragment within pGCgdh was subjected to sequencing using the primers CgdhF, Cgdh2 – Cgdh10, and CgdhR to confirm that no mutations were introduced by the polymerase. Gentamicin resistant complemented colonies were assayed by PCR to confirm integration of the plasmid (see chapter 3, section 3.2.2).

5.5. Working with DNA

5.5.1. Isolation of plasmid DNA from *E. coli*

Plasmid DNA was extracted from *E. coli* cultures using the Wizard Plus SV Minipreps DNA Purification System (Promega, USA) or the NucleoBond PC 100 Plasmid DNA

Purification Kit (Macherey-Nagel, Germany) following the manufacturer's instructions in each case.

5.5.2. Isolation of genomic DNA from *M. bovis* BCG

5.5.2.1. Isolation of crude DNA for PCR

For high fidelity PCR as well as the amplification of long fragments a volume of 1 ml *M. bovis* BCG culture (washed twice with sterile de-ionised water and re-suspended in 50 µl nuclease free water (Ambion, USA)) or a suspension of de-aggregated bacterial colony in sterile de-ionised water were boiled at 102°C for 20 minutes, pelleted by centrifugation (12 000 × g, 1 minute, room temperature), and the supernatant decanted for use as DNA template (2 µl).

5.5.2.2. Isolation of high quality and purity DNA

For PCR applications which required concentrated high purity genomic DNA template, genomic DNA was extracted from a 1 ml *M. bovis* BCG culture grown to an OD of at least 0.8 and washed once with sterile de-ionised water using the Zymo Research Fungal/Bacterial DNA MiniPrep Kit (Zymo Research, USA) according to the manufacturer's instructions. For Southern blotting analysis high quality pure genomic DNA was extracted from *M. bovis* BCG as was previously described (179). Briefly, 7H11 agar containing *M. bovis* BCG growth were incubated at 80°C for 1 hour. Afterwards bacterial growth was dislodged from the agar by adding 3 ml extraction buffer (5% MSG, 50mM Tris-HCl, 25mM EDTA, pH 7) and scraping with an L-shaped spreader. The extraction buffer bacterial suspension was then transferred to a 50ml centrifuge tube (Greiner, USA) containing approximately 5 ml glass balls (5 mm diameter). Bacteria remaining on the plate were transferred to the centrifuge tube with another 3 ml extraction buffer and scraping with a spreader. Bacterial clumps were broken by vortexing the centrifuge tube for 2 minutes. Bacterial cells were lysed by the addition of 500µl lysozyme (Roche, Germany) and 2.5µl RNaseA (Roche, Germany) to the tube and incubation at 37°C for 2 hours. After lysis 600µl proteinase K buffer (Roche, Germany) and 150µl proteinase K (Roche, Germany) was added to the tube and the suspension incubated at 45°C for 16 hours. A volume of 5ml phenol/chloroform/isoamylalcohol (25:24:1 (v/v)) was added and the tube mixed by

inversion every 30 minutes for 2 hours. The tubes were subsequently centrifugation at 1800 × g for 20 minutes at room temperature in order to aid separation into a lower organic phase containing cellular debris and proteins and an upper aqueous phase containing nucleic acids. The top aqueous phase (approximately 5 - 6 ml, containing the gDNA) was transferred to a new 50 ml centrifuge tube. DNA was precipitated from the aqueous phase by addition of 600 µl sodium acetate (3 M, pH 5.5) and 7 ml ice cold isopropanol and immediately collected with the tip of a thin sterile glass rod. The tip of the glass rod with DNA around it was placed inside a sterile 1.5 ml microcentrifuge tube (Axygen, USA) containing 1ml 70% ethanol for 10 minutes. The tip of the glass rod was then transferred to new sterile 1.5 ml microcentrifuge tube and left to dry at room temperature for 2-3 hours. DNA was dislodged from the glass rod by addition of 500µl nuclease free water and allowed to reconstitute overnight at 4°C.

5.5.3. Analysis of plasmid/genomic DNA concentration, purity, and integrity

DNA concentration was measured with a Nanodrop 100 spectrophotometer (Thermo Scientific, USA) and in some instances estimated by gel electrophoresis. Purity of DNA (plasmid or genomic) was also assessed using the nanodrop. A260/A280 and A260/A230 ratios of between 1.80 and 2.30 were used as cut-off values when highly pure plasmid or genomic DNA was desired. DNA integrity was assessed by gel electrophoresis. A single high molecular weight band with negligible smear was considered to be indicative of intact genomic DNA. All construct plasmids made during the study were assessed by restriction mapping with at least three restriction endonucleases.

5.5.4. PCR

5.5.4.1. Conventional polymerase chain reaction (PCR)

Conventional PCR was performed with either HotStarTaq (Qiagen) or FastStart (Roche). The 25 µl HotStartTaq reaction consisted of 1X Q-buffer (supplied as a 5X solution, supplement for high GC-content template), 1X reaction buffer (supplied as a 10X solution), 0.2 mM of each of the deoxyribonucleotide triphosphates (ATP, TTP, GTP, CTP, Bioline, UK), 3.5 mM $MgCl_2$, 1 µM of each primer, 1 u HotStarTaq, and between 2 and 20 ng purified DNA template or 2 µl bacterial suspension or boiled cells

suspension (see chapter, section 5.5.2.1). The thermic cycling conditions of the HotStart PCR reaction were as follows: activation of HotStarTaq enzyme at 95°C for 15 minutes, 35 cycles of denaturation of the template DNA at 94°C for 30 seconds, annealing of the primers to the DNA template at 60°C for 30 seconds, and extension of the PCR product at 72°C for 1 minute per kilobase (kb) of the amplicon, and a final extension step at 72°C for 7 minutes. Upon completion of the thermic cycling reactions were used immediately for subsequent procedures or kept at 4 – 8°C for a few hours or stored at -20°C for later use. The 25 µl FastStart reaction contained 1X GC rich solution (supplied as a 5X solution), 1X reaction buffer containing 20mM $MgCl_2$ (supplied as a 10X solution), 0.2mM of each of the deoxyribonucleotide triphosphates, 1 µM of each primer, 1 u FastStart enzyme, and between 2 and 20 ng purified DNA template or 2 µl bacterial suspension or supernatant from boiled bacterial cells (see chapter 5, section 5.5.2.1). The thermic cycling conditions of the FastStart PCR reaction were essentially the same as for the HotStart reaction with the following differences: activation of FastStart enzyme at 95°C for 4 minutes and denaturation of the template DNA at 95°C for 30 seconds.

5.5.4.2. High fidelity PCR and PCR of long fragments

PCR amplification of long fragments (> 3 kb) and PCR with a low error rate were performed with long PCR enzyme (Fermentas, USA) or Phusion enzyme (Finnzymes, USA) as indicated in the text. The 50 µl long PCR reaction contained 1X long PCR enzyme reaction buffer containing 15mM $MgCl_2$ (supplied as a 10X solution), 0.2 mM of each of the deoxyribonucleotide triphosphates, 1 µM of each primer, 1.25 u long PCR enzyme, and 2 – 20 ng purified DNA template or 2µl supernatant of boiled bacterial cells. The thermic cycling conditions of the long PCR reaction were as follows: activation of the long PCR enzyme at 94°C for 5 minutes, 35 cycles of denaturation of the template DNA at 96°C for 10 seconds, annealing of the primers to the DNA template at 60°C for 30 seconds, and extension of the PCR product at 68°C for 1 minute per kilobase (kb) of the amplicon, and a final extension step at 68°C for 10 minutes. The 50 µl Phusion reaction contained 1X Phusion reaction buffer (supplied as a 5X solution), 1X GC rich solution (from Roche FastStart kit, see previous section), 0.2 µM of each of the deoxyribonucleotide triphosphates, 1 µM of each primer, 1 u Phusion enzyme, and 2 – 20 ng purified DNA template or 2 µl supernatant of boiled

bacterial cells (see chapter 5, section 5.5.2.1). The thermic cycling conditions of the long PCR reaction were as follows: activation of the Phusion enzyme at 98°C for 30 seconds, 35 cycles of denaturation of the template DNA at 98°C for 10 seconds, annealing of the primers to the DNA template at 60°C for 30 seconds, and extension of the PCR product at 72°C for 30 seconds per kilobase (kb) of the amplicon, and a final extension step at 72°C for 10 minutes.

5.5.4.3. High resolution melt analysis

High resolution melt analysis was performed as previously described (180). Briefly a 25 µl HotStarTaq (Qiagen, Germany) reaction was prepared as outlined in chapter 5, section 5.5.4.1, but also containing 2 µM of the fluorescent dye Syto 9 (Invitrogen, USA). The supernatant from boiled bacterial cells (colonies obtained from solid medium and de-aggregated in liquid as explained in section chapter 5, section 5.5.2.1) was used as template. The thermic cycling conditions of the HotStart PCR reaction for HRM analysis were as follows: activation of HotStarTaq enzyme at 95°C for 15 minutes, 35 cycles of denaturation of the template DNA at 94°C for 1 minute, annealing of the primers to the DNA template at 60°C for 1 minute, and extension of the PCR product at 72°C for 1 minute, and a final extension step at 72°C for 7 minutes. Upon completion of the thermic cycling reactions 12.5 µl of each unknown sample reaction was mixed with 12.5 µl of a wild type reaction in a new thin walled 200µl PCR tube (QSP, USA). The remaining 12.5 µl of each unknown sample reaction was transferred to a new thin walled 200µl PCR tube and acted as positive controls. The unknown-wild type mixtures were heated to 95°C for 45 seconds and subsequently cooled to 40°C for 2 minutes to induce heteroduplex formation between wild type amplicons (A61) and A61G in amplicons in unknown sample reactions. Heteroduplex formation was previously used to more easily detect nucleotide transversions (A:T and G:C) in unknown samples (180). In addition, two first derivative peaks are expected for the thermal melt profile for a heteroduplex whereas a single derivative peak is expected for the thermal melt profile of a homoduplex and could be used to more easily discriminate between wild type and mutant. The thermal melt profile was subsequently measured from 85°C to 95°C with fluorometric measurements after each 0.1°C increase in temperature using the Corbett Rotorgene 6000 (Qiagen, USA) instrument. The Rotor-Gene 6000 series 1.7 software was used to obtain first derivative plots of

HRM profiles as well as to analyse the generated HRM profiles. The profile generated for a known wild type negative control which was included in each HRM run was defined as the profile of the wild type genotype. Automatic calling of unknown sample genotypes as wild type or varying from wild type was performed using the HRM software, which also provided an R value (in percentage) as measure of confidence for each call made.

5.5.4.4. Mismatch amplification mutation assay (MAMA) PCR

MAMA-PCR was carried out as previously described (142). Briefly, a standard 25 µl HotStarTaq PCR or FastStart PCR reaction was setup containing three primers. Two of the primers amplified a control product of approximately 1000 bp in size. Along with the forward control primer another reverse primer (MAMA primer) with a single mismatch to wt-BCG template DNA at the penultimate 3'-nucleotide amplified a 400 – 500 bp product from wt-BCG template, but not from mutant BCG template wherein an additional mismatch to the ultimate 3'-nucleotide of the MAMA primer impeded extension by the PCR enzyme. In a separate reaction a MAMA primer was used which along with the forward control primer selectively amplified a 400-500 bp product from mutant BCG and not from wt-BCG template.

5.5.4.5. Site directed mutagenesis by double-joint PCR

Single nucleotide substitutions were introduced into target sequences by a modification of the previously described double-joint PCR technique (181). Briefly, a standard 50 µl Phusion PCR reaction was setup (see chapter 5, section 5.5.4.2) with a reverse primer that was complementary to the site of mutagenesis, but with a substitution of the nucleotide to be mutagenized (up-stream reaction). Similarly another standard 50 µl Phusion PCR reaction was setup (down-stream reaction), but in this case the forward primer was totally complementary to the reverse primer from the up-stream reaction. Care was taken during design of the mutagenesis primers that the substitutions were at least 3 bp from the 3'-ends of the primers so as not to affect elongation by the PCR enzyme. Standard cycling conditions for a Phusion PCR reaction was used to amplify the products in both reactions (see chapter 5, section 5.5.4.2). PCR products were verified by gel electrophoresis and 2 µl each of the up-

and downstream reactions added to a 50 µl (final volume) assembly reaction containing 1X Phusion High Fidelity buffer (supplied as a 5X solution), 1X FastStart GC rich solutions (supplied as a 5X solution), 0.2mM of each deoxyribonucleotide triphosphate, and 1 unit Phusion polymerase. A thermal step at 98°C for 1 minute which both activated the Phusion polymerase enzyme and denaturated DNA double strands was followed by a 60°C step for 10 minutes which allowed renaturing of double stranded DNA and elongation by the polymerase enzyme from the 3'-recessive ends in hybrids of up- and downstream amplicons. Subsequently, 40 µl of the assembly reaction was removed to a new PCR tube and 2 µl of 5X High Fidelity Phusion buffer, 2 µl of the up-stream amplicon forward primer, 2 µl of the down-stream amplicon reverse primer, and 4 µl of nuclease free water added. Thermal cycling ensued with the following steps: 35 cycles of denaturation of the template DNA at 98°C for 10 seconds, annealing of the primers to the DNA template at 60°C for 30 seconds, and extension of the PCR product at 72°C for 30 seconds per kilobase (kb) of the amplicon, and a final extension step at 72°C for 10 minutes. The correct PCR amplicon was excised from the gel and purified as detailed in chapter 5, section 5.5.6.

5.5.4.6. Extraction of DNA from PCR reactions

DNA was extracted from PCR reactions using the Wizard SV Gel and PCR Clean-up system (Promega, USA) according the manufacturer's guidelines.

5.5.5. Southern blotting

Pure gDNA (6 µg, see chapter 5, section 5.5.2.1) was digested for 16 hours at 37°C in a 100 µl reaction containing 30 units of restriction endonuclease (see chapter 5, section 5.5.7). Digested gDNA was precipitated and re-constituted in 20 µl loading buffer (see chapter 5, section 5.5.7.1) and subjected to gel electrophoresis at 70 V for 4 hours in a 1% agarose gel (1 × TAE, pH 8, see chapter 5, section 5.5.6). DNA fragments were chemically denatured and transferred from the agarose gel to a Hybond N1 membrane (GE Healthcare, UK) by capillary action according to the manufacturer's recommendations. Hybridisation and detection was performed with the Amersham ECL Nucleic acid Labelling kit (GE Healthcare, UK) according to the manufacturer's recommendations. The PCR products obtained from UgltBDF and

UgltBDR as well as DgltBDF and DgltBDR (see chapter 5, section 5.5.4.1) were used as probes for the southern blotting analysis of *ΔgltBD*. A probe for southern blotting analysis of *Δgdh* was generated by PCR using the specific oligonucleotides PgdhF and PgdhR (Table 14), HotStarTaq polymerase (Qiagen, Germany) and the pGEMΔgdh construct as template.

5.5.6. Gel electrophoresis and extraction of DNA from agarose gels

For visualisation of PCR products in screening tests and with small amplicon sizes (< 1 kb) 2 – 4 % agarose (Lonza, USA) gels were prepared with 1X sodium tetraborate decahydrate (SB) buffer. SB buffer offers the advantage of greater heat tolerance of gels and thus electrophoresis at higher voltages (> 120 V) and more rapid electrophoretic migration of DNA fragments (182). For visualisation and excision of larger fragments and Southern blots (1 – 10 kb) 0.7 – 1.0 % agarose gels were prepared with 1X tris TAE buffer (40 mM Tris, 40 mM acetate, 1mM EDTA, pH 8.0). After electrophoretic separation of DNA fragment, ethidium bromide (0.5 µg/ml Sigma, Germany) stained gels were subjected to UV-B light (302 nm) or blue light (470 - 530 nm, in combination with an orange emission post-filter) and bands of interest excised with a scalpel. DNA fragments were purified from gel slices using the Wizard SV Gel and PCR Clean-up system (Promega, USA) according the manufacturer's guidelines.

5.5.7. Restriction, dephosphorylation, ligation and sequencing of DNA

Restriction digests of DNA was performed with restriction endonucleases obtained from Roche (Germany), New England Biolabs (UK), Fermentas (USA), or Promega (USA) according to the respective manufacturer's recommendations. Dephosphorylation of restricted vector fragments in order to decrease re-circularisation frequencies during ligation reactions were carried out with Antarctic phosphatase (New England Biolabs, UK) or with rAPid alkaline phosphatase (Roche) according to the respective manufacturer's recommendations. Ligations were carried out using T4 ligase (Roche, Germany) according to the manufacturer's guidelines. DNA sequencing was performed at the Stellenbosch University Central Analytical Facility and was analysed with Sequencher 5.1 software (Gene Codes, USA).

5.5.7.1. Precipitation of DNA in order to increase concentrations

DNA in reaction mixtures in 1.5 ml microcentrifuge tubes was precipitated in order to increase the concentration of the samples or to decrease sample volume without a loss of nucleic acid yield. Briefly, 1/10th volume 3M sodium acetate pH 5.5 (Ambion, USA) was added to the solution and distributed by pipetting. Precipitation of DNA was induced by addition of 3 volumes of 100% ethanol (Sigma, Germany) and incubation at -20°C for 16 hours (overnight). Precipitated nucleic acids were collected by centrifugation at 12 000 × g for 30 minutes at 4°C. The supernatant was discarded and the resulting DNA pellet washed twice with 70% ethanol. The DNA pellet was dried at room temperature for 1 – 16 hours and reconstituted in nuclease free water or buffer solution as specified in the text.

5.6. Working with RNA

5.6.1. Isolation of total RNA from *M. bovis* BCG

Bacteria (15 ml) were pelleted by centrifugation, re-suspended in 1 ml RNApro solution (MP Biomedicals, Germany) and transferred to a Lysing Matrix B tube (MP Biomedicals, Germany). Bacterial cells were homogenised with a FastPrep-24 tissue and cell homogeniser (MP Biomedicals, Germany) for 40 seconds at a speed setting of 6.5 m/s, and cooled on ice for 2 – 4 minutes. Afterwards, homogenisation was repeated once with the same settings. The Fast RNA Pro Blue Kit protocol (MP Biomedicals, Germany) was subsequently followed to extract RNA up until the point where ethanol was added to precipitate nucleic acids. At this point, the ethanol-containing solution was transferred directly to the membrane of a NucleoSpin RNA II column (Macherey Nagel, Germany). RNA was subsequently purified according to the manufacturer's recommendations (Macherey Nagel, Germany), which included an on-column DNase-treatment step. RNA extraction, analysis and cDNA conversion was performed in duplicate for each assayed bacterial culture.

5.6.2. Analysis of purity and integrity of RNA

RNA purity was analysed by spectrophotometric profiling on the NanoDrop 1000 spectrophotometer (Thermo Scientific, USA). Samples with A260/A280 and A260/A230 ratios between 1.80 and 2.20 were considered to be pure of contaminating reverse transcriptase or DNA polymerase inhibitors. Integrity of RNA was assessed as well as RNA concentration determined by automated electrophoresis with the Agilent 2100 Bioanalyzer (Agilent Technologies, USA). Samples with RIN values greater than 7.5 were considered undegraded and used in subsequent analyses.

5.6.3. DNase treatment of total RNA and further purification

DNA contamination was removed from purified RNA (100 ng/µl) using Turbo DNase (Ambion, USA) and the protocol for rigorous DNase treatment according to the manufacturer's recommendations. The Turbo DNase treatment was terminated by the addition of the DNase Inactivation Reagent (Ambion, USA).

5.6.4. First strand cDNA synthesis

RNA (400 ng) was converted to cDNA using the PrimeScript 1st Strand cDNA Sunthesis kit (Takara, Japan) and random hexamer primers according to the manufacturer's recommendations. After synthesis a 1:2 dilution of the cDNA reaction was prepared for use in subsequent steps (see next section). For the gene expression analysis of the high copy number reference genes *sigA* and *16S* rRNA, further 1:100 and 1:100 000 dilutions were made, respectively. This was done in order for the threshold cycle (Ct) values of assays with these genes to occur in the linear range of the PCR reaction (between 15 and 25 cycles). A no reverse transcriptase (-RT) control was included for each sample.

5.6.5. Quantitative real-time PCR (qPCR)

Real time PCR was carried out in a 384-well plate format with the 7900HT real time instrument (Applied Biosystems, USA) using the TaKaRa SYBR Premix Ex Taq (Tli RNaseH Plus) kit (Takara, Japan), according to the manufacturer's recommendations.

Each reaction (10 µl) contained 10 ng cDNA template and was performed in duplicate. In order to control for gDNA contamination of cDNA samples –RT controls (10 ng nucleic acid) as wells as Turbo DNase-treated RNA (100 ng) were assayed in parallel with sample assays. The assay for the reference gene, 16S, was used in the qPCR reactions of RNA and –RT controls. A threshold cycle (Ct) value of lower than 32 for a –RT control resulted in exclusion of a sample from further analysis. A standard curve of Ct over target template number was obtained for each assay in a plate from a ten-fold dilution series of purified wt-BCG gDNA (see chapter 5, section 5.5.2.2) ranging from 10^6 genomes/qPCR reaction to 10 genomes/qPCR reaction.

5.6.6. Analysis of qPCR data and determination of relative gene expression

Absolute expression was determined from the linear range of the standard curve obtained for each assay (see previous section). Absolute gene expression data for gene of interest was normalised to that of the reference gene *16S*. It was found in this study that expression of the reference gene, *sigA*, was altered by the investigated conditions, therefore only *16S* data was used. 16S-normalised data of treatment groups were compared to 16S-normalised data of untreated groups to obtain a measure of relative gene expression in response to treatment and analysed statistically (as indicated in the text).

5.7. Working with proteins

5.7.1. Analysis of protein concentration in whole cell lysates of *M. bovis* BCG

M. bovis BCG (25 ml) was pelleted (2000 × g, 10 minutes, 4°C), re-suspended in 1 ml of 100mM NaH_2PO_4/K_2HPO_4 buffer (pH 7.0), transferred to a 2 ml screw cap tube containing approximately 200 µl zirconium balls (0.1 mm diameter), homogenised with a FastPrep-24 tissue and cell homogeniser (MP Biomedicals, USA) for 40 seconds at a speed setting of 6.5 m/s, and cooled on ice for 2 – 4 minutes. Homogenisation was repeated once more with the same settings. The homogenate was centrifuged (12 000 × g, 10 minutes, 4°C) and the clear cell lysate transferred to a sterile 1.5 ml microcentrifuge tube. Total protein concentration in lysates was determined by method

of the Bio-Rad Protein Assay (Bio-Rad, USA) and the manufacturer's standard protocol for a microtiter plate.

5.7.2. GS activity assay

The standard GS γ-glutamyl transferase reaction was carried out as previously described (183). Briefly, a reaction mixture (500 µl, pH = 7.0) consisted of 20 mM imidazole, 30 mM L-glutamine, 0.4 mM Na-ADP, 60 mM hydroxylamine, 20 mM K_2HAsO_4 and 3 mM $MnCl_2$, and 6 µg total protein. A reaction was initiated by the addition of a master mix solution of reaction components to sample containing protein. The enzymatic reaction occurred at 37°C for 30 minutes and was stopped with the addition of 125 µl of a solution containing 2% (w/v) $FeCl_3$, 8% (w/v) trichloroacetic acid, and 2 M HCl. The mixed imidazole buffer-system GS γ-glutamyl transferase reaction was carried according to the method described by (129). Briefly, a reaction mixture (500 µl, pH was varied as indicated in text) consisted of 50 mM imidazole, 50 mM 2-methylimidazole, 50 mM 2,4-dimethylimidazole, 20 mM L-glutamine, 0.4 mM Na-ADP, 20 mM hydroxylamine, 20 mM K_2HAsO_4 and 0.3 mM $MnCl_2.4H_2O$, 60 mM $MgCl_2.6H_2O$ (or not) and 6 µg total protein. The assay was initiated by the addition of a master mix solution of reaction components to sample containing protein and occurred at 37°C for 30 minutes. The reaction was stopped with the addition of 1 ml of a solution containing 0.2 M $FeCl_3$, 0.2 M trichloroacetic acid and 0.25 M HCl. Samples (200µl) were subsequently transferred to a 96 well plate and spectrophotometric measurements were taken at 540 nm with a Synergy HT Luminometer (Bio-Tek Instruments, USA). L-γ-glutamyl hydroxamate production was determined from an L-γ-glutamyl hodroxamate standard curve. Control reactions were included in which L-glutamine as excluded from the assay system. One unit (U) of GS activity was defined as the amount of enzyme which produced 1 µmole of γ-glutamyl hydroxamate per minute. Specifc GS activity was expressed as mU per mg of total protein (mU/mg protein).

5.7.3. GOGAT activity assay

GOGAT was assayed at 37°C according to the method of Ahmad et al. (1986) (18). A single reaction mixture (200µl, pH 7.5) contained 50 mM Tris-HCl (replaced as indicated in the text), 2mM L-glutamine, 1mM 2-oxoglutarate, 1mM EDTA, 0.15mM NADPH, and 10 - 20 µg total protein. Reactions were initiated with the addition of the cofactor NADPH. The continuous enzyme activity assay tracks the oxidation of NADPH to $NADP^+$ over 1-minute intervals for a 10 minute period by measuring a decrease in optical density at 340nm. Spectrophotometric measurements were made in a 96 well plate format with a Synergy HT Luminometer (Bio-Tek Instruments, USA). The molar extinction coefficient of NADH, expressed in units of $OD_{340nm}.\mu mol^{-1}.well^{-1}$, was determined empirically using a standard curve of OD_{340nm} over [NADPH]. For each sample a control reaction was included in which L-glutamine was omitted. One unit (U) of GOGAT activity was defined as the amount of enzyme which consumed 1 nanomole of NADPH per minute. Specifc GOGAT activity was expressed as mU per mg of total protein (mU/mg protein).

5.7.4. GDH activity assay

GDH activity was assayed at 37°C in the forward or reverse direction in a 96 well plate format according to the method of Miñambres *et al.* (2000) (56). A single forward reaction mixture (200 µl, pH = 7) contained 100 mM NaH_2PO_4/K_2HPO_4, 100 mM NH_4Cl, 15 mM 2-oxoglutarate, 0.15 mM NADH and 10 - 20 µg total protein. A single reverse reaction mixture (200 µl) contained 100 mM NaH_2PO_4/K_2HPO_4, 100 mM L-glutamate, 0.5 mM NAD^+ and 10 - 20 µg total protein. Reactions were initiated with the addition of the cofactor NADH (forward reaction) or NAD^+ (reverse reaction). The continuous enzyme activity assay tracks the oxidation of NADH to NAD^+ over 1-minute intervals for a 10 minute period by measuring a decrease in optical density at 340nm. Spectrophotometric measurements were made in a 96 well plate format with a Synergy HT Luminometer (Bio-Tek Instruments, USA). As the path length of the light through the enzyme reaction is not fixed at 1cm in the microtiter plate assay the molar extinction coefficient of NADH, expressed in units of $OD_{340nm}.\mu mol^{-1}.well^{-1}$, was determined empirically using a standard curve of OD_{340nm} over [NADH]. For each sample a control reaction was included in which 2-oxoglutarate was omitted. One unit

(U) of GDH activity was defined as the amount of enzyme which consumed 1 nanomole of NADH per minute. Specifc GDH activity was expressed as mU per mg of total protein (mU/mg protein).

5.8. *M. bovis* BCG intracellular survival

5.8.1. Culturing and infection of BMDM monolayers

The intracellular survival assay was performed as previously described with some modifications (184, 185). Briefly, tibia and femur bones were dissected from 6-10 week old female C57/BL6 mice and the marrow flushed out and dispersed with 2.5 ml of RPMI 1640 medium with L-glutamine and sodium bicarbonate (Sigma, USA) and a 25-GA syringe needle. The bone marrow cell suspension was adjusted to 2×10^5 cells.ml^{-1} in RPMI-20 medium (consisted of RPMI 1640 medium with L glutamine and sodium bicarbonate, 10% fetal bovine serum (Biochrom, UK) and 20% supernatant from L929 cells (prepared as previously described (186)). The cells were plated in 10ml volumes on bacterial Petri dishes (Greiner, USA) and incubated at 37°C with 5% CO_2 for 7 days. Cells were fed with 10ml RPMI-20 after 4 days. Non-adherent cells were removed in two washes with PBS (Lonza, USA) before adherent cells were released with 10ml ice cold PBS. Released macrophages were adjusted to 2×10^5 cells.ml^{-1} in RPMI-10 (as described before but with 10% supernatant from L929 cells). Cells were seeded in 24 well plates (1ml.well^{-1}) and allowed to adhere for 24 hours. Bacteria grown to early exponential growth phase (OD_{600} = 0.5-0.8) were washed once with PBS (Lonza, USA). Bacterial aggregates were removed by low speed centrifugation (200 × g for 10 minutes) and the resulting supernatant passed through a 5µm surfactant free cellulose acetate syringe filter (Sartorius, Germany). Bacterial suspensions were prepared in RPMI-10 to yield a multiplicity of infection (MOI) of 1:1; namely 1 bacterial cell to 1 macrophage. The RPMI-10 medium was replaced with 0.5ml bacterial suspension in infection wells. In previous experiments using a different protocol and an M.O.I. of 5:1, we observed a loss of the BMDM monolayer and extracellular growth of bacteria. In the current protocol at an M.O.I. of 1:1, the monolayers remained intact. Infection of monolayers lasted for 4h before they were washed four times with pre-warmed PBS to eliminate non-phagocytosed bacteria and re-fed with RPMI-10. The medium covering each monolayer was replaced every 48h.

5.8.2. Harvesting bacteria and enumeration of BCG infection

Infected macrophages were lysed with 0.1% Triton X-100 solution (Sigma, Germany). Duplicate serial dilutions of the lysates were prepared in 7H9 and spread on 7H11 agar supplemented with OADC in 24 well plates. Bacterial colonies became visible and were enumerated under a stereoscopic microscope (Nikon, Japan) at 10X to 40X magnification after 7-14 days of incubation at 37°C.

5.9. Bioinformatic approaches

Sequence alignments were carried out with the basic local alignment search tool (BLAST) available on the National Centre for Biotechnology Information website (http://blast.ncbi.nlm.nih.gov/Blast.cgi). PCR primers were designed with primer 3 software (187) or with the Integrated DNA Technologies (IDT) PrimerQuest Assay Design Tool (http://eu.idtdna.com/PrimerQuest/Home/Index). Secondary structures in some PCR assays, such as qPCR assays were analysed with the IDT UNAfold webserver (http://eu.idtdna.com/UNAFold?). Metabolic pathway data was obtained from the Kyoto Encyclopedia of Genes and Genomes (KEGG) and from the Pathosystems Resource Integration Centre (PATRIC) (15–17).

5.10. Growth curve analysis

Growth curves were modelled in GraphPad Prism 5 version 5.01 (GraphPad Software) using non-linear regression to fit the Logistic or Gompertz sigmoidal growth functions to OD data (188). OD data have been fit with mathematical models to obtain parameters of growth for several bacterial species (189–192). Biological parameters of bacterial growth were obtained, including maximal achieved growth (A) defined as the asymptote of the functions, maximal growth rate (R) defined as the first derivative of the functions at the inflection point and lag time (L) defined as the value at the x-axis intercept of the tangential line through the inflection point (Figure 33A). These growth functions were written with the syntax allowed in the GraphPad Prism 5 software (Table 16). For each growth curve a comparison using Akaike's Information Criteria was made between the Logistic and Gompertz models to select the model

which was most likely to have generated the curve. The parameters obtained for the selected model was used in subsequent analyses. A general observation in this study was that instead of maintaining a plateau once stationary phase was reached, the OD measurements of *M. bovis* BCG cultures started to decrease within 2 – 3 days of when the highest OD reading was made. It was reasoned that inclusion of the OD measurements post when the highest OD reading was taken may result in underestimation of the A-parameter. However, modelling with only the OD-measurements in the increasing range of the growth curves frequently led to non-convergence of the sigmoidal models or to overestimation of the A-value particularly by the Gompertz function (Figure 33B, broken line), therefore, the smallest possible number of decreasing OD readings succeeding the highest reading and permitting convergence of one of the two models were included in analyses (Figure 33B). Growth curve data was collected over a minimum of 15 days, which was usually sufficient time for *M. bovis* BCG cultures to reach stationary phase, however in isolated instances (indicated in the text) no declining data was available. In these cases the logistic function, which was found to be less prone to overestimate the A-value (Figure 33B, solid line) than the Gompertz model was used to model the data. A limitation in the modelling of growth curves was observed for the L parameter when the inflection point occurred very early on the x-axis and was accompanied by a low R-parameter value, which resulted in very low or even negative L-parameter estimations. Therefore, only significant increases in L values from control groups were considered.

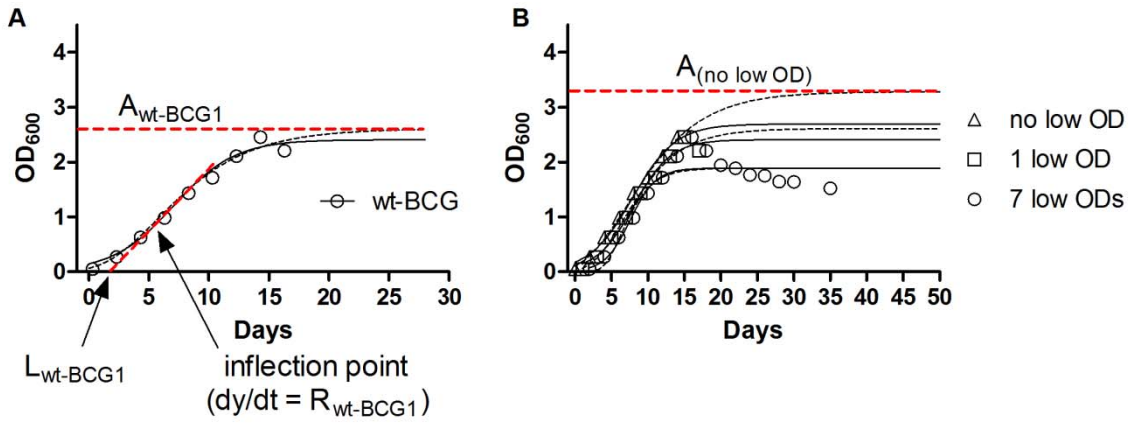

Figure 33: Estimation of lag time (L), maximum growth rate (R) and maximum growth achieved (A) by modelling growth curve data with the sigmoidal growth functions. The solid line indicates modelling with the Logistic function, while the broken line indicates modelling with the Gompertz

function. A) How the growth parameters (L, R and A are determined). (B). While estimation of growth rate and lag time was relatively stable between the two models, the Gompertz function over-estimated maximum growth rate achieved in comparison with the logistic function, especially when the model was only fit to data in the increasing OD range.

Table 16: Original re-parameterized logistic and Gompertz functions as well as their forms in the allowed GraphPad Prism 5 syntax:

Logistic growth model	
$Y(t) = \frac{A}{1 + e^{[\frac{4R}{A}.(L-t)+1]}}$	(188)
Y=A/(1+exp((4R/A)*(L-x)+2))	GraphPad Prism syntax
Rules for curve-fit initial values: parameter: A, initial value: 1.0, rule: *YMAX parameter: R, initial value: 10.0, rule: *YMIN parameter: L, initial value: 1.0, rule: /(Value of X at YMID)	
Gompertz growth model	
$Y(t) = A.e^{-e^{[\frac{R.e}{A}.(L-t)+1]}}$	(188)
Y=A*exp(-exp((R*exp(1)/A)*(L-x)+1))	GraphPad Prism syntax
Rules for curve-fit initial values: parameter: A, initial value: 1.0, rule: *YMAX parameter: R, initial value: 1.0, rule: *YMIN parameter: L, initial value: 1.0, rule: /(Value of X at YMID)	

5.11. Statistical analysis

Statistical analyses were carried out with the statistics software GraphPad Prism 5 version 5.01 (GraphPad Software). Repeated experiments were regarded as randomized block designs and assessed by repeated measures one-way or two-way ANOVA tests with Bonferroni post-testing to compare pairs of columns. For analyses of growth curves, the best bit-fit values obtained for the three parameters of growth (see chapter 5, section 5.10) were compared between different growth curves using a one-way ANOVA with Bonferroni post testing. Probabilities of < 0.05 were considered significant.

References

1. **World Health Organization**. 2012. Global tuberculosis report 2012. World Health Organization, Geneva, Switzerland.

2. **Cox HS, McDermid C, Azevedo V, Muller O, Coetzee D, Simpson J, Barnard M, Coetzee G, van Cutsem G, Goemaere E**. 2010. Epidemic levels of drug resistant tuberculosis (MDR and XDR-TB) in a high HIV prevalence setting in Khayelitsha, South Africa. PLoS ONE **5**:e13901.

3. **Strauss OJ, Warren RM, Jordaan A, Streicher EM, Hanekom M, Falmer AA, Albert H, Trollip A, Hoosain E, van Helden PD, Victor TC**. 2008. Spread of a low-fitness drug-resistant *Mycobacterium tuberculosis* strain in a setting of high human immunodeficiency virus prevalence. J. Clin. Microbiol. **46**:1514–1516.

4. **Klopper M, Warren RM, Hayes C, Gey van Pittius NC, Streicher EM, Müller B, Sirgel FA, Chabula-Nxiweni M, Hoosain E, Coetzee G, David van Helden P, Victor TC, Trollip AP**. 2013. Emergence and spread of extensively and totally drug-resistant tuberculosis, South Africa. Emerging Infect. Dis. **19**:449–455.

5. **Ayé R, Wyss K, Abdualimova H, Saidaliev S**. 2010. Household costs of illness during different phases of tuberculosis treatment in Central Asia: a patient survey in Tajikistan. BMC Public Health **10**:18.

6. **Ayé R, Wyss K, Abdualimova H, Saidaliev S**. 2010. Illness costs to households are a key barrier to access diagnostic and treatment services for tuberculosis in Tajikistan. BMC Res Notes **3**:340.

7. **Gülbay BE, Gürkan ÖU, Yıldız ÖA, Önen ZP, Erkekol FÖ, Baççıoğlu A, Acıcan T**. 2006. Side effects due to primary antituberculosis drugs during the initial phase of therapy in 1149 hospitalized patients for tuberculosis. Respiratory Medicine **100**:1834–1842.

8. **Awofeso N**. 2008. Anti-tuberculosis medication side-effects constitute major factor for poor adherence to tuberculosis treatment. Bull. World Health Organ. **86**:B–D.

9. **DeJesus MA, Zhang YJ, Sassetti CM, Rubin EJ, Sacchettini JC, Ioerger TR**. 2013. Bayesian analysis of gene essentiality based on sequencing of transposon insertion libraries. Bioinformatics **29**:695–703.

10. **Griffin JE, Gawronski JD, Dejesus MA, Ioerger TR, Akerley BJ, Sassetti CM**. 2011. High-resolution phenotypic profiling defines genes essential for mycobacterial growth and cholesterol catabolism. PLoS Pathog. **7**:e1002251.

11. **Murphy DJ, Brown JR**. 2007. Identification of gene targets against dormant phase *Mycobacterium tuberculosis* infections. BMC Infect Dis **7**:84.

12. **Voskuil MI, Bartek IL, Visconti K, Schoolnik GK**. 2011. The response of *Mycobacterium Tuberculosis* to reactive oxygen and nitrogen species. Front Microbiol **2**.

13. **Zhang YJ, Ioerger TR, Huttenhower C, Long JE, Sassetti CM, Sacchettini JC, Rubin EJ**. 2012. Global assessment of genomic regions required for growth in *Mycobacterium tuberculosis*. PLoS Pathog. **8**:e1002946.

14. **Sassetti CM, Boyd DH, Rubin EJ**. 2003. Genes required for mycobacterial growth defined by high density mutagenesis. Molecular Microbiology **48**:77–84.

15. **Gillespie JJ, Wattam AR, Cammer SA, Gabbard JL, Shukla MP, Dalay O, Driscoll T, Hix D, Mane SP, Mao C, Nordberg EK, Scott M, Schulman JR, Snyder EE, Sullivan DE, Wang C, Warren A, Williams KP, Xue T, Yoo HS, Zhang C, Zhang Y, Will R, Kenyon RW, Sobral BW**. 2011. PATRIC: the comprehensive bacterial bioinformatics resource with a focus on human pathogenic species. Infect. Immun. **79**:4286–4298.

16. **Kanehisa M, Goto S, Sato Y, Furumichi M, Tanabe M**. 2012. KEGG for integration and interpretation of large-scale molecular data sets. Nucleic Acids Res. **40**:D109–114.

17. **Kanehisa M, Goto S**. 2000. KEGG: kyoto encyclopedia of genes and genomes. Nucleic Acids Res. **28**:27–30.

18. **Ahmad S, Bhatnagar RK, Venkitasubramanian TA**. 1986. Changes in the enzyme activities involved in nitrogen assimilation in *Mycobacterium smegmatis* under various growth conditions. Ann Inst Pasteur Microbiol **137B**:231–7.

19. **Amon J, Titgemeyer F, Burkovski A**. 2009. A genomic view on nitrogen metabolism and nitrogen control in mycobacteria. J. Mol. Microbiol. Biotechnol. **17**:20–29.

20. **O'Hare HM, Durán R, Cerveñansky C, Bellinzoni M, Wehenkel AM, Pritsch O, Obal G, Baumgartner J, Vialaret J, Johnsson K, Alzari PM**. 2008. Regulation of glutamate metabolism by protein kinases in mycobacteria. Mol Microbiol **70**:1408–23.

21. **Gómez-Valero L, Rocha EPC, Latorre A, Silva FJ**. 2007. Reconstructing the ancestor of *Mycobacterium leprae*: the dynamics of gene loss and genome reduction. Genome Res. **17**:1178–1185.

22. **Titgemeyer F, Amon J, Parche S, Mahfoud M, Bail J, Schlicht M, Rehm N, Hillmann D, Stephan J, Walter B, Burkovski A, Niederweis M**. 2007. A genomic view of sugar transport in *Mycobacterium smegmatis* and *Mycobacterium tuberculosis*. J. Bacteriol. **189**:5903–5915.

23. **Merrick MJ, Edwards RA**. 1995. Nitrogen control in bacteria. Microbiol Rev **59**:604–622.

24. **Harth G, Clemens DL, Horwitz MA**. 1994. Glutamine synthetase of *Mycobacterium tuberculosis*: extracellular release and characterization of its enzymatic activity. Proc Natl Acad Sci U S A **91**:9342–6.

25. **Almassy RJ, Janson CA, Hamlin R, Xuong N-H, Eisenberg D**. 1986. Novel subunit—subunit interactions in the structure of glutamine synthetase. Nature **323**:304–309.

26. **Gill HS, Pfluegl GMU, Eisenberg D**. 2002. Multicopy crystallographic refinement of a relaxed glutamine synthetase from *Mycobacterium tuberculosis* highlights flexible loops in the enzymatic mechanism and its regulation. Biochemistry **41**:9863–9872.

27. **Liaw SH, Villafranca JJ, Eisenberg D**. 1993. A model for oxidative modification of glutamine synthetase, based on crystal structures of mutant H269N and the oxidized enzyme. Biochemistry **32**:7999–8003.

28. **Rhee SG, Park SC, Koo JH**. 1985. The role of adenylyltransferase and uridylyltransferase in the regulation of glutamine synthetase in *Escherichia coli*. Curr. Top. Cell. Regul. **27**:221–232.

29. **Harth G, Horwitz MA**. 1997. Expression and efficient export of enzymatically active *Mycobacterium tuberculosis* glutamine synthetase in *Mycobacterium smegmatis* and evidence that the information for export is contained within the protein. J Biol Chem **272**:22728–35.

30. **Harth G, Maslesa-Galić S, Tullius MV, Horwitz MA**. 2005. All four *Mycobacterium tuberculosis glnA* genes encode glutamine synthetase activities but only GlnA1 is abundantly expressed and essential for bacterial homeostasis. Mol Microbiol **58**:1157–72.

31. **Tullius MV, Harth G, Horwitz MA**. 2001. High extracellular levels of *Mycobacterium tuberculosis* glutamine synthetase and superoxide dismutase in actively growing cultures are due to high expression and extracellular stability rather than to a protein-specific export mechanism. Infect Immun **69**:6348–63.

32. **Harth G, Horwitz MA**. 1999. An inhibitor of exported *Mycobacterium tuberculosis* glutamine synthetase selectively blocks the growth of pathogenic mycobacteria in axenic culture and in human monocytes: extracellular proteins as potential novel drug targets. J Exp Med **189**:1425–36.

33. **Harth G, Zamecnik PC, Tang JY, Tabatadze D, Horwitz MA**. 2000. Treatment of *Mycobacterium tuberculosis* with antisense oligonucleotides to glutamine synthetase mRNA inhibits glutamine synthetase activity, formation of the poly-L-glutamate/glutamine cell wall structure, and bacterial replication. Proc Natl Acad Sci U S A **97**:418–23.

34. **Harth G, Horwitz MA**. 2003. Inhibition of *Mycobacterium tuberculosis* glutamine synthetase as a novel antibiotic strategy against tuberculosis: demonstration of efficacy *in vivo*. Infect Immun **71**:456–64.

35. **Lee S, Jeon B-Y, Bardarov S, Chen M, Morris SL, Jacobs WR**. 2006. Protection elicited by two glutamine auxotrophs of *Mycobacterium tuberculosis* and *in vivo* growth phenotypes of the four unique glutamine synthetase mutants in a murine model. Infect. Immun. **74**:6491–6495.

36. **Tullius MV, Harth G, Horwitz MA**. 2003. Glutamine synthetase GlnA1 is essential for growth of *Mycobacterium tuberculosis* in human THP-1 macrophages and guinea pigs. Infect Immun **71**:3927–36.

37. **Chandra H, Basir SF, Gupta M, Banerjee N**. 2010. Glutamine synthetase encoded by *glnA-1* is necessary for cell wall resistance and pathogenicity of *Mycobacterium bovis*. Microbiology (Reading, Engl.) **156**:3669–3677.

38. **Collins DM, Wilson T, Campbell S, Buddle BM, Wards BJ, Hotter G, De Lisle GW**. 2002. Production of avirulent mutants of *Mycobacterium bovis* with vaccine properties by the use of illegitimate recombination and screening of stationary-phase cultures. Microbiology (Reading, Engl.) **148**:3019–3027.

39. **Hasan S, Daugelat S, Rao PSS, Schreiber M**. 2006. Prioritizing genomic drug targets in pathogens: application to *Mycobacterium tuberculosis*. PLoS Comput Biol **2**:e61.

40. **Carroll P, Waddell SJ, Butcher PD, Parish T**. 2011. Methionine sulfoximine resistance in *Mycobacterium tuberculosis* is due to a single nucleotide deletion resulting in increased expression of the major glutamine synthetase, GlnA1. Microb Drug Resist **17**:351–355.

41. **Proler M, Kellaway P**. 2008. The methionine sulfoximine syndrome in the cat. Epilepsia **3**:117–130.

42. **Rowe WB, Meister A**. 1970. Identification of L-methionine-S-sulfoximine as the convulsant isomer of methionine sulfoximine. PNAS **66**:500–506.

43. **Gising J, Nilsson MT, Odell LR, Yahiaoui S, Lindh M, Iyer H, Sinha AM, Srinivasa BR, Larhed M, Mowbray SL, Karlén A**. 2012. Trisubstituted imidazoles as *Mycobacterium tuberculosis* glutamine synthetase inhibitors. J. Med. Chem. **55**:2894–2898.

44. **Nilsson MT, Krajewski WW, Yellagunda S, Prabhumurthy S, Chamarahally GN, Siddamadappa C, Srinivasa BR, Yahiaoui S, Larhed M, Karlén A, Jones TA, Mowbray SL**. 2009. Structural basis for the inhibition of *Mycobacterium tuberculosis* glutamine synthetase by novel ATP-competitive inhibitors. Journal of Molecular Biology **393**:504–513.

45. **Nordqvist A, Nilsson MT, Lagerlund O, Muthas D, Gising J, Yahiaoui S, Odell LR, Srinivasa BR, Larhed M, Mowbray SL, Karlén A**. 2012. Synthesis, biological evaluation and X-ray crystallographic studies of imidazo[1,2-a]pyridine-based *Mycobacterium tuberculosis* glutamine synthetase inhibitors. Med. Chem. Commun. **3**:620–626.

46. **Odell LR, Nilsson MT, Gising J, Lagerlund O, Muthas D, Nordqvist A, Karlén A, Larhed M**. 2009. Functionalized 3-amino-imidazo[1,2-a]pyridines: a novel class of drug-like *Mycobacterium tuberculosis* glutamine synthetase inhibitors. Bioorganic & Medicinal Chemistry Letters **19**:4790–4793.

47. **Lamichhane G, Zignol M, Blades NJ, Geiman DE, Dougherty A, Grosset J, Broman KW, Bishai WR**. 2003. A postgenomic method for predicting essential genes at subsaturation levels of mutagenesis: application to *Mycobacterium tuberculosis*. Proc Natl Acad Sci U S A **100**:7213–8.

48. **Rengarajan J, Bloom BR, Rubin EJ**. 2005. Genome-wide requirements for *Mycobacterium tuberculosis* adaptation and survival in macrophages. Proc. Natl. Acad. Sci. U.S.A. **102**:8327–8332.

49. **Sassetti CM, Rubin EJ**. 2003. Genetic requirements for mycobacterial survival during infection. PNAS **100**:12989–12994.

50. **Vanoni MA, Curti B**. 2005. Structure–function studies on the iron–sulfur flavoenzyme glutamate synthase: an unexpectedly complex self-regulated enzyme. Archives of Biochemistry and Biophysics **433**:193–211.

51. **Van den Heuvel RH., Svergun DI, Petoukhov MV, Coda A, Curti B, Ravasio S, Vanoni MA, Mattevi A**. 2003. The active conformation of glutamate synthase and its binding to ferredoxin. Journal of Molecular Biology **330**:113–128.

52. **Lamichhane G, Freundlich JS, Ekins S, Wickramaratne N, Nolan ST, Bishai WR**. 2011. Essential metabolites of *Mycobacterium tuberculosis* and their mimics. mBio **2**.

53. **Cheung YW, Tanner JA**. 2011. Targeting glutamate synthase for tuberculosis drug development. Hong Kong Med J **17 Suppl 2**:32–34.

54. **Benachenhou-Lahfa N, Forterre P, Labedan B**. 1993. Evolution of glutamate dehydrogenase genes: evidence for two paralogous protein families and

unusual branching patterns of the archaebacteria in the universal tree of life. J Mol Evol **36**:335–46.

55. **Andersson JO, Roger AJ**. 2003. Evolution of glutamate dehydrogenase genes: evidence for lateral gene transfer within and between prokaryotes and eukaryotes. BMC Evol Biol **3**:14.

56. **Miñambres B, Olivera ER, Jensen RA, Luengo JM**. 2000. A new class of glutamate dehydrogenases (GDH). Biochemical and genetic characterization of the first member, the AMP-requiring NAD-specific GDH of *Streptomyces clavuligerus*. J Biol Chem **275**:39529–42.

57. **Camardella L, Di Fraia R, Antignani A, Ciardiello MA, di Prisco G, Coleman JK, Buchon L, Guespin J, Russell NJ**. 2002. The Antarctic *Psychrobacter* sp. TAD1 has two cold-active glutamate dehydrogenases with different cofactor specificities. Characterisation of the NAD^+-dependent enzyme. Comp Biochem Physiol A Mol Integr Physiol **131**:559–67.

58. **Kawakami R, Sakuraba H, Ohshima T**. 2007. Gene cloning and characterization of the very large NAD-dependent l-glutamate dehydrogenase from the psychrophile *Janthinobacterium lividum*, isolated from cold soil. J Bacteriol **189**:5626–33.

59. **Lu CD, Abdelal AT**. 2001. The *gdhB* gene of *Pseudomonas aeruginosa* encodes an arginine-inducible NAD^+-dependent glutamate dehydrogenase which is subject to allosteric regulation. J Bacteriol **183**:490–9.

60. **Harper CJ, Hayward D, Kidd M, Wiid I, van Helden P**. 2010. Glutamate dehydrogenase and glutamine synthetase are regulated in response to nitrogen availability in *Myocbacterium smegmatis*. BMC Microbiol **10**:138.

61. **Harper C, Hayward D, Wiid I, van Helden P**. 2008. Regulation of nitrogen metabolism in *Mycobacterium tuberculosis*: a comparison with mechanisms in *Corynebacterium glutamicum* and *Streptomyces coelicolor*. IUBMB Life **60**:643–50.

62. **Amon J, Titgemeyer F, Burkovski A**. 2010. Common patterns - unique features: nitrogen metabolism and regulation in Gram-positive bacteria. FEMS Microbiol Rev.

63. **Amon J, Bräu T, Grimrath A, Hänssler E, Hasselt K, Höller M, Jessberger N, Ott L, Szököl J, Titgemeyer F, Burkovski A**. 2008. Nitrogen control in *Mycobacterium smegmatis*: nitrogen-dependent expression of ammonium transport and assimilation proteins depends on the OmpR-type regulator GlnR. J Bacteriol **190**:7108–16.

64. **Helling RB**. 1994. Why does *Escherichia coli* have two primary pathways for synthesis of glutamate? J. Bacteriol **176**:4664–4668.

65. **Helling RB**. 1998. Pathway Choice in Glutamate Synthesis in *Escherichia coli*. J. Bacteriol **180**:4571–4575.

66. **Schulz AA, Collett HJ, Reid SJ**. 2001. Nitrogen and carbon regulation of glutamine synthetase and glutamate synthase in *Corynebacterium glutamicum* ATCC 13032. FEMS Microbiology Letters **205**:361–367.

67. **Reuther J, Wohlleben W**. 2007. Nitrogen metabolism in *Streptomyces coelicolor*: transcriptional and post-translational regulation. J. Mol. Microbiol. Biotechnol. **12**:139–146.

68. **Atkinson MR, Fisher SH**. 1991. Identification of genes and gene products whose expression is activated during nitrogen-limited growth in *Bacillus subtilis*. J. Bacteriol. **173**:23–27.

69. **Tesch M, de Graaf AA, Sahm H**. 1999. *In vivo* fluxes in the ammonium-assimilatory pathways in *Corynebacterium glutamicum* studied by 15N nuclear magnetic resonance. Appl Environ Microbiol **65**:1099–1109.

70. **Beckers G, Nolden L, Burkovski A**. 2001. Glutamate synthase of *Corynebacterium glutamicum* is not essential for glutamate synthesis and is regulated by the nitrogen status. Microbiology (Reading, Engl.) **147**:2961–2970.

71. **Fisher SH**. 1989. Glutamate synthesis in *Streptomyces coelicolor*. J Bacteriol **171**:2372–7.

72. **Ertan H**. 1992. The effect of various culture conditions on the levels of ammonia assimilatory enzymes of *Corynebacterium callunae*. Arch. Microbiol. **158**:42–47.

73. **Jenkins VA, Barton GR, Robertson BD, Williams KJ**. 2013. Genome wide analysis of the complete GlnR nitrogen-response regulon in *Mycobacterium smegmatis*. BMC Genomics **14**:301.

74. **Pashley CA, Brown AC, Robertson D, Parish T**. 2006. Identification of the *Mycobacterium tuberculosis* GlnE promoter and its response to nitrogen availability. Microbiology **152**:2727–34.

75. **Parish T, Stoker NG**. 2000. *glnE* is an essential gene in *Mycobacterium tuberculosis*. J Bacteriol **182**:5715–20.

76. **Carroll P, Pashley CA, Parish T**. 2008. Functional analysis of GlnE, an essential adenylyl transferase in *Mycobacterium tuberculosis*. J Bacteriol **190**:4894–902.

77. **Niebisch A, Kabus A, Schultz C, Weil B, Bott M**. 2006. Corynebacterial protein kinase G controls 2-oxoglutarate dehydrogenase activity via the phosphorylation status of the OdhI protein. J. Biol. Chem. **281**:12300–12307.

78. **Nott TJ, Kelly G, Stach L, Li J, Westcott S, Patel D, Hunt DM, Howell S, Buxton RS, O'Hare HM, Smerdon SJ**. 2009. An intramolecular switch regulates phosphoindependent FHA domain interactions in *Mycobacterium tuberculosis*. Sci Signal **2**:ra12.

79. **Schultz C, Niebisch A, Gebel L, Bott M**. 2007. Glutamate production by *Corynebacterium glutamicum*: dependence on the oxoglutarate dehydrogenase inhibitor protein OdhI and protein kinase PknG. Appl Microbiol Biotechnol **76**:691–700.

80. **Anand N, Singh P, Sharma A, Tiwari S, Singh V, Singh DK, Srivastava KK, Singh BN, Tripathi RP**. 2012. Synthesis and evaluation of small libraries of triazolylmethoxy chalcones, flavanones and 2-aminopyrimidines as inhibitors of mycobacterial FAS-II and PknG. Bioorganic & Medicinal Chemistry **20**:5150–5163.

81. **Cowley S, Ko M, Pick N, Chow R, Downing KJ, Gordhan BG, Betts JC, Mizrahi V, Smith DA, Stokes RW, Av-Gay Y**. 2004. The *Mycobacterium tuberculosis* protein serine/threonine kinase PknG is linked to cellular glutamate/glutamine levels and is important for growth *in vivo*. Mol Microbiol **52**:1691–702.

82. **Jayachandran R, Scherr N, Pieters J**. 2012. Elimination of intracellularly residing *Mycobacterium tuberculosis* through targeting of host and bacterial signaling mechanisms. Expert Review of Anti-infective Therapy **10**:1007–1022.

83. **Scherr N, Müller P, Perisa D, Combaluzier B, Jenö P, Pieters J**. 2009. Survival of pathogenic mycobacteria in macrophages is mediated through autophosphorylation of protein kinase G. J Bacteriol **191**:4546–4554.

84. **Walburger A, Koul A, Ferrari G, Nguyen L, Prescianotto-Baschong C, Huygen K, Klebl B, Thompson C, Bacher G, Pieters J**. 2004. Protein kinase G from pathogenic mycobacteria promotes survival within macrophages. Science **304**:1800–1804.

85. **Feehily C, Karatzas KAG**. 2013. Role of glutamate metabolism in bacterial responses towards acid and other stresses. J. Appl. Microbiol. **114**:11–24.

86. **Goude R, Renaud S, Bonnassie S, Bernard T, Blanco C**. 2004. Glutamine, glutamate, and α-glucosylglycerate are the major osmotic solutes accumulated by *Erwinia chrysanthemi* strain 3937. Appl. Environ. Microbiol. **70**:6535–6541.

87. **Yan D**. 2007. Protection of the glutamate pool concentration in enteric bacteria. Proc Natl Acad Sci U S A **104**:9475–80.

88. **Barry CE 3rd, Boshoff HI, Dartois V, Dick T, Ehrt S, Flynn J, Schnappinger D, Wilkinson RJ, Young D**. 2009. The spectrum of latent tuberculosis: rethinking the biology and intervention strategies. Nat Rev Microbiol **7**:845–55.

89. **Gengenbacher M, Kaufmann SHE**. 2012. *Mycobacterium tuberculosis*: success through dormancy. FEMS Microbiology Reviews **36**:514–532.

90. **Khan A, Akhtar S, Ahmad JN, Sarkar D**. 2008. Presence of a functional nitrate assimilation pathway in *Mycobacterium smegmatis*. Microb. Pathog **44**:71–77.

91. **Malm S, Tiffert Y, Micklinghoff J, Schultze S, Joost I, Weber I, Horst S, Ackermann B, Schmidt M, Wohlleben W, Ehlers S, Geffers R, Reuther J, Bange F-C**. 2009. The roles of the nitrate reductase NarGHJI, the nitrite reductase NirBD and the response regulator GlnR in nitrate assimilation of *Mycobacterium tuberculosis*. Microbiology (Reading, Engl.) **155**:1332–1339.

92. **Chen JM, Alexander DC, Behr MA, Liu J**. 2003. *Mycobacterium bovis* BCG vaccines exhibit defects in alanine and serine catabolism. Infect. Immun. **71**:708–716.

93. **Grode L, Seiler P, Baumann S, Hess J, Brinkmann V, Nasser Eddine A, Mann P, Goosmann C, Bandermann S, Smith D, Bancroft GJ, Reyrat J-M, van Soolingen D, Raupach B, Kaufmann SHE**. 2005. Increased vaccine efficacy against tuberculosis of recombinant *Mycobacterium bovis* bacille Calmette-Guérin mutants that secrete listeriolysin. J. Clin. Invest. **115**:2472–2479.

94. **Lin W, Mathys V, Ang ELY, Koh VHQ, Gómez JMM, Ang MLT, Rahim SZZ, Tan MP, Pethe K, Alonso S**. 2012. Urease activity represents an alternative pathway for *Mycobacterium tuberculosis* nitrogen metabolism. Infect. Immun. **80**:2771–2779.

95. **Mukai T, Maeda Y, Tamura T, Miyamoto Y, Makino M**. 2008. CD4+ T-cell activation by antigen-presenting cells infected with urease-deficient recombinant *Mycobacterium bovis* bacillus Calmette-Guérin. FEMS Immunol. Med. Microbiol. **53**:96–106.

96. **Reitzer L**. 2003. Nitrogen assimilation and global regulation in *Escherichia coli*. Annual Review of Microbiology **57**:155(22).

97. **Fisher SH**. 1999. Regulation of nitrogen metabolism in *Bacillus subtilis*: vive la différence! Mol. Microbiol. **32**:223–232.

98. **Awasthy D, Gaonkar S, Shandil RK, Yadav R, Bharath S, Marcel N, Subbulakshmi V, Sharma U**. 2009. Inactivation of the *ilvB1* gene in *Mycobacterium tuberculosis* leads to branched-chain amino acid auxotrophy and attenuation of virulence in mice. Microbiology **155**:2978–2987.

99. **Bange FC, Brown AM, Jacobs WR**. 1996. Leucine auxotrophy restricts growth of *Mycobacterium bovis* BCG in macrophages. Infect. Immun. **64**:1794–1799.

100. **Gordhan BG, Smith DA, Alderton H, McAdam RA, Bancroft GJ, Mizrahi V**. 2002. Construction and phenotypic characterization of an auxotrophic mutant of *Mycobacterium tuberculosis* defective in l-arginine biosynthesis. Infect Immun **70**:3080–3084.

101. **Hondalus MK, Bardarov S, Russell R, Chan J, Jacobs WR Jr, Bloom BR**. 2000. Attenuation of and protection induced by a leucine auxotroph of *Mycobacterium tuberculosis*. Infect. Immun. **68**:2888–2898.

102. **McAdam RA, Weisbrod TR, Martin J, Scuderi JD, Brown AM, Cirillo JD, Bloom BR, Jacobs WR**. 1995. *In vivo* growth characteristics of leucine and methionine auxotrophic mutants of *Mycobacterium bovis* BCG generated by transposon mutagenesis. Infect. Immun. **63**:1004–1012.

103. **Smith DA, Parish T, Stoker NG, Bancroft GJ**. 2001. Characterization of auxotrophic mutants of *Mycobacterium tuberculosis* and their potential as vaccine candidates. Infect Immun **69**:1142–1150.

104. **Gouzy A, Poquet Y, Levillain F, De Carvalho L, Neyrolles O**. 2012. A novel amino acid permease system for *Mycobacterium tuberculosis* nitrogen acquisition and host colonization. Unpublished paper presented at the EMBO Conference Tuberculosis 2012: Biology, Pathogenesis, Intervention strategies, Pasteur Institute, Paris, France.

105. **Feng Z, Cáceres NE, Sarath G, Barletta RG**. 2002. *Mycobacterium smegmatis* L-alanine dehydrogenase (Ald) is required for proficient utilization of alanine as a sole nitrogen source and sustained anaerobic growth. J Bacteriol **184**:5001–10.

106. **Giffin MM, Modesti L, Raab RW, Wayne LG, Sohaskey CD**. 2011. *ald* of *Mycobacterium Tuberculosis* Encodes Both the Alanine Dehydrogenase and the Putative Glycine Dehydrogenase. J. Bacteriol. **194**:1045–1054.

107. **Wayne LG, Hayes LG**. 1996. An *in vitro* model for sequential study of shiftdown of *Mycobacterium tuberculosis* through two stages of nonreplicating persistence. Infect Immun **64**:2062–9.

108. **Wayne LG, Lin KY**. 1982. Glyoxylate metabolism and adaptation of *Mycobacterium tuberculosis* to survival under anaerobic conditions. Infect. Immun. **37**:1042–1049.

109. **Wayne LG, Sohaskey CD**. 2001. Nonreplicating persistence of *Mycobacterium tuberculosis*. Annu Rev Microbiol **55**:139–63.

110. **Gordon AH, Hart PD, Young MR**. 1980. Ammonia inhibits phagosome-lysosome fusion in macrophages. Nature **286**:79–80.

111. **Sohaskey CD**. 2008. Nitrate enhances the survival of *Mycobacterium tuberculosis* during inhibition of respiration. J Bacteriol **190**:2981–2986.

112. **Tian J, Bryk R, Itoh M, Suematsu M, Nathan C**. 2005. Variant tricarboxylic acid cycle in *Mycobacterium tuberculosis*: Identification of α-ketoglutarate decarboxylase. Proceedings of the National Academy of Sciences of the United States of America **102**:10670–10675.

113. **Young VR, Ajami AM**. 2001. Glutamine: the emperor or his clothes? J. Nutr. **131**:2449S–2459S.

114. **Edson NL**. 1951. The intermediary metabolism of the mycobacteria. Bacteriol Rev **15**:147–182.

115. **Lyon RH, Rogers P, Hall WH, Lichstein HC**. 1967. Inducible glutamate transport in mycobacteria and its relation to glutamate oxidation. J Bacteriol **94**:92–100.

116. **De Carvalho LPS, Zhao H, Dickinson CE, Arango NM, Lima CD, Fischer SM, Ouerfelli O, Nathan C, Rhee KY**. 2010. Activity-based metabolomic profiling of enzymatic function: identification of *Rv1248c* as a mycobacterial 2-hydroxy-3-oxoadipate synthase. Chemistry & Biology **17**:323–332.

117. **De Carvalho LPS, Ling Y, Shen C, Warren JD, Rhee KY**. 2011. On the chemical mechanism of succinic semialdehyde dehydrogenase (GabD1) from *Mycobacterium tuberculosis*. Archives of Biochemistry and Biophysics **509**:90–99.

118. **Miner MD, Chang JC, Pandey AK, Sassetti CM, Sherman DR**. 2009. Role of cholesterol in *Mycobacterium tuberculosis* infection. Indian J. Exp. Biol. **47**:407–411.

119. **Csonka LN**. 1989. Physiological and genetic responses of bacteria to osmotic stress. Microbiol Rev **53**:121–147.

120. **Wood JM**. 2011. Bacterial osmoregulation: a paradigm for the study of cellular homeostasis. Annu. Rev. Microbiol. **65**:215–238.

121. **Brown AD**. 1990. Microbial water stress physiology: principles and perspectives. Wiley, Chichester ; New York.

122. **Lundborg M, Falk R, Johansson A, Kreyling W, Camner P**. 1992. Phagolysosomal pH and dissolution of cobalt oxide particles by alveolar macrophages. Environ Health Perspect **97**:153–157.

123. **Nyberg K, Johansson U, Johansson A, Camner P**. 1992. Phagolysosomal pH in alveolar macrophages. Environ Health Perspect **97**:149–152.

124. **Sreevatsan S, Pan X, Stockbauer KE, Connell ND, Kreiswirth BN, Whittam TS, Musser JM**. 1997. Restricted structural gene polymorphism in the *Mycobacterium tuberculosis* complex indicates evolutionarily recent global dissemination. Proc. Natl. Acad. Sci. U.S.A. **94**:9869–9874.

125. **Jordao L, Bleck CKE, Mayorga L, Griffiths G, Anes E**. 2008. On the killing of mycobacteria by macrophages. Cell Microbiol **10**:529–48.

126. **Gey van Pittius NC, Sampson SL, Lee H, Kim Y, van Helden PD, Warren RM**. 2006. Evolution and expansion of the *Mycobacterium tuberculosis* PE and PPE multigene families and their association with the duplication of the ESAT-6 (esx) gene cluster regions. BMC Evol Biol **6**:95.

127. **Wulff K, Mecke D, Holzer H**. 1967. Mechanism of the enzymatic inactivation of glutamine synthetase from *E. coli*. Biochemical and Biophysical Research Communications **28**:740–745.

128. **Kingdon HS, Shapiro BM, Stadtman ER**. 1967. Regulation of glutamine synthetase. 8. ATP: glutamine synthetase adenylyltransferase, an enzyme that catalyzes alterations in the regulatory properties of glutamine synthetase. Proc Natl Acad Sci U S A **58**:1703–10.

129. **Stadtman ER, Smyrniotis PZ, Davis JN, Wittenberger ME**. 1979. Enzymic procedures for determining the average state of adenylylation of *Escherichia coli* glutamine synthetase. Anal Biochem **95**:275–85.

130. **Bancroft S, Rhee SG, Neumann C, Kustu S**. 1978. Mutations that alter the covalent modification of glutamine synthetase in *Salmonella typhimurium*. J. Bacteriol. **134**:1046–1055.

131. **Heuvel RHH van den, Curti B, Vanoni MA, Mattevi A**. 2004. Glutamate synthase: a fascinating pathway from L-glutamine to L-glutamate. CMLS, Cell. Mol. Life Sci. **61**:669–681.

132. **Djaman O, Outten FW, Imlay JA**. 2004. Repair of oxidized iron-sulfur clusters in *Escherichia coli*. J. Biol. Chem. **279**:44590–44599.

133. **Meers JL, Tempest DW, Brown CM**. 1970. 'Glutamine(amide):2-oxoglutarate amino transferase oxido-reductase (NADP); an enzyme involved in the synthesis of glutamate by some bacteria. J Gen Microbiol **64**:187–94.

134. **Miller RE, Stadtman ER**. 1972. Glutamate Synthase from *Escherichia coli*. Journal of Biological Chemistry **247**:7407 –7419.

135. **Sanwal BD, Lata M**. 1961. The occurrence of two different glutamic dehydrogenases in *Neurospora*. Can J Microbiol **7**:319–28.

136. **Holzer H, Hierholzer G, Witt L**. 1965. The role of glutamate dehydrogenases in the linkage and regulation of carbohydrate and nitrogen metabolism in yeast., p. 407–416. *In* In Colloq. Int. Centre Nat. Rech. Sci.

137. **Grenson M, Dubois E, Piotrowska M, Drillien R, Aigle M**. 1974. Ammonia assimilation in *Saccharomyces cerevisiae* as mediated by the two glutamate dehydrogenases. Molec. Gen. Genet. **128**:73–85.

138. **Miller SM, Magasanik B**. 1990. Role of NAD-linked glutamate dehydrogenase in nitrogen metabolism in *Saccharomyces cerevisiae*. J Bacteriol **172**:4927–35.

139. **Nguyen L, Walburger A, Houben E, Koul A, Muller S, Morbitzer M, Klebl B, Ferrari G, Pieters J**. 2005. Role of protein kinase G in growth and glutamine metabolism of *Mycobacterium bovis* BCG. J Bacteriol **187**:5852–6.

140. **Van Kessel JC, Hatfull GF**. 2008. Efficient point mutagenesis in mycobacteria using single-stranded DNA recombineering: characterization of antimycobacterial drug targets. Mol Microbiol **67**:1094–107.

141. **Hendrickson H, Lawrence JG**. 2007. Mutational bias suggests that replication termination occurs near the *dif* site, not at Ter sites. Mol Microbiol **64**:42–56.

142. **Cha RS, Zarbl H, Keohavong P, Thilly WG**. 1992. Mismatch amplification mutation assay (MAMA): application to the c-H-*ras* gene. PCR Methods Appl. **2**:14–20.

143. **Van Kessel JC**. 2008. Recombineering in mycobacteria using mycobacteriophage protiens. PhD, University of Pittsburgh, Pittsburgh.

144. **Loebel RO, Shorr E, Richardson HB**. 1933. The influence of foodstuffs upon the respiratory metabolism and growth of human tubercle bacilli. J Bacteriol **26**:139–66.

145. **Gengenbacher M, Rao SPS, Pethe K, Dick T**. 2010. Nutrient-starved, non-replicating *Mycobacterium tuberculosis* requires respiration, ATP synthase and isocitrate lyase for maintenance of ATP homeostasis and viability. Microbiology **156**:81–7.

146. **Betts JC, Lukey PT, Robb LC, McAdam RA, Duncan K**. 2002. Evaluation of a nutrient starvation model of *Mycobacterium tuberculosis* persistence by gene and protein expression profiling. Mol Microbiol **43**:717–31.

147. **Hampshire T, Soneji S, Bacon J, James BW, Hinds J, Laing K, Stabler RA, Marsh PD, Butcher PD**. 2004. Stationary phase gene expression of *Mycobacterium tuberculosis* following a progressive nutrient depletion: a model for persistent organisms? Tuberculosis **84**:228–238.

148. **Muttucumaru DGN, Roberts G, Hinds J, Stabler RA, Parish T**. 2004. Gene expression profile of *Mycobacterium tuberculosis* in a non-replicating state. Tuberculosis **84**:239–246.

149. **Voskuil MI, Visconti KC, Schoolnik GK**. 2004. *Mycobacterium tuberculosis* gene expression during adaptation to stationary phase and low-oxygen dormancy. Tuberculosis **84**:218–227.

150. **Talaat AM, Lyons R, Howard ST, Johnston SA**. 2004. The temporal expression profile of *Mycobacterium tuberculosis* infection in mice. PNAS **101**:4602–4607.

151. **Kruh NA, Troudt J, Izzo A, Prenni J, Dobos KM**. 2010. Portrait of a pathogen: the *Mycobacterium tuberculosis* proteome *in vivo*. PLoS ONE **5**:e13938.

152. **Fisher MA, Plikaytis BB, Shinnick TM**. 2002. Microarray analysis of the *Mycobacterium tuberculosis* transcriptional response to the acidic conditions found in phagosomes. J. Bacteriol. **184**:4025–4032.

153. **Hunt DM, Sweeney NP, Mori L, Whalan RH, Comas I, Norman L, Cortes T, Arnvig KB, Davis EO, Stapleton MR, Green J, Buxton RS**. 2012. Long-range transcriptional control of an operon necessary for virulence-critical ESX-1 secretion in *Mycobacterium tuberculosis*. J. Bacteriol. **194**:2307–2320.

154. **Mitra A, Angamuthu K, Nagaraja V**. 2008. Genome-wide analysis of the intrinsic terminators of transcription across the genus *Mycobacterium*. Tuberculosis **88**:566–575.

155. **Lyon RH, Hall WH, Costas-Martinez C**. 1974. Effect of L-asparagine on growth of *Mycobacterium tuberculosis* and on utilization of other amino acids. J. Bacteriol. **117**:151–156.

156. **Kay WW**. 1971. Two aspartate transport systems in *Escherichia coli*. J. Biol. Chem. **246**:7373–7382.

157. **Thanky NR, Young DB, Robertson BD**. 2007. Unusual features of the cell cycle in mycobacteria: polar-restricted growth and the snapping-model of cell division. Tuberculosis **87**:231–236.

158. **Schaefer WB, Marshak A, Burkhart B**. 1949. The growth of *Mycobacterium tuberculosis* as a function of its nutrients. J Bacteriol **58**:549–563.

159. **Van Kessel JC, Hatfull GF**. 2007. Recombineering in *Mycobacterium tuberculosis*. Nat Methods **4**:147–52.

160. **Changsen C, Franzblau SG, Palittapongarnpim P**. 2003. Improved green fluorescent protein reporter gene-based microplate screening for antituberculosis compounds by utilizing an acetamidase promoter. Antimicrob Agents Chemother **47**:3682–3687.

161. **Manabe YC, Chen JM, Ko CG, Chen P, Bishai WR**. 1999. Conditional sigma factor expression, using the inducible acetamidase promoter, reveals that the *Mycobacterium tuberculosis sigF* gene modulates expression of the 16-kilodalton alpha-crystallin homologue. J Bacteriol **181**:7629–7633.

162. **Jayaram HN, Ramakrishnan R, Vaidyanathan CS**. 1968. L-asparaginases from *Mycobacterium tuberculosis* strains H37Rv and H37Ra. Arch. Biochem. Biophys. **126**:165–174.

163. **Soru E, Teodorescu M, Zaharia O, Szabados J, Rudescu K**. 1972. L-asparaginase from the BCG strain of *Mycobacterium bovis*. I. Purification and *in vitro* immunosuppressive properties. Can. J. Biochem. **50**:1149–1157.

164. **Lyon RH, Hall WH, Costas-Martinez C**. 1970. Utilization of Amino Acids During Growth of *Mycobacterium tuberculosis* in Rotary Cultures. Infect Immun **1**:513–520.

165. **Souza G de, Målen H, Søfteland T, Sælensminde G, Prasad S, Jonassen I, Wiker H**. 2008. High accuracy mass spectrometry analysis as a tool to verify and improve gene annotation using *Mycobacterium tuberculosis* as an example. BMC Genomics **9**:316.

166. **Krämer R, Lambert C, Hoischen C, Ebbighausen H**. 1990. Uptake of glutamate in *Corynebacterium glutamicum*. European Journal of Biochemistry **194**:929–935.

167. **Poolman B, Hellingwerf KJ, Konings WN**. 1987. Regulation of the glutamate-glutamine transport system by intracellular pH in *Streptococcus lactis*. J Bacteriol **169**:2272–2276.

168. **Braña AF, Paiva N, Demain AL**. 1986. Pathways and regulation of ammonium assimilation in *Streptomyces clavuligerus*. J Gen Microbiol **132**:1305–1317.

169. **Abrahams GL, Kumar A, Savvi S, Hung AW, Wen S, Abell C, Barry III CE, Sherman DR, Boshoff HIM, Mizrahi V**. 2012. Pathway-selective sensitization of *Mycobacterium tuberculosis* for target-based whole-cell screening. Chemistry & Biology **19**:844–854.

170. **Parish T, Stoker NG**. 2000. Use of a flexible cassette method to generate a double unmarked *Mycobacterium tuberculosis tlyA plcABC* mutant by gene replacement. Microbiology **146 (Pt 8)**:1969–75.

171. **Machowski EE, Barichievy S, Springer B, Durbach SI, Mizrahi V**. 2007. *In vitro* analysis of rates and spectra of mutations in a polymorphic region of the

Rv0746 PE_PGRS gene of *Mycobacterium tuberculosis*. J. Bacteriol **189**:2190–2195.

172. **Bishop PJ, Neumann G**. 1970. The history of the Ziehl-Neelsen stain. Tubercle **51**:196–206.

173. **Hermans J, Boschloo J g., de Bont J a. m.** 1990. Transformation of *Mycobacterium aurum* by electroporation: the use of glycine, lysozyme and isonicotinic acid hydrazide in enhancing transformation efficiency. FEMS Microbiology Letters **72**:221–224.

174. **Snapper SB, Melton RE, Mustafa S, Kieser T, Jacobs WR Jr**. 1990. Isolation and characterization of efficient plasmid transformation mutants of *Mycobacterium smegmatis*. Mol. Microbiol. **4**:1911–1919.

175. **Wards BJ, Collins DM**. 1996. Electroporation at elevated temperatures substantially improves transformation efficiency of slow-growing mycobacteria. FEMS Microbiol Lett **145**:101–5.

176. **Lee S-H, Cheung M, Irani V, Carroll JD, Inamine JM, Howe WR, Maslow JN**. 2002. Optimization of electroporation conditions for *Mycobacterium avium*. Tuberculosis (Edinb) **82**:167–74.

177. **Sambrook J, Russell DW**. 2001. Molecular Cloning: A Laboratory Manual, 3rd ed. CSHL Press, Cold Spring Harbor, NY.

178. **Hinds J, Mahenthiralingam E, Kempsell KE, Duncan K, Stokes RW, Parish T, Stoker NG**. 1999. Enhanced gene replacement in mycobacteria. Microbiology **145 (Pt 3)**:519–27.

179. **Warren R, Hauman J, Beyers N, Richardson M, Schaaf HS, Donald P, van Helden P**. 1996. Unexpectedly high strain diversity of *Mycobacterium tuberculosis* in a high-incidence community. S. Afr. Med. J. **86**:45–49.

180. **Hoek KGP, Gey van Pittius NC, Moolman-Smook H, Carelse-Tofa K, Jordaan A, van der Spuy GD, Streicher E, Victor TC, van Helden PD, Warren RM**. 2008. Fluorometric assay for testing rifampin susceptibility of *Mycobacterium tuberculosis* complex. J Clin Microbiol **46**:1369–73.

181. **Yu J-H, Hamari Z, Han K-H, Seo J-A, Reyes-Domínguez Y, Scazzocchio C**. 2004. Double-joint PCR: a PCR-based molecular tool for gene manipulations in filamentous fungi. Fungal Genet. Biol. **41**:973–981.

182. **Brody JR, Kern SE**. 2004. Sodium boric acid: a Tris-free, cooler conductive medium for DNA electrophoresis. Biotechniques **36**:214–6.

183. **Woolfolk CA, Shapiro B, Stadtman ER**. 1966. Regulation of glutamine synthetase. I. Purification and properties of glutamine synthetase from *Escherichia coli*. Arch Biochem Biophys **116**:177–92.

184. **Muñoz-Elías EJ, McKinney JD**. 2005. *Mycobacterium tuberculosis* isocitrate lyases 1 and 2 are jointly required for *in vivo* growth and virulence. Nat. Med. **11**:638–644.

185. **Awasthy D, Ambady A, Bhat J, Sheikh G, Ravishankar S, Subbulakshmi V, Mukherjee K, Sambandamurthy V, Sharma U**. 2010. Essentiality and functional analysis of type I and type III pantothenate kinases of *Mycobacterium tuberculosis*. Microbiology **156**:2691–2701.

186. **Weischenfeldt J, Porse B**. 2008. Bone marrow-derived macrophages (BMM): isolation and applications. Cold Spring Harb Protoc **2008**:pdb.prot5080.

187. **Rozen S, Skaletsky H**. 2000. Primer3 on the WWW for general users and for biologist programmers. Methods Mol. Biol. **132**:365–386.

188. **Zwietering MH, Jongenburger I, Rombouts FM, van 't Riet K**. 1990. Modeling of the bacterial growth curve. Appl Environ Microbiol **56**:1875–1881.

189. **Dalgaard P, Koutsoumanis K**. 2001. Comparison of maximum specific growth rates and lag times estimated from absorbance and viable count data by different mathematical models. Journal of Microbiological Methods **43**:183–196.

190. **De Siano T, Padhi S, Schaffner DW, Montville TJ**. 2006. Growth characteristics of virulent *Bacillus anthracis* and potential surrogate strains. Journal of Food Protection **69**:1720–1723.

191. **Membré J-M, Leporq B, Vialette M, Mettler E, Perrier L, Thuault D, Zwietering M**. 2005. Temperature effect on bacterial growth rate: quantitative microbiology approach including cardinal values and variability estimates to

perform growth simulations on/in food. International Journal of Food Microbiology **100**:179–186.

192. **Novak M, Pfeiffer T, Ackermann M, Bonhoeffer S**. 2009. Bacterial growth properties at low optical densities. Antonie van Leeuwenhoek **96**:267–274.